ALMA MATER STUDIORUM · UNIVERSITÀ DI BOLOGNA

Dynamics of Bora wind over the Adriatic Sea: atmospheric water balance and role of air-sea fluxes and orography

Relatore: Presentata da:
Prof. Andrea Buzzi   Riccardo Hénin

Correlatore:
Dott. Silvio Davolio

Abstract

The Bora wind is a mesoscale phenomenon which typically affects the Adriatic Sea basin for several days each year, especially during winter. Most of the time a Bora occurrence is a consequence of synoptic conditions favourable to persistent cold spells over Europe. The Bora wind has been studied for its intense outbreak across the Dinaric Alps. The properties of the Bora wind are widely discussed in the literature and scientific papers usually focus on the eastern Adriatic coast where strong turbulence and severe gust intensity are more pronounced. However, the impact of the Bora wind can be significant also over Italy, not only in terms of wind speed instensity. Depending on the synoptic pressure pattern (cyclonic or anticyclonic Bora) and on the season, heavy snowfall, severe storms, storm surges and floods can occur along the Adriatic coast and on the windward flanks of the Apennines.

In the present work five Bora cases that occurred in recent years have been selected and their evolution has been simulated with the BOLAM-MOLOCH model set, developed at ISAC-CNR in Bologna. Each case study has been addressed by a control run and by several sensitivity tests, performed with the purpose of better understanding the role played by air-sea latent and sensible heat fluxes. The tests show that the removal of the fluxes induces modifications in the wind approching the coast and a decrease of the total precipitation amount predicted over Italy. In order to assess the role of heat fluxes, further analysis has been carried out: column integrated water vapour fluxes have been computed along the Italian coastline and an atmospheric water balance has been evaluated inside a box volume over the Adriatic Sea. The balance computation shows that, although latent heat flux produces a significant impact on the precipitation field, its contribution to the balance is relatively minor.

The most significant and lasting case study, that of February 2012, has been studied in more detail in order to explain the impressive drop in the total precipitation amount simulated in the sensitivity tests with removed heat fluxes with respect to the CNTRL run. In these experiments relative humidity and potential temperature distribution over different cross-sections have been examined. With respect to the CNTRL run a drier and more stable boundary layer, characterised by a more pronounced wind shear at the lower levels, has been observed to establish above the Adriatic Sea.

Finally, in order to demonstrate that also the interaction of the Bora flow with the Apennines plays a crucial role, sensitivity tests varying the orography height have been considered. The results of such sensitivity tests indicate that the propagation of the Bora wind over the Adriatic Sea, and in turn its meteorological impact over Italy, is influenced by both the large air-sea heat fluxes and the interaction with the Apennines that decelerate the upstream flow.

Sommario

Il vento di Bora è un fenomeno alla mesoscala che interessa il bacino del Mare Adriatico per molti giorni all'anno, soprattutto in inverno: il più delle volte infatti è effetto dello stabilirsi sul continente Europeo di condizioni sinottiche che favoriscono prolungati periodi di freddo intenso. Il fenomeno della Bora ha da sempre destato interesse scientifico per gli aspetti legati alla sua violenta irruzione nel bacino del Mediterraneo attraverso le Alpi Dinariche. In letteratura si è molto dibattuto sull'origine dinamica della Bora e si è focalizzata l'attenzione sulla costa adriatica orientale dove gli effetti turbolenti e le raffiche di vento sono più intensi. Tuttavia anche sull' Italia l'impatto della Bora è significativo e non solo in termini di velocità del vento: in base alle condizioni sinottiche (Bora ciclonica o anticiclonica) e alla stagione si possono sviluppare estese precipitazioni nevose, fenomeni temporaleschi, mareggiate ed episodi alluvionali sulle aree più esposte.

Per questa tesi sono stati selezionati cinque episodi di Bora avvenuti negli ultimi anni la cui evoluzione è stata simulata con i modelli meteorologici BOLAM e MOLOCH sviluppati presso l'istituto ISAC-CNR di Bologna. Per ciascun caso di studio sono stati svolti un run di controllo e dei test di sensitività con l'obiettivo di comprendere il ruolo dei flussi di calore latente e sensibile all'interfaccia aria-mare. I test hanno mostrato che l'azzeramento dei flussi provoca delle modifiche alla propagazione della Bora sul mare e un forte calo della precipitazione prevista sull'Italia. Per caratterizzare meglio questo aspetto sono stati calcolati i flussi di vapore acqueo integrati verticalmente lungo il profilo della costa italiana ed è stato formulato un bilancio di acqua in atmosfera attraverso una box tridimensionale definita sul Mare Adriatico. Proprio quest'ultima analisi ha mostrato che, nonostante i flussi di calore latente abbiano un forte impatto sul campo di precipitazione, essi risultano di piccola entità rispetto agli altri termini del bilancio, soprattutto per gli episodi di Bora ciclonica.

A titolo di esempio si è considerato il caso più significativo e duraturo, quello del Febbraio 2012, per valutare se oltre all'effetto dei flussi ci siano delle ragioni di tipo dinamico in grado di spiegare il forte calo di precipitazione osservato nei test di sensitività. Analizzando la distribuzione spaziale dell'umidità relativa e della temperatura potenziale lungo opportune sezioni verticali è stata osservata, proprio per i test con i flussi azzerati, la formazione di uno strato limite sul Mare Adriatico più secco e più stabile, esteso per poche centinaia di metri, che confina il vento di Bora alle quote superiori.

Infine sono stati effettuati dei test di sensitività variando l'orografia per dimostrare che anche l'interazione del flusso di Bora con l'Appennino ha un ruolo cruciale nel determinare l'evoluzione dell'evento. I risultati dei diversi test di sensitività si sono rivelati coerenti tra loro nell'indicare sia negli intensi flussi di calore aria-mare sia nell'azione di decelerazione a monte esercitata dalla catena appenninica i fattori che influenzano le modalità con cui la Bora si propaga sull'Adriatico e interessa il territorio italiano.

Contents

List of Figures

List of Tables

Chapter 1

Introduction

The first chapter gives an outlook on the main themes that will be treated in the present work with proper reference to state-of-the-art knowledge and to published papers and articles. It goes through the steps that build-up the whole thesis, from the choice of the argument, the investigation among data and curiosities till the final discussion and the experimental verification of working hypotesis.

1.1 The starting point

Andrija Mohorovičić, a Croatian geophysicist who lived in the XIX century wrote what has been then considered the first essay about the effects of a gale-force wind that frequently affected his hometown, Bakar, Croatia [Grubišic and Orlic, 2007]. Here are his words [Mohorovičic, 1889]:

It is impossible to imagine the existence of such a permanent mass of cumulus unless on the assumption of a rotary motion about a horizontal axis .....We do not often read of a whirlwind with its axis horizontal, and I have not been able to find any notice of such a phenomenon.... I think, therefore, that what I say may be of interest.

He outlined what is now recognized as a typical feature of Bora wind: the development of rotor-type clouds remarking the presence of atmopsheric rotors, on the lee-side of mountains. Bora wind belongs to the broader class of local downslope winds and in wider terms to those events strictly connected with the orographic complexity of the area they affect. It's undeniable that such extremely moody phenomenon arouses scientific curiosity.

Local Bora-like winds belong to the class of downslope winds that can be recognised in many parts of the world, besides Northern Adriatic, everytime an air flow of polar origin runs over a well-organized mountain ridge characterized by a certain slope on the leeside

and spreads beyond it. The onset of the Bora wind and the first phases of its outbreak in the Adriatic Sea are described in Ch. 2. Among the best known Bora-like winds, it should be mentioned Boulder and Sierra Nevada windstorms in the USA, Hokkaido wind in Japan as well as Antarctic slope winds. Concerning Europe, Novorossiyskaja Bora is the most famous, which blows into the namesake city located in the northeastern coast of the Black Sea, in Russia.

Although being a local wind, the Bora blowing on Trieste (or *kraška burja* in Croatian) deeply influences the climate of a larger area: climatological studies show that it blows 177 days annually in the town of Senj, not so far from Bakar [Belušić et al., 2013], [Poje, 1992], [Yoshino, 1976], and 160 days annually in Trieste [Stravisi, 1987], with a peak of occurences in the cold season. The most severe winters in Italy and South Europe as well, those with record-breaking temperatures, snowfalls and dramatic damages (1929, 1956, 1985, 2012), are all connected with Bora-favourable synoptic patterns.

Bora wind carries very cold and dry air from Eastern Europe down the Dinaric Alps, directly into the warmer Adriatic area. Large differences between the temperature of the incoming air and the sea water is known to enhance heat fluxes through evaporation [Dorman et al., 2006]. The consequence of such a moistening of the air is still discussed especially the capacity to yield to High Precipitation Events (HPE) affecting more exposed areas [Ludwig et al., 2014], [Senatore et al., 2014].

Several extensive projects have faced the problem of correctly forecasting occurences of high-impact or even catastrophic events, matching the increasing demand for accuracy from common users, Governments and insurance companies, interested in risks evaluation. Currently, the most important project for the meteorology and climatology of the Mediterranean area is the HYdrological MEditerranean Cycle (HyMeX) experiment, a multi-year European programme including also HPE and water cycle analysis over selected areas that have been recognised over the years as the most vulnerable ones [Ducrocq, 2014], [Drobinški, 2014]. On the other hand, a continuous effort is done in order to improve the capability of Numerical Weather Prediction (NWP) models to correctly reproduce the physical phenomena in the atmosphere and, as a consequence, to increase the realiability of the forecasts. Ricerca Italiana per il Mare (RITMARE) is an italian project with the aim of evaluating and implementing a NWP modeling chain for high resolution meteorological forecasts on marine environment, paying specific attention to air-sea interface processes [Davolio et al., 2013]. The choice of the case studies (Ch. 4) for the present thesis has made having in mind the above two projects, to better connect at least part of the present work to study areas and individual episodes of proved scientific interests.

1.2   Main objectives

The present work pertains to the research related to the investigation of the Bora wind mechanism. More specifically, the main objective is to determine to what extent the Adriatic Sea influences the Bora wind and its impact on the Italian Pensinsula and how NWP models can serve this issue. The work is organised through an initial phase (Ch. 2) during which the problem of flow interaction with orography is discussed in general terms, followed by an overview on the numerical models that have been used to perform the simulations of the events (Ch. 3). Then the selection and the characterization of the case studies is presented. The chosen episodes are lead back to known classification criteria and commented on the basis of the simulations results (Ch. 4). Finally the experimental section is the core of the thesis: a discussion on the water vapour profiles and atmospheric water balances is provided in Ch. 5 and a more detailed examination of the February 2012 case, including cross-section analysis and orography sensitivity tests, is presented in Ch. 6. For simplicity the individual objectives are sketched as follows:

- identifying remarkable Bora events, classifying them into a literature-known scheme and qualitatively describying their main features (Ch. 2 and Ch. 4);

- verifying the accordance between the model output and observations recorded by official weather stations networks (Ch. 4);

- performing different kinds of sensitivity tests, making comparisons with respect to control runs to assess which factors influence the most the dynamics of Bora wind (Ch. 4);

- evaluating the relative contribution of the Adriatic Sea, via water vapour fluxes at air-sea interface, in enhancing or diminishing precipitation and convection (Ch. 5);

- investigating all the dynamic aspects that lead to HPE occurences inshore by implementing new ad-hoc tools to analyze the role of water vapour fluxes (Ch. 5);

- probing the role of the downstream orography (the Apennines chain) in modifying the flow dynamics (Ch. 6).

The classification of Bora occurences is proposed mainly belonging to a cyclonic or anticyclonic pattern, but other criteria are suggested. The observational data used to validate the models are collected inquirying regional agencies archives. The sensitivity of Bologna Limited Area Model (BOLAM) and MOdello LOCale in coordinate H (MOLOCH) numerical models forecasts to SST departures from reference values, to modifications of heat fluxes and finally to orography alteration is tested. The model results are discussed on the basis of graphical outputs, cross-sections analysis and comparisons among the events (mainly the cyclonic ones which appear to be the most challenging and intense).

Chapter 2

The Bora wind: main features

Pioneering studies on Bora features trace-back to the seventies [Yoshino, 1976], [Jurčec, 1981] before specific campaigns were planned by scientific community; remarkable advances came actually with Alpine Experiment (ALPEX) project, a joint effort involving twenty-nine nations, World Meteorological Organization (WMO)-driven, in 1982 that was the first campaign dedicated solely to study wind patterns over the Alps and the lee cyclogenesis [Smith, 1985], [Smith, 1987]. Some years later the Mesoscale Alpine Project (MAP) campaign was also fundamental in providing general undestanding of the physical issue regarding wind regimes of a flow crossing a barrier [Bougeault et al., 2001]. The new millenium brought local Bora features to be addressed by means of different technologies acting in concert: improved in-situ measurements networks, aircraft flights, numerical simulations and RADAR observations. Efforts focused on 3D patterns and wind-jets structure that have been also captured by RADARSAT [Askari et al., 2003], [Dorman et al., 2006] and Synthetic-aperture radar (SAR) [Alpers et al., 2009] [Signell et al., 2010] , [Kuzmić et al., 2013]. A masterly review of the up-to-date knowledge and open questions for a full-scale comprehension of Bora events is that one by Grisogono [Grisogono and Belušić, 2009].

Bora features can be faced from different points of view belonging to the reasearch fields of different branches of the earth physics: dynamic meteorology, oceanography, climatology, Planetary Boundary Layer (PBL) turbulence. A summary of the main topics is presented in this chapter with extensive use of references, focusing on the observed phenomena connected with Bora and on the feedback mechanisms that lead to enhancement of its effects.

2.1   Morphology of the Adriatic basin

Tha Adriatic Sea extends over an area of the order of 10^5 km^2 enclosed by the Dinaric Alps on the East, by the Apennines chain on the West, by eastern Alps and Venetian plain on the North and by the Otranto channel on the South. Such a configuration makes the basin prone to the channelling of wind.

It is common to divide the Adriatic basin in three sub-areas belonging mainly to the bathymetric differences [Orlic et al., 1992]: the northern one (NA) which comprises the Gulf of Trieste, the Venice lagoon, the Po delta till the Conero promontory, the central one (CA) and the southern one (SA) where exiting of water masses towards the Ionian Sea is allowed. NA is shallow with an average depth lower than fifty meters whereas CA starts deepening up to Central Adriatic Pit in the middle (Jabuka Pit, 270 m depth) and SA is characterized by the well-known South Adriatic Pit (SAP) which reaches a depth of 1200 m and is a key-structure for the whole Adriatic Sea water circulation and for biology as a source of biodiversity (see Fig. 2.1 for pattern matching).

The shape of the basin, his narrowness and enclosing borders, induce specific ocean dynamic responses to external stresses like superposition of seiches, enhancing tides and gale surges [Lionello et al., 2012]. The wind fetch can be very large for southeasterly wind and lower but still important for northeasterly and southwesterly ones leading to high value of momentum exchange between air flow and water body in terms of Significant Wave Height (SWH) offshore and to regular occurrences of coastal storm surges (better known as *acqua alta*). Moreover the huge number of islands and narrow peninsulae latitudinally stretched on the eastern seaside favours the development of local turbulence, funneling, rotors and gustiness. Another key-factor is the changeable water runoff of several rivers, mainly Po, Timavo, Piave and the minor ones falling from Dinaric Alps and Karstic springs, whose water is fresh, lightly salted, rich of organic compounds and affect deeply the water properties. Finally, the thermal response of water mass is faster because of shallowness.

As regards the orography surrounding the basin while Dinaric Alps steepen approaching the Balcanic coastline (at least for the northern part, slightly gentler moving southward) the Apennines raise wherever more softly. The mountain chains belonging to Dinaric Alps closer to the sea show a distinct sequence of gaps and peaks (Fig. 2.7), the latter ones standing all below 1800 m height (higher values are reached only in the southern inland). It will be shown (Sec. 2.4.2) that this distinctive features is crucial for wind propagation across the sea. The Apennines on the contrary are sharper, 1500 km long and, on average, attain higher altitude with several peaks above 2000 m (Monte Cimone - 2165 m, Monte Terminillo - 2217 m and Monte Vettore - 2476 m among the others) and the highest one which reaches 2912 m (Corno Grande, Abruzzo).
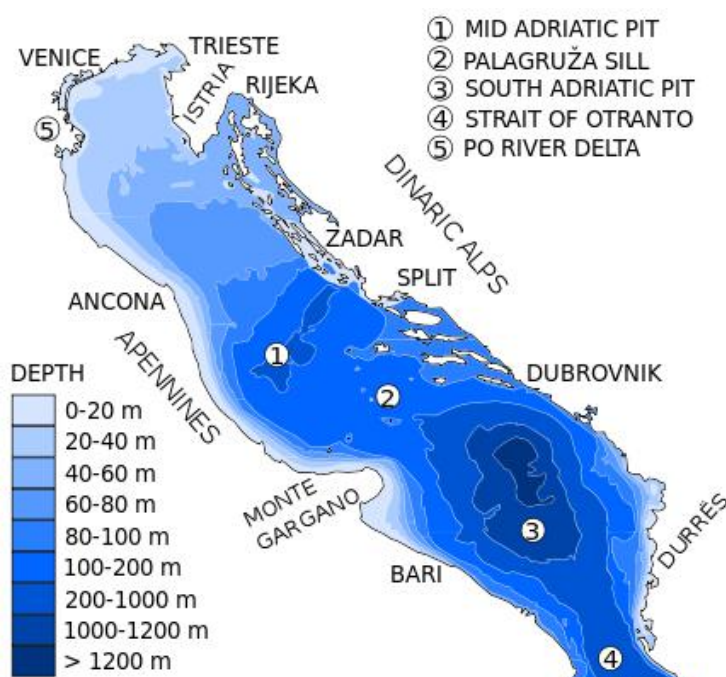
Figure 2.1: Bathymetry of the Adriatic Sea: main terrain features are listed.

2.2 Brief climatology and typical synoptic conditions of Bora events

The main wind regimes northern Adriatic experiences are well-known since past climatological studies [Poje, 1992], [Makjanić, 1978]: northwesterly (Maestrale), northeasterly (Bora), southeasterly (Sirocco, also known with the local name *Jugo*) and southwesterly (Libeccio, whose local name is *Garbin*). Among them Bora is the prevalent one especially in the wintertime [Yoshino, 1976], [Belušić et al., 2013]. Earlier researches concerning Bora events all focused on the northern part of the Adriatic basin and only recently the southern part has been equally taken into account [Horvath et al., 2009]. The reason for this gap is due to the complexity of the terrain orography along the southeastern Adriatic border that makes evidences of Bora outflows difficult to match with the hydraulic theory and with the others typical Bora features (Sec. 2.3).

It is common in literature to distinguish Bora events on the basis of the weather pattern (e.g. synoptic conditions) that produces them [Yoshino, 1976], [Jurčec, 1981], [Pandžić and Likso, 2005]. Bora is triggered always in the same way that is when an oversupply of cold and dry air in the lower levels is confined windward to the Dinaric Alps and Karst plateau thus building-up a large pressure gradient across the mountains with respect to the Adriatic Sea. Synoptic conditions however can be different and can lead to various

evolutions with some local effects more enhanced than others and a specific pattern in terms of rainfalls, sky overcast and air-sea interactions for each case. Therefore the distinction reads as follows:

- **anticyclonic Bora**

  Bora is termed anticyclonic when a solid high pressure is settled over central-eastern Europe and isobars are stretched over the Mediterranean basin. The sky tends to be clear, the air flow is from the North or the North-East all along the vertical profile and precipitations are hardly to occur. A reinforced variation of this type takes place when a very stable high pressure system embraces longitudinally all-Europe as a product of an Atalantic blocking high (the so called Voejkov-bridge). Such a configuration is very effective in blocking the Atlantic westerly flow and conveying continental air towards the Adriatic Sea.

- **cyclonic Bora**

  It is referred to as cyclonic Bora when a Low Pressure (LP) settles over the Adriatic Sea or over the Ionian Sea, mainly as the final step of a lee Alpine cyclogenesis previously originated and migrated southeasterly. Typically the air flow at upper levels is no more easterly and the cyclonic circulation superimposes warmer and moist air with the Bora flow at lower levels too. It is observed in this work that depending on the strenght of this forcing the Bora wind can be overrun and confined more or less to the northern and central Adriatic. Thus the vertical wind shear can be a key-factor to recognise whether the Bora occurrence is cyclonic or not.

In the northern Adriatic (Gulf of Trieste and Venice lagoon) another classification is in use that is more informal and quite slangly but actually matches with some texts [Camuffo, 1981]: that of dark Bora (which eventually can turn into *borino*) and clear/white Bora. This classification does not replace the preceeding one but simply overlaps [Camuffo, 1990], [Cesini et al., 2004]. It can be said to a certain extent that dark Bora belongs to cyclonic Bora and clear Bora to anticyclonic Bora. It is worth pointing that an excess in detailed categorization can be misleading and other different schemes can be found indeed ([Grisogono and Belušić, 2009] and reference therein, [Jurčec, 1981]).

A well-posed classification on the contrary, concerns the origin of the air masses that flows out in the Adriatic Sea and mirrors the two main Bora-type listed above; belonging to the known general classification of air massess [Calwagen, 1926] it can be said that in most cases anticyclonic Bora drains in the Adriatic basin continental air of polar origin whilst cyclonic Bora drains air of artic origin, maritime or continental depending on each case.

2.3 The onset of Bora: the problem of a flow crossing a barrier

The onset of Bora is strictly related to the larger-scale synoptic pattern while the speed, the direction and the development of fine-scale features depend on the local topography of the Dinaric Alps and Dalmatian Islands. It has been clearly shown by means of orographic sensistivity tests [Lazić and Tošić, 1997] that a mountain barrier of at least 1000 m height is a necessary requirement for the triggering of a downslope windstorm considering the typical values of flow parameters for this area.

Bora wind was initially explained by means of katabatic-wind theory that applies to other well-known downslope winds like foëhn and chinook; this concept held for years until inconsistencies were found during ALPEX and MAP campaigns and related measurements. Even though the first stage of a Bora occurrence is reliably illustrated in the context of downslopes wind the thermodynamical forcing expected would require an unrealistic temperature difference between the two flanks of the mountain up to 25°C to mantain a wind speed of about 20 $m \cdot s^{-1}$. Moreover a pure katabatic wind results in a leeside warming while in those cases air that spills over Dinaric Alps is so cold that, even taking into account a compressional warming which anyway would affect no more than a small area, a general leeside cooling is observed. The wind speed maximum is not always recorded at the surface as expected but few hundreds meters above [Grisogono and Belušić, 2009].

Deficiencies in katabatic theory encouraged the research for a new paradigm: the breakthoughts was the discover that, apparently, the mechanism that lead to strong-to-severe Bora is the wave breaking of gravity waves which means, conceptually, that the linear theory of stationary waves crossing a mountain ridge is inadequate and the role of non-linear processes is straightforward.

The basic paradigm [Markowski and Richardson, 2010] is therefore that of vertical and horizontal propagation of gravity waves induced by the orography at significant distances downstream (and upstream as well) in the context of a 2-dimensions linear theory. The steady-state solution for idealised cases (simple and regular topography, uniform and homogeneous flow, constant stratification).

Gravity waves can propagate or decay with height. A special case is that of trapped lee waves that are encouraged by non homogeneous atmosphere and are associated with rotor circulation in between (Fig. 2.2). Vertical parcel displacement, rotor-induced too, can be large enough to reach the Lifting Condensation Level (LCL) and results in typical cloud pattern (laminar lenticular clouds and roll clouds).

More accurate observations show that especially if we consider high amplitude gravity waves the flow experiences substantial acceleration as it passes over a barrier leading to
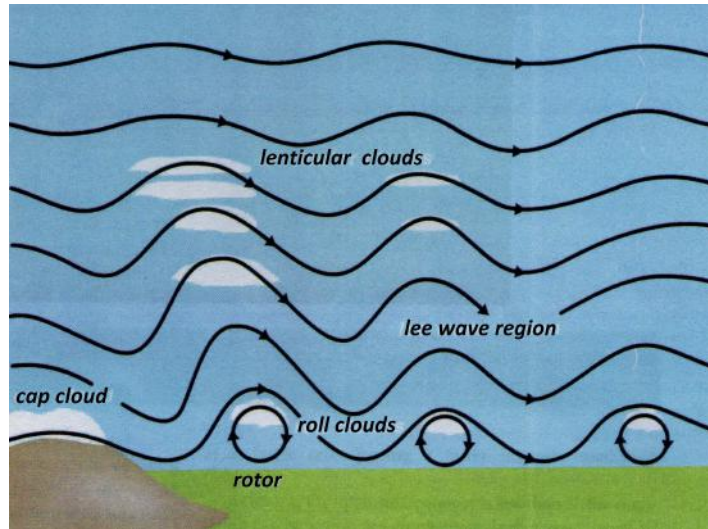
Figure 2.2: Schematic illustration of the main features regarding gravity waves propagation beyond a mountain barrier.

gravity wave breaking and to the formation of an hydraulic jump downstream. Linear theory no longer holds in these cases that are characterized by a nondimensional parameter

$$Fr^{-1} = \frac{Nh_m}{U} \tag{2.1}$$

greater than unity (N is Brunt-Väisälä frequency, h_m is the mountain height, U is the zonal wind speed of a uniform flow). This parameter is in such a way a measure of the nonlinearity produced in the flow and its reciprocal is known as *Froude number* which is a very important parameter to characterise a flow impinging onto a barrier. Another important non-dimensional parameter describing an airflow is the *Rossby number*

$$Ro = \frac{U}{fL} \tag{2.2}$$

which respresents the ratio of intertial to Coriolis forces.

It was firtsly observed that wave breaking takes place above the boundary layer inducing a dynamical response of the flow resembling the hydraulic model that is a pattern with a steep descent and a sudden ascent of isentropes connected with a large TKE zone [Jiang and Doyle, 2005]. This means that wave-breaking induces turbulent phenomena through energy dissipation such as PV banners ([Smith, 1989], [Grubišíc, 2004]), rotors, gusts and shooting flows.

The Froude number is a widely used parameter in fluid dynamics. It expresses the ratio of inertial to gravitational forces and it is useful to distinguish two main flow regimes and the critical threshold between them for a flow crossing an idealised barrier in a two-dimension approximation (Fig. 2.3):

- $Fr > 1$ supercritical:
  the fluid thickens going uphill and thins downstream; consequently the cross-mountain velocity also changes: minimun velocity is reached on the top of the mountain while it attains the same value before and after climbing the top. The kinetic energy a parcel possesses before is converted in potential energy during the lifting and then back to kinetic.

- $Fr \to 1$ critical:
  is defined as the layer where phase speed of buoyancy waves equals the ambient wind speed and mountain waves are thus stationary

- $Fr < 1$ subcritical:
  opposite to supercritical: the fluid thins during the lifting and reaches the minimum thickness and the maximun velocity at the top; then it comes back to initial condition. energy conversions are opposite too.

In hydraulic jump the air parcel attains higher wind speeds as it moves from windward side to leeward side thus a regime favourable to a continuous flow acceleration is needed on both flanks of the mountain. This means that the region upstream should be in subcritical condition whilst as the flow crosses the mountain it undergoes a transition and becomes supercritical. The subcritical condition can be eventually restored by the hydrauic jump and by farther adjustments to environmental conditions to take place leeward. It is worth noting that a proper treatment of a realistic atmosphere would involve stratification instead of free surfaces approximation with internal waves playing an importan role.

Flow regimes described hitherto account for *flow over* only (with respect to an obstacle) whilst the Bora wind we are dealing with is tipycally connected with a blocking of the air impinging on the eastern flank of Dinaric Alps and a *flow around* regime is experienced too. The Froude number can be still used as a threshold value to decide weather an air parcel belonging to the flow can rise up to the top of the obstacle or not. Generally speaking an air parcel tends to go around than over a mountain with increasing stratification, decreasing speed and increasing distances to be ascended. This means that $Fr < 1$ is the condition for blocking. To calculate a proper Froude number for each case is challenging because of not obvious estimations of layer depths. However, it is not the only parameter to be considered: both the slope and the aspect ratio of the mountain ridge affect the tendency for blocking.

Due to the blocking, orographically trapped surge of cold air develops upstream, as it is observed on the Karst Plateau (it is termed *cold air damming*) and flow around tendency is observed resulting in a barrier wind appearance, equatorward if considering the northern emisphere (Sec. **??**).

Conversely, if enough rising is allowed by dynamical constraints, air mass flows into the gaps of the barrier. A further circumstance that expands the model discussed up to
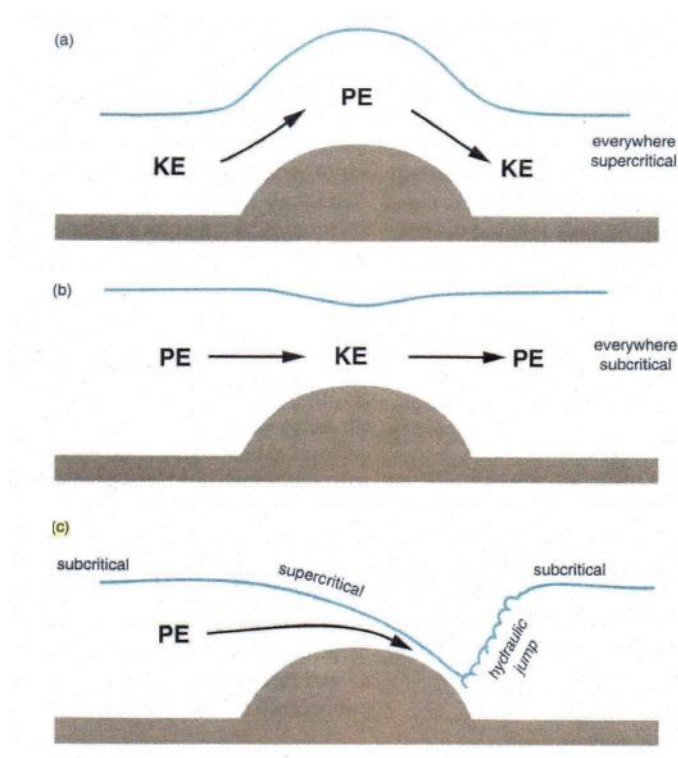
Figure 2.3: Schematic illustration of flow regimes depending on Froude number. Case (a) is referred to $Fr > 1$, case (b) to $Fr < 1$ and case (c) shows the transition between the two regimes that produecs the hydraulic jump pattern (from [Durran, 1990]).

now is that of wind speed enhancement and shooting flows developing close to mountain passes [Gaberšek and Durran, 2004]. The fact that gap flows would amplify Bora locally is well known [Gohm, Alexander and Mayr, Georg J. and Fix, Andreas and Giez, Andreas, 2008] but it is important to clarify the dynamical reason for this behaviour that can be applied worlwide also belonging to sea channels (Gibraltar for example). The key factors for strong gap flows are the settling of a pressure gradient and a temperature difference on the opposite sides of the barrier usually produced by larger-scale motions (Sec. 2.2) and cold air trapping. Thermal and pressure forcing acting on the air mass would produce an acceleration of the flow along the gap but maximum wind speed, with gusts exceeding 45-50 $m \cdot s^{-1}$, are rather recorded downstream at the gap exit (Fig. 2.5). Vertical momentum exchange must be taken into account as well: it is exerted by gravity waves and is responsible for that shifting.

Gap width finally determines how the flow re-adjusts to environmental conditions after it came out: narrower gaps induce a sharply transition, exactly that observed in hydraulic jumps.

To summarize, in Fig. 2.4 the interaction between an airflow and the orography is

explained by the different regimes that establish. Depending on the aspect ratio linear or non-linear regimes has to be considered and the Earth's rotation influence becomes relevant. The flow is assumed to be adiabatic on a f-plain and the latent heat release effect is neglected.

A wide variety of phenomena are shown to be connected with a Bora outbreak. Clearly those phenomena are better observed as the Bora severity increases but there is not a unique criterion to establish when a Bora occurrence can be identified as a truly Bora event. Depending on the area involved different standards have been setted mainly belonging to Bora flow lifetime and persistence: for example, Bora has been defined as a northeasterly 3-days lasting wind that blow over Senj with a speed always greater than 5 $m/cdots^{-1}$ [Milivoj et al., 2006] or similarly as a northeasterly wind at least 24h-lasting that exceeds 2.6 $m/cdots^{-1}$ at Zadar [Dorman et al., 2006].
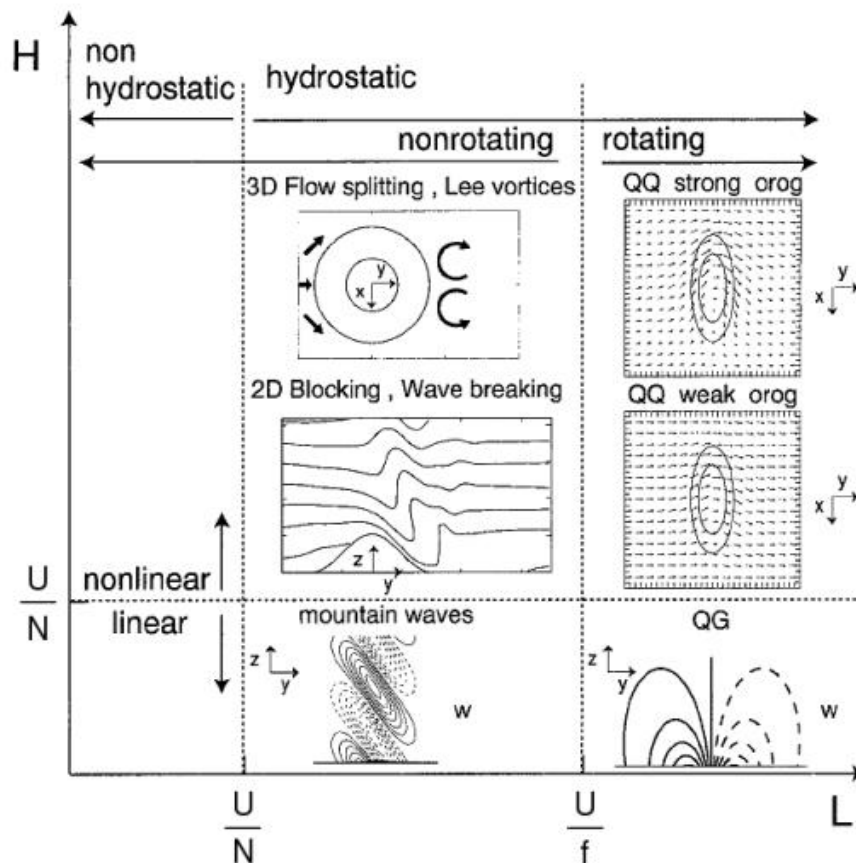
Figure 2.4: Regime diagram for an air flow of constant wind speed U, stratification N, impinging on a mountain (H and L are mountain height and width, respectively).
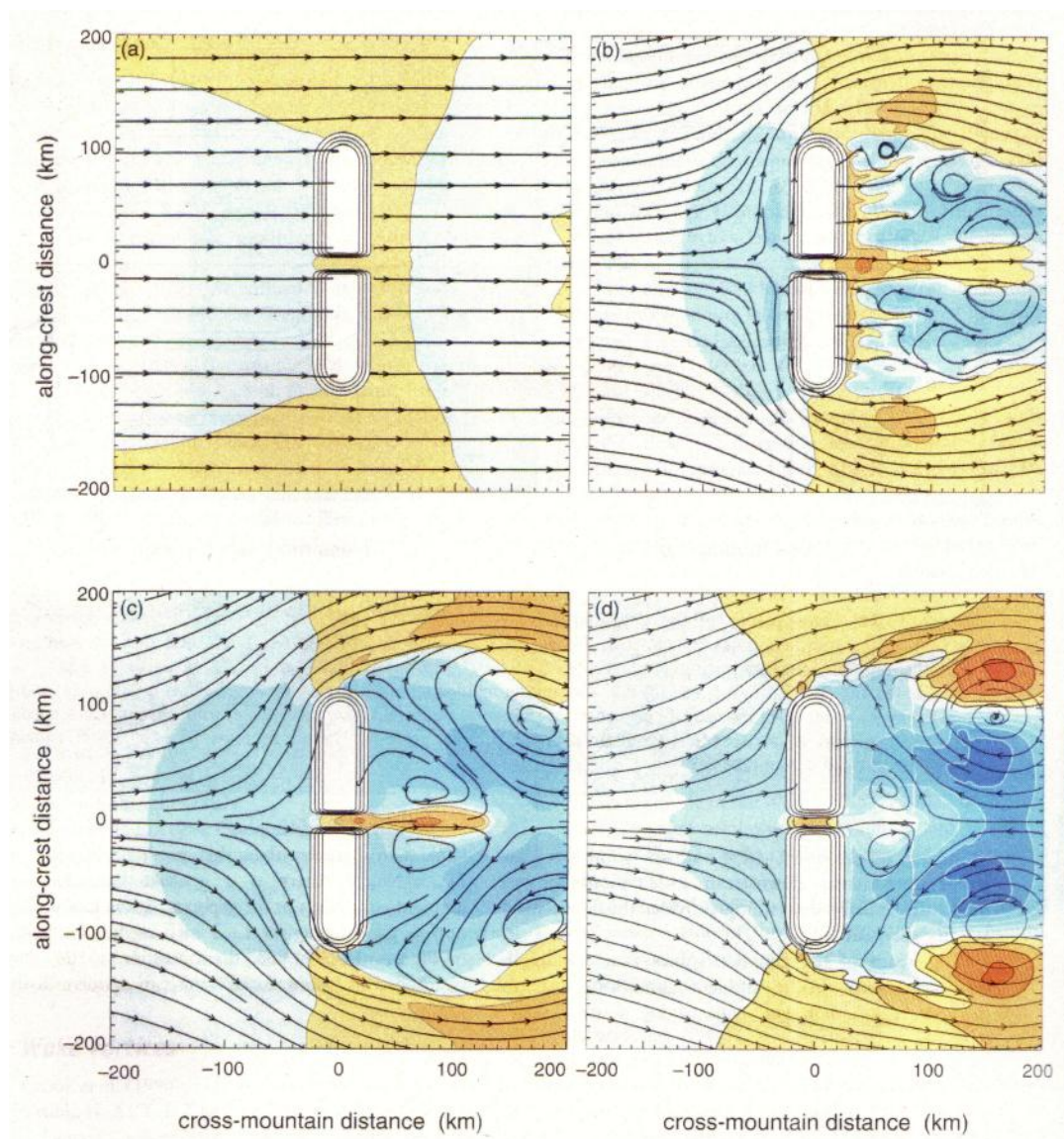
Figure 2.5: Idealised gap flow regimes depending on Froude number: $Fr = 4.0$ for (a), $Fr = 0.7$ for (b), $Fr = 0.4$ for (c), $Fr = 0.2$ for (d). Horizontal streamlines and normalized perturbation velocity at $z = 300m$ are shown; warm shading corresponds to positive values; terrain contours are 300m-staggered [Gaberšek and Durran, 2004].

2.4 The passage over the Adriatic Sea

It has been pointed out how Bora wind, belonging to downslope windstorms, is strictly connected with the local topography; the complex features of the Dinaric Alps trigger the first Bora gusts downstream. From that point on the offshore Bora front propagation experiences other forcings apart from orography, mainly those connected with air-sea fluxes. The sea state, described in terms of SWH, roughness, SST and mixing of upper layers become crucial in order to understand the dynamical evolution of the flow. Sea roughness can be considered as a fingerprint of the wind blowing over, whose intensity and direction can be thus retrieved by SAR images providing an accurate fine-scale representation (on the order of hundreds of meters) of Bora overwater structures otherwise very difficult to achieve. The majority of those structures are associated with strong turbulence and a parametrization approch is recommended. A remarkable feature of this type is the possible lee rotors formation downstream, in proximity to coastal cities, exactly what Mohorovičić tried to describe in the quotation reported at the beginning of the thesis. The vertical development of lee rotors, with reversed wind direction, is expected within the theoretical frame of a flow crossing a barrier (Sec. 2.3): their occurrences and persistence can be facilitated in this specific case by the unique distribution of the Croatian islands, all stretched alongshore nearly shaping a second lower barrier. Rotors over the eastern Adriatic, mainly referred to the city of Bakar and Senj in front of Krk island, have been reported in a number of studies [Ž.Večenaj et al., 2012], [Belušić et al., 2013], [Gohm, Alexander and Mayr, Georg J. and Fix, Andreas and Giez, Andreas, 2008] but no systematic knowledge exists about their characteristics and locations.

Once the flow propagates offshore it spreads cone-shaped above the sea surface with a unique pattern composed by strong Low Level Jets (LLJ) and wakes in between (Sec. 2.4.2). Typical timescales of the air-sea interaction range from a few days to a few hours: the surface fluxes and roughness variations response is quite istantaneous while SST feedback mechanism and divergence-driven sea current appereance are longer issues; the strong influence of Bora wind on winter and springtime Adriatic Sea circulation is described in Sec. 2.4.3.

As regards SST it has been outlined that its effects can be remarkable. For example sea minus air temperature difference sets the amount of sensible heat exchanged even if it is the depth of sea mixed layer that tells how much energy should be given to cool down the surface. SST is typically a relatively slow-evolving parameter because of the thermal inertia of the water body and usually a decimal of degree Celsius drop in a typical time-span of a short-range forecast (24h) can be considered as a significant tendency value [Lebeaupin et al., 2006]. Nevertheless it has been observed, even in the simulations performed in the present work, that impressive drops by several degrees can be experienced in case of strong Bora flow; the response of heat surface fluxes to SST changes is strongly connected with the strenght of the low level winds (the LLJ) that clearly promote a strong evaporation through a continuous air renewal.

A number of SST sensistivity tests ([Enger and Grisogono, 1998], [Vickers and Mahrt, 2004], [Kraljević and Grisogono, 2006]) pointed out another crucial topic: the higher the SST with respect to that of the land, the longer the Bora fetch (e.g. the overwater trajectory followed by an air parcel belonging to the flow) above the sea because of a lee side extention of supercritical regime due to a decrease in buoyancy. Consequently a stronger Bora front, heavily moistened by longer exposition to surface fluxes, reached the western coast of the Adriatic Sea where conditional convective instability might be released and rainfall is observed. Actually this behaviour has been widely observed in the Mediterranea area [Lebeaupin et al., 2006] and further investigations are needed for the specific case of Adriatic Bora.

The precipitation enhancing effect that is observed inland due to favourable convection conditions lead to associate this feature with the phenomenon of Lake-Effect Snow (LES), an instability driven mesoscale weather feature, long recognized by forecasters in the Great Lakes region which produces impressive snowfall on the southern banks and a typical cloud pattern over the water body. This linkage can be controversial since the observed rain rates are much larger in the USA but it's a matter of fact that some local features are the same; the acronimon Adriatic Sea Effect (ASE) is currently used by several weather services. The American Meteorological Society (AMS) definition of lake effect sounds like this: "localized convective snow bands that occur in the lee of lakes when relatively cold air flows over warm water ". Wind-parallel bands, sometimes exhibiting multiple-band structure and snowfall or rainfall peaks inland are clearly observed in some Bora occurrences as well (Fig. 2.6).

2.4.1 Surface fluxes

Sensible heat flux is related to changing temperature and it is non-zero everytime a thermal gradient between two mediums exists whereas latent heat flux is released during a phase transition. As long as a water storage is available or, more generally, above the sea surface, latent heat flux is greater than sensible heat flux because phase transitions (evaporation in case of an air-sea interface) prevail. An experiment on a 2002 Bora occurrence reveals that mean latent heat fluxes were approximatly 70% greater than sensible ones [Pullen et al., 2006]. The ratio between sensible heat flux and latent heat flux is known within turbulent phenomena physics as Bowen ratio.

Surface heat fluxes experience very high values up to hudreds $W \cdot m^{-2}$ during a Bora oubreak exhibiting a pattern that typically superimposes to that of the LLJ. A table, based on 1945-1984 May's dataset, with monthly surface heat flux components of the radiative balance for the whole Adriatic basin is proposed as a reference for a further comparison (Tab. 2.1, quoted and commented in [Artegiani et al., 1997]). It is worth noting that the annual average is negative ($-22\ W \cdot m^{-2}$).
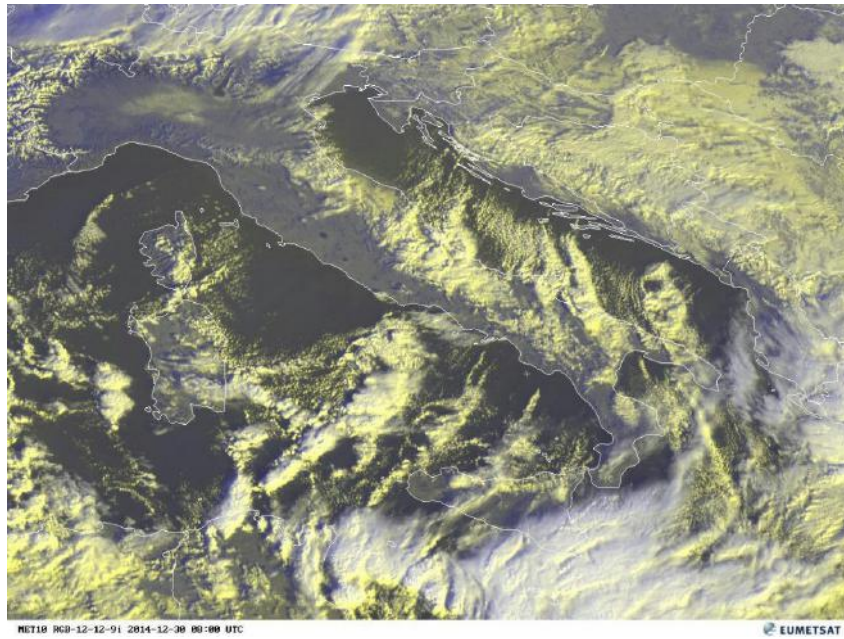
Figure 2.6: Satellite image of cloud bands over the Adriatic Sea during the 31/12/2014 Bora event, suggesting a possible ASE (EUMETSAT).

month	Q_S	Q_B	Q_H	Q_E	Q
Jan	66	-76	-48	-148	-207
Feb	99	-73	-36	-123	-133
Mar	153	-69	-16	-88	-20
Apr	201	-67	-9	-74	52
May	251	-61	-2	-61	128
Jun	283	-59	0	-69	155
Jul	296	-64	-2	-105	124
Aug	254	-66	-6	-117	65
Sep	196	-69	-12	-125	-10
Oct	133	-70	-13	-112	-62
Nov	77	-71	-30	-135	-159
Dec	55	-70	-38	-141	-193

Table 2.1: Monthly surface radiative balance over the Adriatic Sea ($W \cdot m^{-2}$): sensible heat flux (Q_H), latent heat flux (Q_E), incident solar radiation flux (Q_S), backward solar radiation (Q_B) and total heat flux (Q) are reported [Artegiani et al., 1997].

2.4.2 Wind pattern (LLJ)

It has been shown (Sec. 2.3) that the topic of air flow crossing a barrier gets more difficult when the mountain ridge exhibits a pattern of alternated gaps and peaks. In situ measurements and in recent years SAR-derived wind speed retrieval [Kuzmić et al., 2013] confirmed the theoretical prediction of a spatial modulations of wind propagation offshore in terms of topographically controlled LLJ.

All the occurrences of strong-to-severe Bora winds are connected with a jet-like structure above the sea, more pronounced over the NA and CA and sometimes roughly sketched in SA. Those jets appeared as terrain-locked features because they follow the similar pattern of gaps and peaks shaping the Dinaric Alps. Wind speed is higher at the heads of the jets and progressively weakens going farther off the coastline. It has been found that the southern jets experience a greater weakening of the wind speed.

It is worth noting that by contrast wake regions form in between the jets on the wake of higher mountains; the largest one extends westward from the Istrian peninsula and it's clearly visible in the italian along-coast wind speed measurements where a drop is observed over a certain area [Dorman et al., 2006]. Moving to the South the propagation turns out to be more irregular and the interchange between wakes and jets is still detectable although less defined.

A complete classification of LLJ pattern can be controversial since, to some extent, especially for the southern jets, it is rather subjective. It has been said that the northern jets have received more attention and actually the denomination of *Bora* as local wind is mainly referred to the area of Trieste and Senj (see the list) and it is less common moving southward. Nevertheless up to seven corridors have been identified [Askari et al., 2003] whereas a greater number of papers focused on a lower number: four distinct jets have been strictly addressed by Signell [Signell et al., 2010] and several articles can be found regarding the two main jets [Grubišíc, 2004], [Dorman et al., 2006]. On the basis of published articles and simulations performed in the present work the following scheme is suggested:

- *Trieste jet*
  Trieste-affecting jet is due to the channelling effect of air stucked above Karst Plateau and impinging on Postojna Pass (609 m) between Nanos and Snežnik massifs; it propagates offshore in the Gulf of Trieste and finds no obstacles along the way spreading over the plain of Northern Italy. It is known that the Trieste jet is actually divided into two distinct bands due to a thin ridge behind the city [Dorman et al., 2006] but this pattern is hardly reproduced by numerical models, LAMs included; subkilometer resolution would be necessary to resolve fine-scale topography such in this case.

- *Senj jet*
  Two jets originates at the two sides of Velika Kapela massif. The northern gap is in the back of Bakar village and the southern is Vratnik Pass (698 m) located upstream of the town of Senj. The former usually attains larger speeds and most of the time reveals as the most intense Bora jet according to data recorded at Krk bridge weather station; for that reason it has been deeply studied and the present work is no excepetion. Bakar and Senj jets appear to coalesce offshore Cres Island.

- *Karlobag/Pag jet*
  A narrow gap (Ostarijska Pass, 920 m) that breaks the Velebit range is responsible for the last of the northern well-recognizable jets; the main inflow hits the village of Karlobag on the coast and runs over Pag Island (also known as Novalja jet). Sometimes it blows through a second path, undergoing a slight deflection towards the southern Velebit flank and an outbreak in correspondence to Zadar is observed; actually Maslenica bridge that is right outside the city is a well-known measurements site for Bora gusts ([Horvath et al., 2009], [Mihanović, 2013]).

- *Sibenik jet*
  This jet arises from running air along Krka river wide valley that flows into the sea nearby the town of Sibenik.

- *Makarska jet*
  This jet originates from Biokovo-range blocking; the flow can be deflected further north or further south to the city of Makarska.

- *Pelijesac jet*
  It is observed at the mouth of Neretva river.

- *Dubrovnik jet*
  It is weak and sporadic but two features can be responsible for this jet: a narrow sea patch that goes inland and the hill behind the city.

- *Scutari jet*
  Defining the outcoming flow from the large plain around Scutari Lake as the southernmost Bora jet can be controversial since the flow orientation is merely easterly and it often drives no such well-defined air masses. However, in case of anticyclonic Bora and persistent northeasterly flow a heavy outbreak is observed as in two of the case studies considered in the present work. Looking at wind direction at upper levels (typically above 1000m) the properties of flow are the same as for the northern jets.

The exact path of the istantaneous maximum wind speed bands is a consequence of the geographical orientation of the mountain gaps and strongly depends on several factors: the sea forcing in terms of roughness, the air-sea heat fluxes, the Apennines. For example the Trieste jet can turn totally from the North, the jets south to Istria (those of Senj and Bakar) typically follow a clear northeasterly direction while the southern ones blow more from the East.
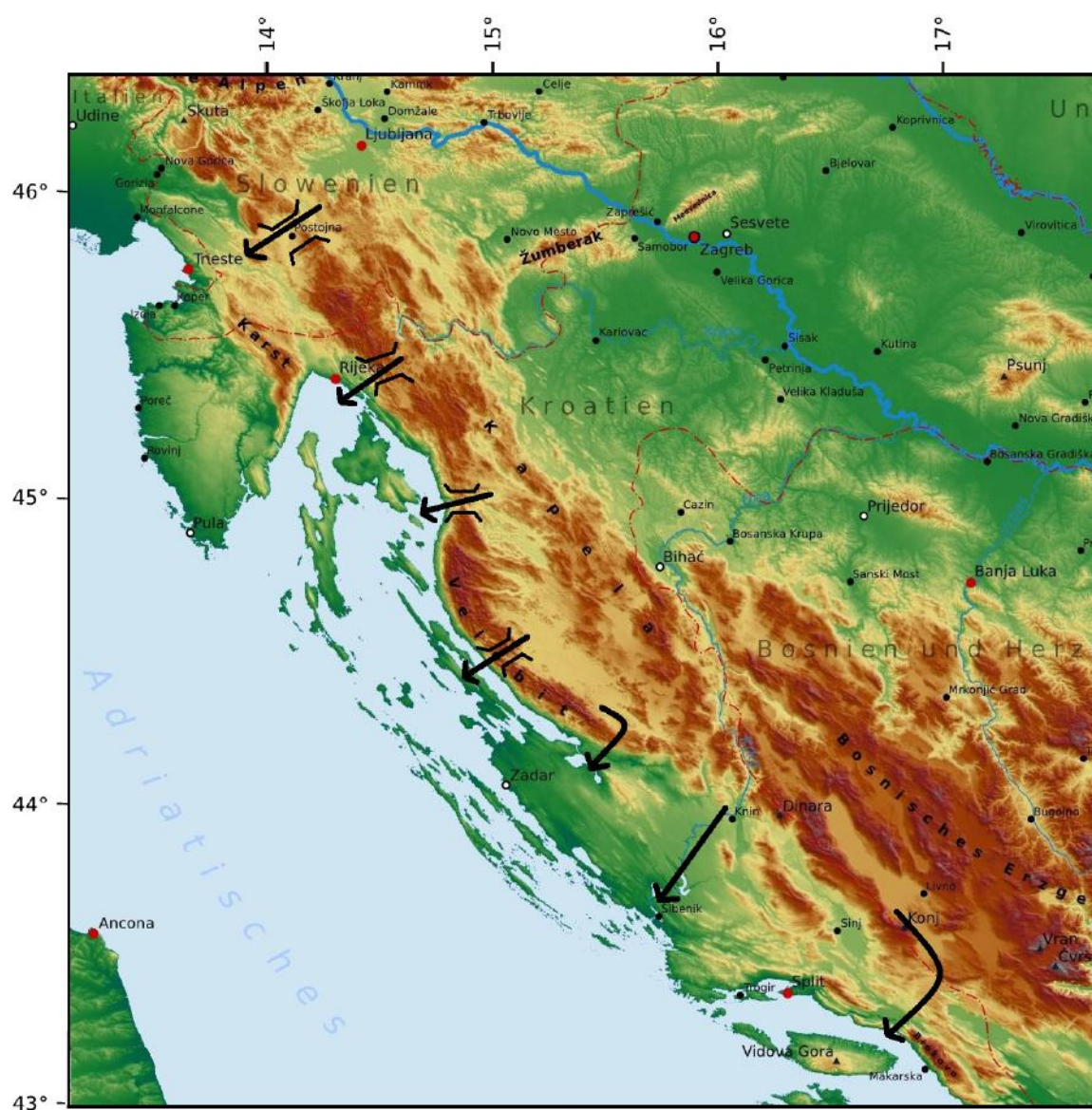
Figure 2.7: Focus on northern Adriatic basin orography: Dinaric Alps gaps and main Bora outbreaks are indicated.

2.4.3   Adriatic Sea circulation

The oceanographic point of view is one of the more interesting because it faces the wide question of how air masses and water masses mutually interact. One of the unsolved issues in meteorology is actually to completely understand the role of the oceans and it is quite a few years that efforts are made to improve the forecast performances by the development of proper two-way coupled numerical models [Ferrarese et al., 2009], [Pullen et al., 2006].

Climatological studies concerning the predictability of the sea-state showed that some typical winter features of Adriatic Sea water circulation are due to the persistence of windy Bora conditions over the area [Supić et al., 2012], [Jeffries and Lee, 2007]. Basically the wind plays an important role in affecting vertical mixing and mass transport because it changes water properties such as density, temperature and salinity due to large heat losses. It has been already pointed out that the pattern of the largest sensible and latent heat fluxes above the sea clearly follows the spatial modulation of LLJ as will be shown graphycally hereinafter (Ch. 4).

It can be stated that the NA sea circulation is wind-driven [Rachev and Purini, 2001]: the counterclockwise gyre in the NA is powered by the Trieste jet and it is regognised as the site of North Adriatic Dense Water (NAdDW) formation; slight southerly the strongest Senj jet drives water masses towards the western slope of the basin triggering the Western Adriatic Current (WAC) and a consequently upwelling of deep water along the eastern side of the basin is observed [Rachev and Purini, 2001]. A weaker clockwise gyre sets up off the coast in the wake of the Istrian Peninsula in between the northern gyre and the southern WAC [Milivoj et al., 2006] (see Fig. 2.8). In opposition to upwelling on eastern boundaries, WAC sinks once reached the western coast and falls down in the Jabuka Pit and SAP that are considered to be the Adriatic Dense Water (AdDW) formation sites where old waters are replaced and finally flow out through the Otranto Channel [Supić et al., 2012]. An incoming flow is needed in the basin to fulfill mass conservation: that is the intrusion of Levantine Intermediate Water (LIW) which guarantees the whole thermoaline circulation scheme of the Mediterranean Sea. It is suggested that Bimodal Oscillating System (BiOS) mechanism controls the exchanges of AdDW and LIW with a decadal scale depending on the changes in the Ionian gyre spin [Gačić et al., 2010]. It has been estimated that a water particle typically takes a couple of months to reach Jabuka Pit and another month to exit across the Otranto channel [Vilibić et al., 2001]. This means that signs of severe long-lasting Bora conditions can be retrieved forward in time by looking at sea properties.

Apart from the Dense Water Formation (DWF) sites identified offshore, several underground rivers of dense water has been recently discovered over the eastern shelf of the basin, thanks to improving NWP resolution and to several mesurements campaigns [Janecović et al., 2014], [Mihanović, 2013] that took place during the 2012 winter which experiences one of the most intense cold period of recent decades.
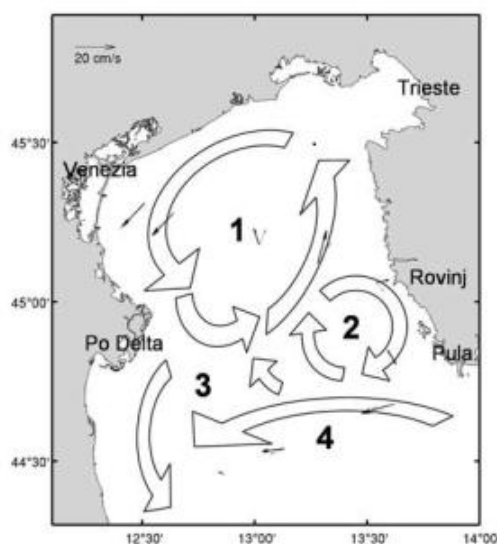
Figure 2.8: Schematic representation of northern Adriatic Sea circulation and main features: (1) NA gyre, (2) Roviny gyre, (3) and (4) WAC [Milivoj et al., 2006].

2.5 The interaction with the orography of the Italian peninsula

As the wind jets approch the Italian coastline they impinge against the foothills of the Apennines whose effects on the upstrem flow can be compared with that of the Dinaric Alps even if the slope of the Apennines is typically lower and the flow impinging on them typically less stable. Relevant wind speeds are recorded at the coastal stations of Dalmatia and on mountain peaks. Looking at sea level the LLJ pattern is clearly recognisable while usually at upper levels the flow becomes more homogenous.

On the other side of the mountains, the one exposed to the Tyrrhenian Sea, a channeling effect is once more observed in the northern part (mainly Tuscany). Although the flow is generally weaker and less defined, wind gusts can reach very high speed value, especially in steep valleys but sometimes also at sea level as occured in the last 2015 Bora outbreak occured in March, when severe damages affected the seaboard (see Fig. 2.9).

The Bora flow interaction with the Italian orography results in the two regimes already described: *flow over* which in this case includes a stronger frontal uphill lifting because of higher mountains and *flow around* associated with low level blocking which can lead to the appearance of South-pointing barrier wind along the mountain ridge.
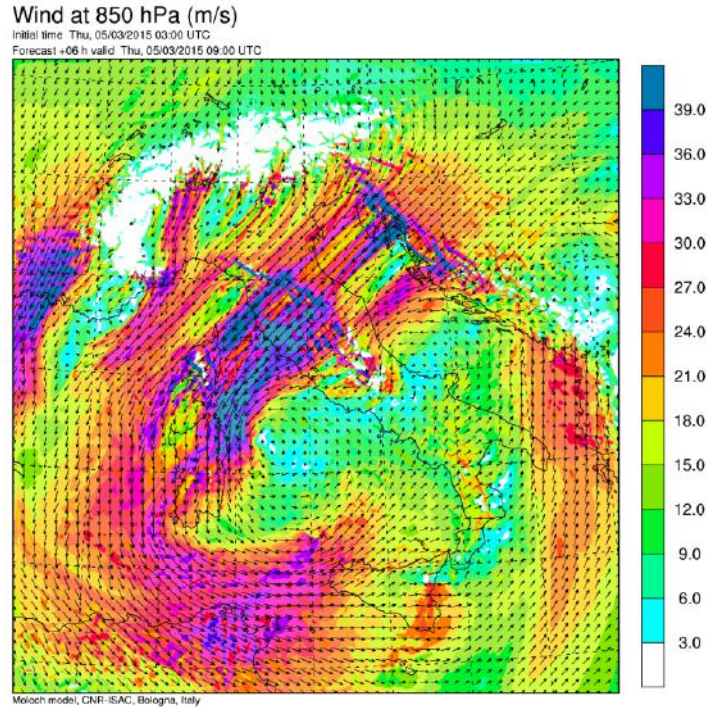
Figure 2.9: Wind speed forecast by MOLOCH at 850 hPa on 05 March 2015 at 09 UTC.

Forced lifting drags the air masses up to LCL causing hydrometeors to precipitate. The simultaneous blocking that slows down the motion at larger-scale favours the persistence of heavy rainfall cells over the same areas. The saturation level is more easily reached if the air mass has been moistened by sea-surface fluxes for a long time thus the importance of the fetch.

Barrier winds originate on the windward side of a mountain as a response to the forcing induced by cold air stagnation, blocking of the upstream flow, wind deceleration and *flow around* regime. It has been shown how a stable and stratified atmosphere tends be blocked by a barrier instead of ascending it, depending on Fr^{-1}.

Flow around tendency can be defined by a dimensional parameter associated with barrier wind formation:

$$L_r = \frac{N h_m}{f} \tag{2.3}$$

where N is Brunt-Väisälä frequency, f is the Coriolis parameter and h_m is the mountain height. L_r is the Rossby radius of deformation. This expression holds for $Ro << 1$. Rossby radius can be qualitatively defined as the upstream distance where the flow starts being affected by topography. The smaller L_r the stronger will be the barrier wind.

The barrier winds affect the Adriatic coast with the starting point typically located south to Monte Conero where the Apennines ridge approches the coast and it is, on

average, higher. They blow northwesterly (and 90° tilted to northeasterly Bora), covering a narrow band aligned with the coast and streched for hundreds kilometers in some cases, with maximum wind speed up to 20 $m \cdot s^{-1}$ centered at an altitude roughly half the height of the mountain crest. SAR technique revealed very useful in describing fine-scale features of the barrier wind. For examples several works point out the existence of a very narrow band (1-2 km wide) of stronger winds within the broader band [Signell et al., 2010], [Alpers et al., 2009].

A daily signature in the barrier wind affecting the western Adriatic coast has been noticed in specific Bora cases. The barrier wind strength seems to depend on daily insolation cycle being stronger early in the morning and weakening during daytime; [Pullen et al., 2007], [Askari et al., 2003] in the same way as breeze regime is influenced by differntial cooling over land relative to the sea. This suggests that an interaction between the barrier wind and the breeze winds occurs and must be taken into account.

Chapter 3

The Numerical models

In the present work outputs of three different NWP models are used for running short range simulations of the atmospheric evolution. The models are not used separately but nested one inside the other with incrasing resolution and decreasing integration domain, a well-known process in numerical modelling whose details will be explained hereinafter.

Each model needs initial and boundary conditions (e.g. grided values of several variables at earlier state) to inizialize a system of Partial Differential Equation (PDE) describing the physical processes and dynamical state of the atmosphere. An analytic solution, continuous in space, for this system is not possible so variables are typically represented on a discrete 3d-grid. The parametrizations introduced in the equation system, the ability to reproduce complex physical processes such as those connected with the water cycle, the maximum achievable resolution and the computational cost characterize a model and its usefulness. A Global Model (GM) is a suitable model for the prediction of planetary scale motions and for long-range forecasts, while a Limited Area Model (LAM) is eligible for synoptic and mesoscale phenomena and for a shorter-term outlook.

It is decided in this case to make use of Integrated Forecast System (IFS) of the European Centre for Medium-range Weather Forecast (ECMWF) as GM and, starting from this, to run the two LAMs developed at Istituto di Scienze dell'Atmosfera e del Clima (ISAC)-Consiglio Nazionale delle Ricerche (CNR) namely BOLAM and MOLOCH. They represent a unique example of a totally italian-developed product for NWP task.

This chapter goes through the main features and parametrizations implemented for each one (Sec. 3.1 and 3.2) and a clear scheme of the specific set-up used for running the simulations is presented in Sec. 3.3. A brief explanation of the strictly software procedure that has been followed can be lastly found in Sec. 3.4.

3.1 The BOLAM model

BOLAM stands for BOlogna Limited Area Model and has been developed by the Dynamic Meteorology research group at ISAC-CNR since early nineties [Buzzi et al., 1994], [Malguzzi and Tartagione, 1999], [Buzzi and Foschini, 2000]. The model performances tests were carried out worldwide over the years during Comparison of Mesoscale Prediction and Mesoscale Experiment (COMPARE) I and II projects by WMO, during EU RAPHAEL project and more recently during MAP campaign [Richard et al., 2003], [Buzzi et al., 2003], [Richard et al., 2007]. It was compared with other analogous mesoscale models and many times it permormed the best, especially in forecasting cyclogenesis and precipitation fields over Europe.

Nowdays BOLAM is part of the set of available models for research and operational tasks at ISAC-CNR. It was profitably used for research purposes regarding heavy precipitation episodes and lee cyclogenesis [Buzzi and Foschini, 2000], [Davolio et al., 2009b], [Orlandi et al., 2010] as well as for marine forecasting [Cavaleri et al., 2010], [Ferrarin et al., 2013] and idealized studies, using a channel version of the model grid. More recently, a stand-alone chemical and aerosol transport model has been developed at ISAC, starting from the BOLAM dynamical core.

Daily BOLAM outputs are currently used by several regional meteorological services (ARPA Liguria among the others) and by national agencies (e.g. ISPRA) for their regular activity of weather forecasting. A permanent collaboration exists with National Civil Protection Department which also supports the whole project. The model has been successfully exported abroad to Greece, where it is used by the National Observatory of Athens, to Vietnam and Ethiopia.

3.1.1 BOLAM features

BOLAM is a hydrostatic LAM providing real-time weather forecasts with a parametrization scheme for atmospheric convection. In a hydrostatic model the vertical equation of motion is diagnostic, given by the hydrostatic approximation thus neglecting friction and Coriolis terms that would be some orders of magnitude lower. The approximation holds as long as synoptic scale are considered so there is a threshold of usefulness for hydrostratic models, typically around 10 km. Moreover since vertical motion is inhibited, sound waves are filtered and a wider integration time step can be used. This is another reason why hydrostatic models have a low computational cost.

The prognostic variables of the model are wind components u and v, absolute temperature T, surface pressure p, specific umidity q and Turbulence Kinetic Energy TKE plus five water species for stratiform precipitation processes namely cloud ice (q_{ci}), cloud water (q_{cw}), precipitable water (q_{pw}), snow (q_{ip1}) and graupel (q_{ip2}).

Variables values are assigned to each node of a 3d-grid. On the horizontal plane a

staggered regular lat-lon Arakawa-C grid [Arakawa and Lamb, 1977] is used. The user can optionally chose a rotated grid defining a proper centre of rotation. In such a way it is like a virtual equator passes over it thus reducing considerably the error otherwise introduced by the convergence of meridians towards the Pole. On the vertical plane values are distributed on a non-regular Lorentz grid with vertical levels non-uniformly staggered: basically the vertical coordinate σ is an hybrid one, terraing following at lower levels and gradually relaxing going further on the top where it tends to a pure pressure coordinate, on horizontal planes (Fig. 3.1).
The definition of σ is pressure-based as follows

$$P = P_0\sigma - (P_0 - P_s)\sigma^\alpha \tag{3.1}$$

where P_0 is a reference value, typically 1000 hPa, P_s is the surface pressure and α is the relaxing factor in turn defined as

$$\alpha \leq \frac{P_0}{P_0 - minP_s}. \tag{3.2}$$

α parameter depends on orography via $minP_s$ value and sets the rapidity of the transition from σ-surfaces to pure p-surfaces. Typical values exceed 2 but lower ones are required in case of high mountains embedded in the integration domain.

Boundary conditions are not roughly applied on the grid points at the edges but values gradually relax within a frame of points (typically 8) via a linear formula [Lehmann, 1993] to be applied for each time step. Relaxing parameters are defined through a minimization process for the maximum reflection coefficient in a well-defined range of Courant number. This is done to avoid reflection of outgoing waves at the border where fields from different models (in a cascade run) can be unbalanced. Moreover the coefficients are grid-dependent thus the adjustment to grid resolution is automatic.
Weighted Average Flux (WAF) scheme [Billet and Toro, 1997] is implemented to reproduce 3d-advection at second order of accuracy in time and space. A second order diffusion scheme is also used, except for surface pressure.

The fundamental primitive equations system (to be integrated in time) that governs the evolution of large-scale atmospheric motions is defined in several textbooks with a general notation (Holton, Wallace and Hobbs). The system is composed by (the following equations are already arranged in the form they are implemented in BOLAM):

- 3 equations of motion, namely the three components of Navier-Stokes equations that state the momentum conservation principle. They are implemented in BOLAM in a non-cartesian system with the triad (λ, ϕ, z) as coordinates. λ stands for longitude,
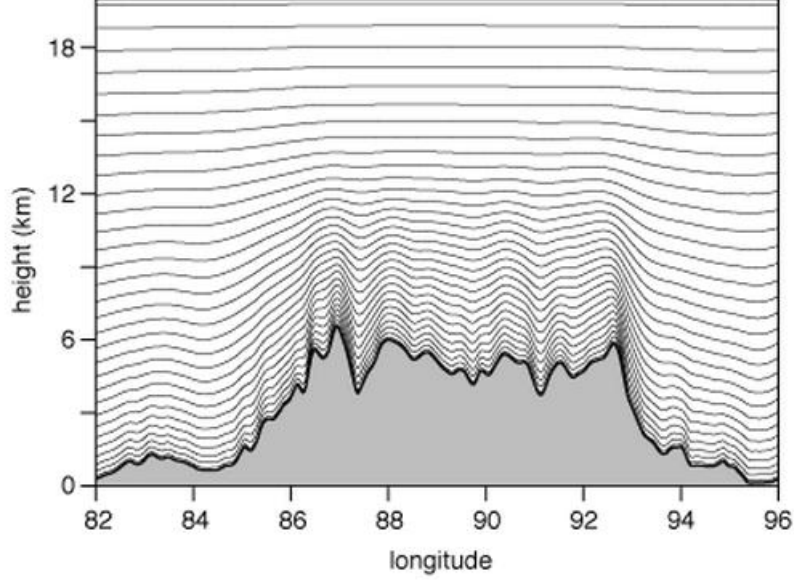
Figure 3.1: Exemple of a terrain following vertical coordinate; mountains profile is that of Himalayas.

ϕ stands for latitude and z is the altitudine with respect to the sea level.

$$\frac{\partial u}{\partial t} = \frac{uvtan\phi}{a} - \frac{u}{acos\phi}\frac{\partial u}{\partial \lambda} - \frac{v}{a}\frac{\partial u}{\partial \phi} - \dot{\sigma}\frac{\partial u}{\partial \sigma} + fv - \frac{R_dT_v\sigma^\alpha}{acos\phi P}\frac{\partial P_s}{\partial \lambda} - \frac{1}{acos\phi}\frac{\partial \Phi}{\partial \lambda} + K_u \quad (3.3)$$

$$\frac{\partial v}{\partial t} = -\frac{u^2tan\phi}{a} - \frac{u}{acos\phi}\frac{\partial v}{\partial \lambda} - \frac{v}{a}\frac{\partial v}{\partial \phi} - \dot{\sigma}\frac{\partial v}{\partial \sigma} + fv - \frac{R_dT_v\sigma^\alpha}{acos\phi P}\frac{\partial P_s}{\partial \phi} - \frac{1}{acos\phi}\frac{\partial \Phi}{\partial \phi} + K_v \quad (3.4)$$

$$\frac{\partial \Phi}{\partial \sigma} = -R_dT_v\frac{P_0 - \alpha(P_0 - P_s)\sigma^{\alpha-1}}{P} \quad (3.5)$$

Further notation is needed: f is the Coriolis parameter ($f = 2\Omega sin\phi$ where Ω is the Earth angular velocity), g is the gravity acceleration, σ, α, P_0 and P_s were mentioned above, Φ is the geopotential and the K terms account for the contributions of the parameterization of vertical turbulent processes. R_d is the gas constant for dry air and T_v the virtual temperature as defined in Eq. 3.10.

- Continuity equation which states the mass conservation principle:

$$0 = \frac{\partial}{\partial t}\left(\frac{\partial P}{\partial \sigma}\right) + \frac{\partial}{\partial x}\left(u\frac{\partial P}{\partial \sigma}\right) + \frac{\partial}{\partial y}\left(v\frac{\partial P}{\partial \sigma}\right) + \frac{\partial}{\partial \sigma}\left(\dot{\sigma}\frac{\partial P}{\partial \sigma}\right) \quad (3.6)$$

- Energy conservation equation that is expressed by the first thermodynamic principle:

$$\frac{\partial T_v}{\partial t} = -\frac{u}{a cos\phi}\frac{\partial T_v}{\partial \lambda} - \frac{v}{a}\frac{\partial T_v}{\partial \phi} - \dot{\sigma}\frac{\partial T_v}{\partial \sigma} - \frac{R_d T_v}{c_p P}\frac{DP}{Dt} + K_T + F_T \qquad (3.7)$$

K_q accounts for vertical turbulent parametrization and F_q is related to contributions arising from non-adiabatic processes such as cooling, heating or phase transitions.

- Prognostic equation for specific umidity q

$$\frac{\partial q}{\partial t} = -\frac{u}{a cos\phi}\frac{\partial T_v}{\partial \lambda} - \frac{v}{a}\frac{\partial q}{\partial \sigma} - \dot{\sigma}\frac{\partial q}{\partial \sigma} + K_q + F_q \qquad (3.8)$$

K_T and F_T are defined as to Eq. 3.7.

- Finally, it is supposed that ideal gas state equation holds. The form with explicit reference to virtual temperature is (ρ is air density)

$$P = \rho R_d T_v \qquad (3.9)$$

where

$$T_v = T\left[1 + \left(\frac{1}{\epsilon} - 1\right)q - q_{cw} - q_{ci} - q_{pw} - q_{ip1} - q_{ip2}\right]. \qquad (3.10)$$

ϵ is the ratio of R_d to R_v (gas constant for moist air) while q-terms account for specific umidity of water species.

This equations system is the full core of the physics to be described although lot of simplifications are used: first of all hydrostatic approximation holds thus vertical acceleration is negligible and the third equation of motion is reduced to the hydrostatic equation (Eq. 3.5) then scale analysis leads to neglect viscosity, curvature terms and Coriolis effects in Eq. 3.3 and Eq. 3.4. Adiabatic approximation states that on top levels there is no heat flux because the parcel undergoes adiabatic motion. Meanwhile a general parametrization of bottom fluxes is also used (Sec. 3.1.2).

3.1.2   BOLAM parametrizations

Parametrizations define the so called *physics* of the model. It includes all those phenonema that necessarily happen on typical spatial scale smaller than model resolution and the way they are resolved. Approximated methods become crucial in this cases because it would be impossible to resolve the equation system for distances smaller than grid-spacing.

Parametrization of PBL is defined belonging to the theory of similarity [Monin and Obukhov, 1954] whereas a turbulence closure model is used, on the basis of the mixing lenght proposed by Blackadar [Blackadar, 1962] for buoyancy properties and for turbulent vertical diffusion of momentum, heat and moisture in a stratified Atmospheric Boundary Layer (ABL). In cases of unstable boundary layers a modified value is applied [Bougeault and Lacarrère, 1989]. Turbulence Kinetic Energy (TKE) is evaluated within a turbulence scheme whose closure is of order 1.5 (E-l scheme, [Zampieri et al., 2005]). The roughness length is computed as a function of vegetation and of sub-grid orography variance on dry land while Charnock roughness [Charnock, 1955], that evaluates the wave height as a function of the surface wind speed, is introduced over the sea.

The SST is computed taking into account all the terms that contribute to the energy balance at the surface (latent and sensible heat fluxes, radiative Short Wave (SW) and Long Wave (LW) fluxes) using a simple slab ocean model and a relaxation parameter to a reference value for deep layers.

Radiation fluxes derived from the superposition of two different schemes: the RG scheme [Ritter and Geleyn, 1992] and that used at ECMWF [Morcrette, 1991] with updating [Mlawer et al., 1997], [Morcrette et al., 2008]. Due to the higher computational cost of the latter, while RG scheme is continuously updated at each grid point and at each time step, ECMWF scheme is less frequently updated and only on alternated points. ECMWF scheme is therefore more detailed: for exemples its libraries include astronomical functions, the definition of atmospheric composition climatology and the mean seasonal and geographical distributions of different types of aerosol. A 2012 upgrade of the scheme introduced the Rapid Radiative Transfer Model (RRTM) algorithm for spectral bands and the Monte-Carlo Independent Column Approximation (McICA) for computing the radiative effects of clouds [Barker et al., 2008]. A recent model update made possible to use consistently inputs from both schemes.

A parametrized model for Earth surface is used: it includes a soil model based on 4-6 layers with increasing depht moving downward, a land-sea mask (that is a water fraction index) and a model for orography, a database of vegetation coverage and soil types and routines for all the processes that take place at the surface as well as underground. This model is continually updated to take into account more and more specific sub-processes

such as surface energy, momentum, water and snow balances, heat and water vertical transfer, vegetation effects (evapo-transpiration, interception of precipitation, wilting and canopy effects) and the whole water cycle (melting and freezing of groundwaters, extraction of water by roots, runoff).

A smoothing of orography at the border is required when BOLAM is applied in cascade to better fit with the orography of the other models. Orographic wave drag and related deceleration of the mean flow passing over obstacles, are parametrized too.

Microphysical parametrization scheme has been updated [Drofa and Malguzzi, 2004] from the original one with noticeable improvements. The new scheme is based on explicit assumptions of spectral distributions of clouds (both droplets and ice crystals) and of liquid and solid hydrometeors assuming a generalized *gamma function* distribution. It serves mainly stratiform precipitation processes since convective ones are parametrized. The main processes attached to the microphysical scheme are:

- nucleation of cloud water and cloud ice;

- condensation and evaporation of cloud water;

- freezing of cloud water ;

- nucleation, sublimation and melting of cloud ice;

- auto-conversion of cloud water and cloud ice;

- sublimation of snow and graupel in both directions;

- a set of 13 specific hydrometheor interaction processes (involving rain, hail, snow, graupel, cloud water, cloud ice);

- melting and evaporation of hydrometheors;

- specific routine for terminal fall speed computation and fall processes (a conservative-diffusive backward-upstream integration scheme is used);

- thermodynamic feedback mechanism entalpy conservation based.

Convective precipitations are parametrized by means of the Kain–Fritsch scheme [Kain and Fritsch, 1990] with following updates [Kain, 2004]; it has been further adjusted regarding downdraft processes and shallow moist convection. The main mechanism of this parametrization is based on stability: essentially when a coloumn of air is unstable condensation and precipitation are forced until they consume all the Convective Potential Available Energy (CAPE) giving back a stable or neutral profile.

3.2 The MOLOCH model

First works about MOLOCH go back to more than ten years ago [Tettamanti and Zardi, 2002] when BOLAM was effectively widely used and the demand for a new LAM became a crucial task. It is a Convection Resolving Model (CRM), non-hydrostatic, which treats the atmosphere as a totally compressible fluid. It provides Quantitative Precipitation Forecast (QPF) with better spatial resolution, up to 1 km and 100 vertical levels nowdays and with an explicit resolution scheme for convective phenomena, without parametrizations. Thus MOLOCH has actively contributed to research branches regarding HPE, flooding and, more generally, environmental hazard conditions [Davolio et al., 2007], [Davolio et al., 2009a] having been a key-instrument for Weather Risk Reduction for the Mediterannean (RISKMED) and MAP D-PHASE projects [Bartzokas et al., 2010], [Rotach et al., 2009] and for the HyMeX field campaign Special Observation Period (SOP) [Ducrocq, 2014], [Ferretti, 2014]. Furthermore a collaboration with Istituto di Scienze MARine (ISMAR) is active for sea state forecast (KASSANDRA project) [Ferrarin et al., 2013]. The MOLOCH model is mostly used together with BOLAM in the same agencies mentioned in the previous section.

3.2.1 MOLOCH features and parametrizations

Some basic features are similar to BOLAM ones with just few adjustments. For example the horizontal grid is still of Arakawa-C type [Arakawa and Lamb, 1977] while the hybrid vertical coordinate ζ is now height-depending. If h is orography-height and H a scale value for tropospheric heigh the definition of the vertical coordinate turns out to be

$$\zeta = H \left(1 - e^{-\frac{z - h(1 - \frac{\zeta}{H})}{H}} \right).$$ (3.11)

The model runs with an implicit scheme for sound waves vertical propagation and an explicit, timpe-split scheme for the time integration of the other terms of the equations of motion. All the other schemes making up the physics of the model descend directly from BOLAM: radiation, sub-grid turbulence and interactions between the soil model and the atmosphere are faced in the same way. Horizontal second order diffusion scheme and a small divergence damping are still included to prevent energy accumulation on the shorter space scales.

As regards the mycrophysical parametrization an improved scheme is used. The basis is the one of [Drofa and Malguzzi, 2004] with the addition of specific routines to resolve the so-called two-moment microphysics, by integrating in time the spatial distribution of the number density of cw and ci thus describing the cloud spectra evolution.

On the other hand, the convection is no more parametrized. Vertical motion which becomes predominant in extreme rainfall at smaller scales is explicitly computed in the equation since hydrostatic approximation no longer holds.

3.3 BOLAM and MOLOCH set up for simulations

The NWP models can be customised depending on specific purposes. The BOLAM and MOLOCH models allow to choose the area over which equations are integrated, its borders and its horizontal and vertical grid-step, the external data sources such as for SST and allow to custom the time issue: the nesting time shift, the diagnostic and output time step and, obviously, the forecast range.

The choice of integration domains is due mainly for practical needings: generally the covered area should be large enough to describe the whole evolution of the event but at the same time it should be small enough to permit the resolution of the equations on a typical LAM grid-step. Considering that resolution and computational requirements grow together, a compromise has to be achieved. A single precaution has to be considered that is to avoid that the domain border passes across mountains that can be a source of numerical errors especially due to the smoothing of the orography mask.

The chosen BOLAM domain (Fig. 3.2) extends longitudinally from the Atlantic Ocean to the eastern boundaries of the Mediterranean Sea and latitudinally from Scotland to North Africa since the typical synoptic conditions over Europe are often driven by the Westerlies and by the conflict between cold and dry air moving from Russia and Arctic latitudes and warm and moist air moving from the South. The Mediterranean Sea also plays an important role in triggering the convection.
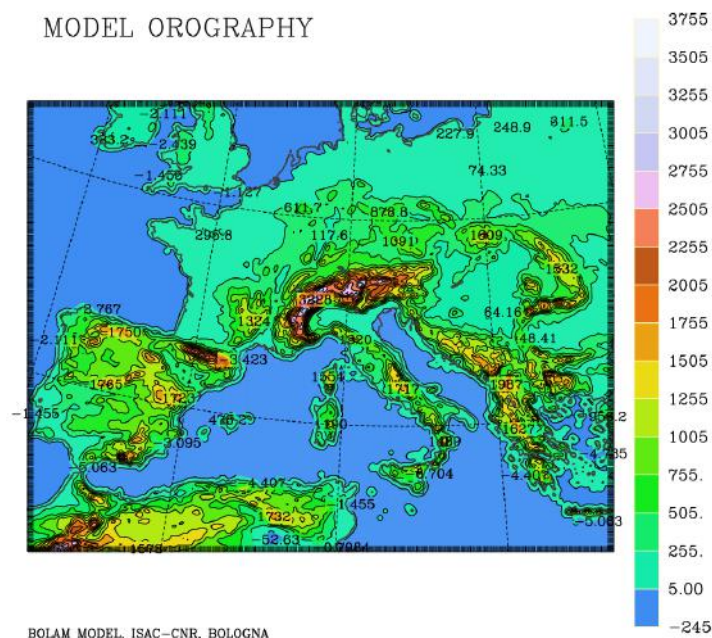
Figure 3.2: BOLAM integration domain.

The MOLOCH domain is centered over Italy (Fig. 3.3), slightly East-shifted to better include the Dinaric Alps. Even if Bora winds affected mainly the northern part of the Adriatic basin the domain includes the southern too, up to the Otranto Channel and the Tyrrhenian Sea where it is known that the circulation connected with LP in cyclonic episodes is able to deeply affect the Bora flow.
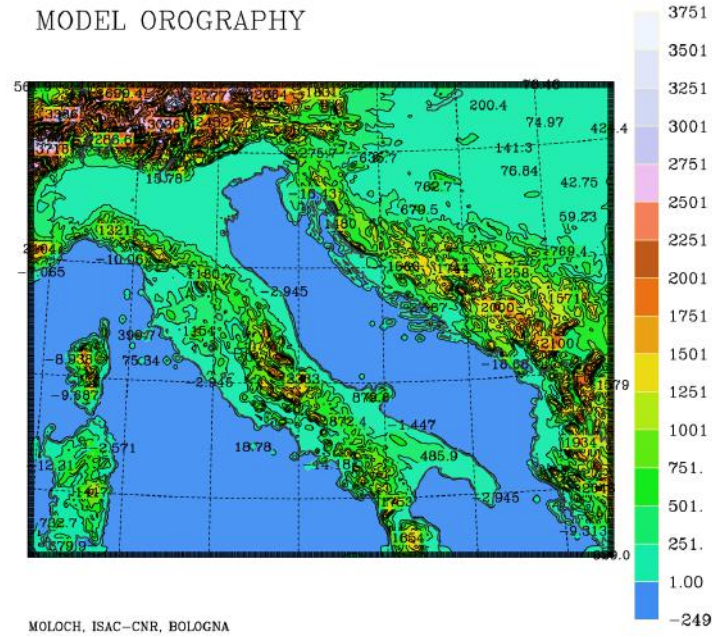
Figure 3.3: MOLOCH integration domain.

BOLAM horizontal resolution is set to 0.075° that corresponds to a grid-step of 8.3 km while MOLOCH to 0.02° (2.2 km). The time resolution attains to Courant-Friedrichs-Lewy (CFL) criterion so it is different as well. The forecast range is smaller for MOLOCH than for BOLAM (45h instead of 48h) because a 3h-shift in the initial time is applied during the nesting process (Sec. 3.4).

The SST field for the MOLOCH model can be derived from MyOcean, an oceanographic project supported by several institutes (ISMAR-CNR among them) for the Mediterranean and Black Sea joined with OSTIA project by United Kingdom Meteorological Office (UKMO) which covers the global ocean or from IFS-ECMWF. For the simulation performed in the present work the latter source has been used.

The number of vertical levels are the same in both models, both over and under the ground, as well as the centre of rotation that has been fixed in the middle of the area of main interest that is in the open water of the Northern Adriatic Sea. The prognostic variables are evaluated hourly but the output step is set to be 6h for BOLAM and 3h or 1h for MOLOCH depending on necessity.

The ECMWF radiation scheme is updated with a 3h-step. For a full overview on the parameter choosen for the simulations see Tab. 3.1 while a first list of the control runs performed is discloled in Tab. 3.2.

parameter	BOLAM value	MOLOCH value
spatial domain	54° N −8° W 26° E 34° S	48° N 8° W 21° E 40° S
centre for rotated coordinates	LAT 44° N LON 14° E	LAT 44° N LON 14° E
grid points	382x294	510x414
spatial resolution (km)	8.3	2.2
vertical levels	50	50
ground levels	7	7
forecast time (h)	+48	+45
time resolution (s)	90	30
diagnostic step	1	1
output step	6	3/1
clustering	2x2	2x2
α value	0.06	0.06

Table 3.1: List of main custom parameters for BOLAM and MOLOCH simulations.

event	model	initial time	fcst time (h)	res (km)	initial conditions
Feb 2012	BOLAM	09/02/2012 12:00	+48h	0.075	ECMWF-analysis
	MOLOCH	09/02/2012 15:00	+45h	0.02	BOLAM-forecast
Sept 2012	BOLAM	13/09/2012 00:00	+48h	0.075	ECMWF-analysis
	MOLOCH	13/09/2012 03:00	+45h	0.02	BOLAM-forecast
Nov 2013	BOLAM	11/11/2013 00:00	+48h	0.075	ECMWF-analysis
	MOLOCH	11/11/2013 03:00	+45h	0.02	BOLAM-forecast
Dec 2010	BOLAM	15/12/2010 00:00	+48h	0.075	ECMWF-analysis
	MOLOCH	15/12/2010 03:00	+45h	0.02	BOLAM-forecast
Dic 2014	BOLAM	30/12/2014 00:00	+48h	0.075	ECMWF-analysis
	MOLOCH	30/12/2014 03:00	+45h	0.02	BOLAM-forecast

Table 3.2: Main features of the control runs performed.

3.4   Execution and nesting

High resolution weather forecasts are obtained by means of a models cascade in which each step concurs to increase the reliability of the forecast over a smaller and smaller area. The reason which makes this process (*nesting*) essential is twofold: from the operational point of view it would be a rough mistake to perform mesoscale phenomena forecasts without taking into account the larger scale circulation but, even if this issue is considered, a remarkable inaccuracy would be introduced by a simple transition from a GM dataset output to the most accurate LAM. It is still a matter of interpolation since the physical consistency of a LAM whose initial conditions have been obtained by a coarse interpolation (typical GM grid steps are of the order of tens of km while LAM best performance can be less then a km) is arguable. An intermediate step, namely a medium-resolution LAM, is the best way to overcome the problem.

Furthermore a time interval, 3 or 6 hours long, between the nested model starting time and the parent model is introduced so that the initial and boundary conditions of the nested model come from a true forecast. On the contrary, it should be faced the same problem of interpolation discussed above and nesting would be useless.
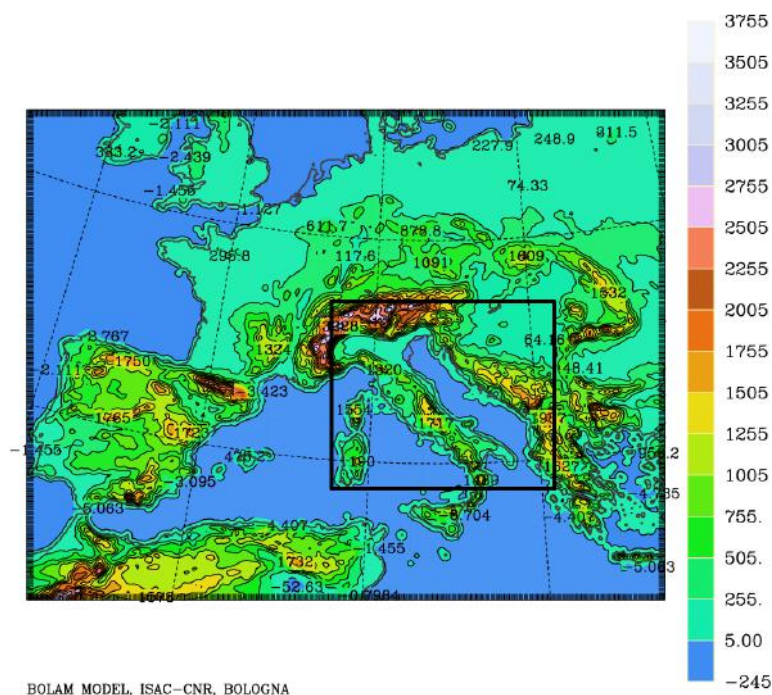
Figure 3.4: MOLOCH integration domain nested in the BOLAM one.

Therefore, the models are arranged to run in cascade in the present work : BOLAM is nested into ECMWF analysis and MOLOCH into BOLAM (Fig. 3.4). ECMWF analysis are scheduled every 6h so that a continuous adjustment to real data (properly assimilated) is done. Analysis instead of forecasts (both provided by ECMWF GM) are used mainly because the aim is not to perform simulations to account for an operational demand but to produce the best control run achievable. Actually both of them have been addressed to initialise the two 2012 cases runs but only the analysis-driven ones are shown. For the other cases the ECMWF analysis have been always considered.

The execution of the simulations is carried out by executable FORTRAN-based codes following a strict procedure. A single run, both BOLAM and MOLOCH, can be divided into three different steps: preprocessing, processing and postprocessing.

3.4.1   Preprocessing

The preprocessing phase realizes what has been called nesting. It deals with an interpolation of data from the grid of the parent model to the finer grid of the nested model. This process is carried out at each time-step the parent model has been set to produce the output from which a new input file is created. It contains the initial and boundary conditions for the nested model. A further interpolation has to be done in case of rotated grid in order to redefine meteorological fields and wind vectors.

Global ECMWF data are written in *grib* or *grib2* binary format. Preprocessing creates a list of binary input files, one for each hour, progressively named *inputNN.mhf* (NN stands for the forecast instant) that includes the initial and boundary conditions to be conveyed to the nested BOLAM. Conceptually, the same procedure is carried out between BOLAM and MOLOCH with the semplification that there is no format conversion to be accounted for.

Both spatial and temporal model parameters, most of them listed in the previous section, have to be defined in a *.inp* file that will be part of the process. The executable code is written in FORTRAN90 language and includes a call to the *.inp* file and to other database files containing fundamental informations about soil type, vegetation coverage and orography. It is necessary to custom this input files to carry out sensitivity tests (Ch. 4). Preprocessing runs with a single processor.

3.4.2 Clustering

The execution of the model is clearly the most computational demanding step. The available computational power is not always adequate for the spatial resolution to be achieved. A well-known device to optimise the computational issue is that of parallel computing connected with domain splitting technique.

In this technique the physical domain is properly divided in sub-areas depending on the number of processors of the computer cluster. Each sub-area must be assigned a process to be run on core processors (or on virtual processes of the same processor). To resolve derivatives in proximity of the borders of each subdomain a frame of external points is added, thus realizing a superposition with other subdomains or with the parent larger integration domain. The whole BOLAM and MOLOCH codes are fully parallelized and compatible with MPICH2 and OpenMP parallel computing environments.

In the present work a 2x2 clusterization is used with 2 processors for x and y direction respectively so that 4 subareas are provided (Fig. 3.5). A discretization is done over the whole domain (a GNLONxGNLAT matrice is produced) while NLON and NLAT are the dimensions of the matrices defining the subdomains including the frame at the border. Their values can't be arbitrary but have to fulfill the constraint

$$NLON = \frac{GNLON - 2}{NPROCSX} - 2 \qquad NLAT = \frac{GNLAT - 2}{NPROCSY} - 2 \qquad (3.12)$$

where NPROCSX and NPROCSY are the number of processor for each direction. This means that GNLON and GNLAT have to be choosen in order to get integer values for NLON and NLAT.
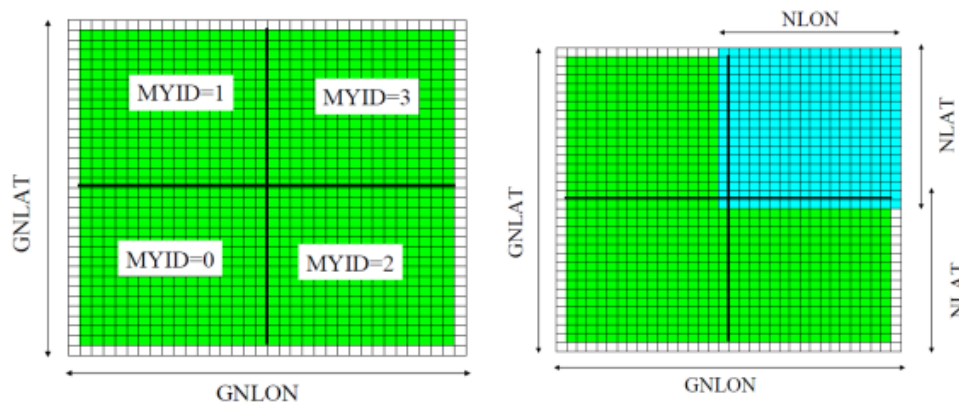
Figure 3.5: Domain splitting technique: enhanced areas belong to forecast integration domain (green) and to the border frames (white).

3.4.3 Postprocessing and graphic Outputs

The postprocessing phase serves the purpose of creating a *.ppf* file in ASCII format which is readable by the National Center for Atmospheric Research (NCAR) Graphics software in order to create the final output maps.

An executable FORTRAN code has to be launched and it expects to be given instructions by a *postprocessing.inp* file where it is possible to choose the fields to be converted and the related model vertical levels, selecting the standard isobaric ones. Another important choice is that of the frequency of the output step, typically 3h for a LAM, but often a 1h-step is used.

Finally, some shorter scripts, one for each specific map type (cumulative variables, analysis and evolution maps, cross-sections) produce graphic files ready to be plotted.

(manca schema)

Chapter 4

Case studies

This chapter goes through the five case studies considered: they are presented from Sec. 4.3 to Sec. 4.7 by analysing the synoptic maps and the mesoscale phenomena occurred. For three of them an evaluation of the quality of the numerical simulations through a comparison with observed data is presented. In Sec. 4.1 the selection criteria followed to chose the case studies are explained while Sec. 4.2 provides general informations to better understand the analysis and the tests performed for each case.

4.1   Selection of case studies

A full-scale climatology of Adriatic wind regimes has been firstly carried out decades ago [Makjanić, 1978] with more recent assesments [Prtenjak and Grisogono, 2007, Pasarić et al., 2009] (more details are given in Sec. 2.2); nevertheless it would have been helpful for the aim of this work to consult an almanac or an updated meteorological year-book where Bora events details are recorded but a full peer-reviewed published work of this type is still lacking.

On the other hand, the ISAC Dynamic Meteorology research group resources, namely the full-archive of BOLAM and MOLOCH simulations outputs as well as the GFS analysis, allow to identify past meteorological events, Bora occurrences included.

It has been decided to proceed picking out, among the large number of occurences of Bora winds in the recent past, those events that match specific requirements stated beforehand that are:

- long-lasting events, characterized by at least 3 days of easterly flow

- events that stand out for severity or damaging effects

- events that led to high precipitation rates and high total rainfall over the Adriatic area and in particular the eastern slopes of the Apennines

- both synoptic set-up with and without a Mediterranean low pressure system settled over Central Italy (referred as to cyclonic and anticyclonic pattern, respectively)

The previous keypoints lead to the exclusion of some significant Bora events that deserve anyway to be mentioned such as the one occured on March, 1, 2011 characterized by the record wind-speed of $171 km \cdot h^{-1}$ at Trieste Nautical Institute or the one occured on March, 10, 2010.

The final choice is on the following cases:

- 2012, February, 9-11

- 2012, September, 13-15

- 2013, November, 11-13

- 2010, December, 15-17

- 2014, December, 30-31

The February, September and November events are characterized by a cyclonic pattern while the December ones by anticyclonic Bora. It is worth noting that the September event is a case study (Intesive Observation Period (IOP)4) of HyMeX SOP1 campaign [Ferretti, 2014] while the February event is of great interest within RITMARE project and other studies are currently carried on at ISAC on the same episode [Davolio et al., 2015]. It is noticeable that they all belong to autumn-wintertime, the most favorable period for Bora onset, when typical temperature differences at sea-air interface are known to be higher, as well as heat fluxes, and main Bora features are observed to be reinforced.

4.2   Overview of the case studies

For the analysis of the case studies the same procedure is followed for each episode. At first it is provided an overview of the meteorological pattern prior to the period of main interest. Then the distinctive features of the event are described and a verification of the main simulated fields is presented. The validation is carried out by comparing model forecast fields with both in-situ measurements and remote-sensing data are considered. Wind profilers, satellite images, radar reflectivity maps have been examined too for a complete survey of the dynamics of the events.

Actually a detailed comparison with real data is presented only for the two 2012 events that are included in larger-scale effort projects and for which the availability of data is higher (and for November 2013 event too). We are dealing with severe events, that have been long monitored by weather regional agencies whose technical reports are helpful in providing and collecting a large number of recorded data.

After the validation, sensistivity tests are devised in order to analyse in detail the role of two meteorological parameters, SST and surface heat fluxes. In order to attain this aim a different set of simulations is performed for each Bora case (Tab. 4.1): the cyclonic episodes (February 2012, September 2012, November 2013) are more carefully inspected since they were characterized by much larger amount of precipitation and among them more attention is paid to the February case for which a dedicated dissertation is presented in Ch. 6 in addition to the results described in this section. For the cyclonic cases a $\pm 2°C$ change in SST is introduced over an area that covers the whole Adriatic basin (Fig. 4.1) while heat fluxes are removed separately in the southern part (latent and sensible heat fluxes together) and in the northern part (both together and one-by-one individually).

The distinction between northern and southern Adriatic (Fig. 4.2) is proposed on the basis of the typical circulation pattern that establishes in these situations characterized by southwesterly currents in the southern part of the basin, driven by the low pressure system, that merge with the northeasterly Bora flow south of Ancona. Such a configuration suggests that the two areas experience different dynamics: the northern one is affected by the Bora outbreak and the southern one by the cyclonic circulation. Results show that there is a different response to different heat fluxes removals.

For the anticyclonic cases (December 2010 and December 2014) the easterly flow is homogeneous all along the Adriatic basin and no low pressure systems moves over central Italy. Therefore, there are no differences between North and South Adriatic and the heat flux sensitivity tests are performed by removing the total fluxes over the whole basin. SST variation are not tested since the experiments performed for the cyclonic cases demonstrated a very limited impact.

When dealing with the heat fluxes sensitivity tests for the cyclonic cases, the caption *noflux-tests* indicates results to be associated to all the experiments.

To better compare sensitivity tests results regarding cumulative precipitation field, three different sub-domains (Fig. 4.3) are identified for a quantitative evaluation of the total rainfall (including snowfall) amount. The domains are chosen to be representative of the areas affected by heaviest precipitation: two peaks are usually recorded at the border dividing Emilia-Romagna from Marche and Marche from Abruzzo.
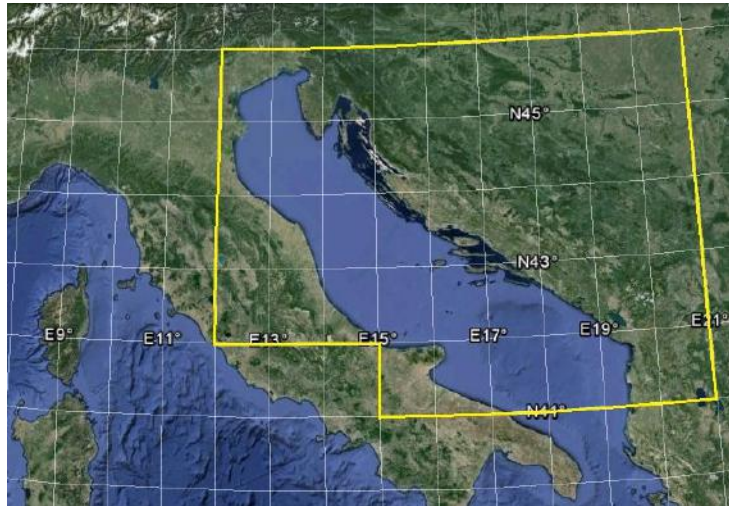
Figure 4.1: Area affected by modified SST.
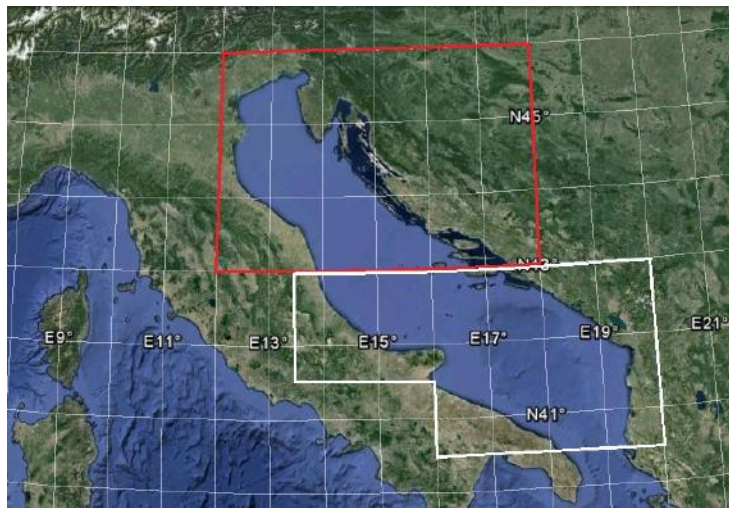
Figure 4.2: Areas affected by modified surface heat fluxes: the red box is referred to *nofluxN*, *nolatN* and *nosenN* cases, white box to *nofluxS* cases. Heat fluxes are modified only over the sea.

event	initial time	fcst range	run code	description
Feb 2012	09/02/2012 12 UTC	+45h	CNTRL	control run
			SST+	SST +2 in the Adriatic Sea
			SST-	SST -2 in the Adriatic Sea
			nofluxN	both fluxes removed in the N-box
			nolatN	latent flux removed in the N-box
			nosenN	sensible flux removed in the N-box
			nofluxS	both fluxes removed in the S-box
			orogplus	orography increased by a factor 2
			orogless	orography decreased by a factor 0.5
Sept 2012	13/09/2012 00 UTC	+45h	CNTRL	control run
			SST+	SST +2 in the Adriatic Sea
			SST-	SST -2 in the Adriatic Sea
			nofluxN	both fluxes removed in the N-box
			nolatN	latent flux removed in the N-box
			nosenN	sensible flux removed in the N-box
			nofluxS	both fluxes removed in the S-box
Nov 2013	11/11/2013 00 UTC	+45h	CNTRL	control run
			SST+	SST +2 in the Adriatic Sea
			SST-	SST -2 in the Adriatic Sea
			nofluxN	both fluxes removed in the N-box
			nolatN	latent flux removed in the N-box
			nosenN	sensible flux removed in the N-box
			nofluxS	both fluxes removed in the S-box
Dic 2010	15/12/2010 00 UTC	+45h	CNTRL	control run
			noflux	both fluxes removed on the sea
Dic 2014	30/12/2014 00 UTC	+45h	CNTRL	control run
			noflux	both fluxes removed on the sea

Table 4.1: List and codes of all the simulations performed.

Figure 4.3: Selected areas for the evaluation of the sensitivity tests results on precipitation: Romagna box (a), Central Apennine box (b), Adriatic Sea box (c).

4.3 February 2012

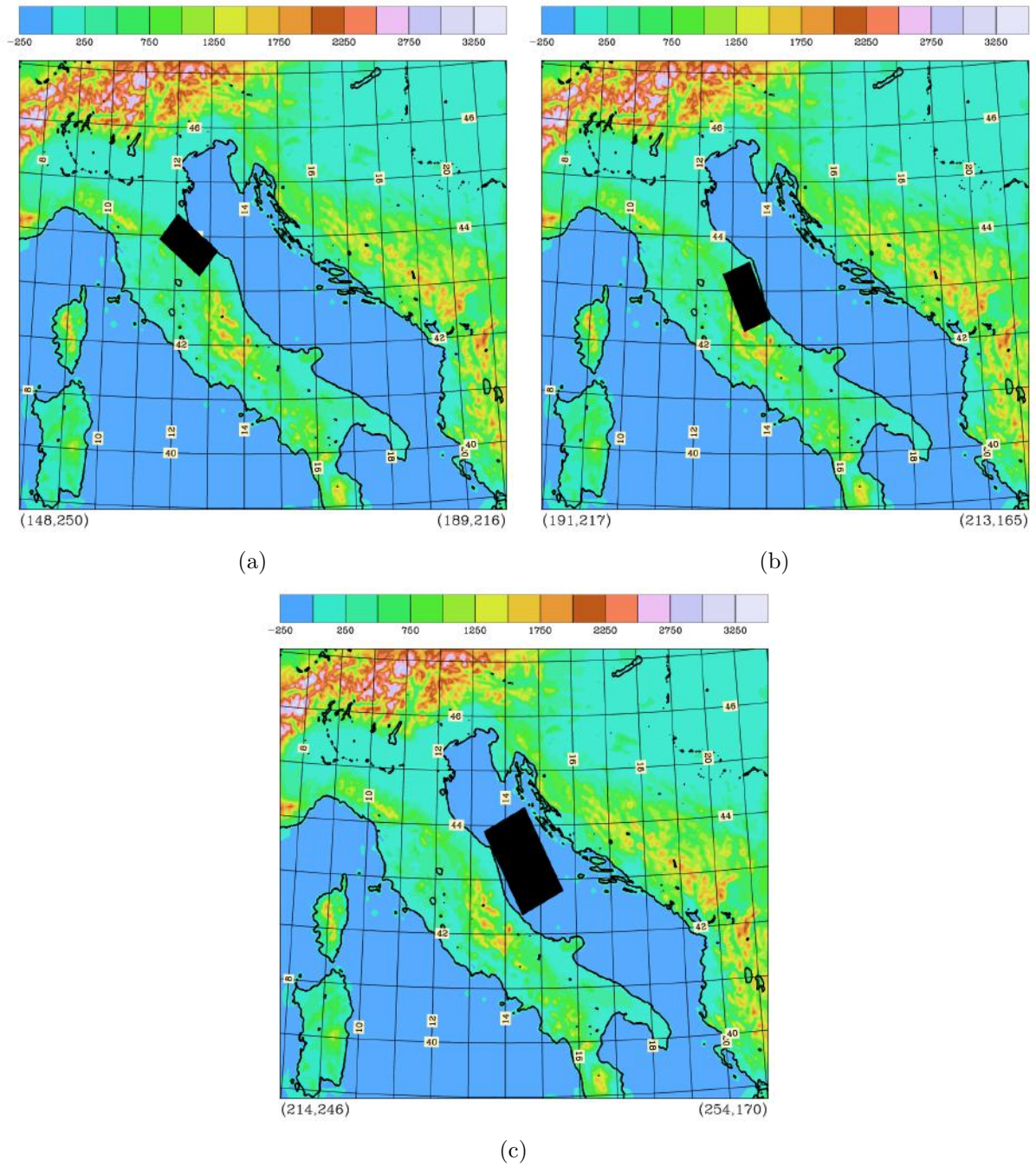The 2012 winter cold spell which lasted from the end of January to the mid of February is considered as one of the most severe event the Mediterranean basin experienced over the last century. Climatological data confirm that the period is known to have decadal recurrence interval: past events to be compared with are those occurred in 1985, 1956 and 1929.

For this reason the event has already been subject of several studies, also from the ocenographical point of view since its effects on the Adriatic Sea properties and circulation were remarkable: the persisting wind caused a considerable evaporation of the water body which was estimated in the order of 0.2 m over the whole period of the Bora event [Raicich et al., 2013]. A paper addressing the validation of the BOLAM-MOLOCH model chain specifically applied to the February 2012 Bora episode has just been published [Davolio et al., 2015].

In the present work simulations are performed concerning with the second phase of strong wind conditions, occurred in the period 9-12 February. The eastern flow persisted over the same area for almost three weeks, characterized by a first outbreak on 29 January that lasted few days followed by a short break and a second phase with larger snowfalls and wind gusts affecting the Apennines [ARPA-SIMC, 2012b]. The final period is more interesting as the area was already stressed by a long exposure to Bora wind and some phenomena were in their most intensive phase. Record-breaking values regarding daily tememperature, snowfall amounts and especially the northern Adriatic Sea water column properties (temperature, density and salinity) were recorded right at the end of the cold period [Pratizzoli, 2012].

The sensitivity tests performed for this case are listed in Tab. 4.2.

event	initial time	fcst range	run code	description
			CNTR	control run
			SST+	SST +2 in the Adriatic Sea
			SST-	SST -2 in the Adriatic Sea
			nofluxN	both fluxes removed in the N-box
Feb 2012	09/02/2012 12 UTC	+45h	nolatN	latent flux removed in the N-box
			nosenN	sensible flux removed in the N-box
			nofluxS	both fluxes removed in the S-box
			orogplus	orography increased by a factor 2
			orogless	orography decreased by a factor 0.5

Table 4.2: List and codes of the simulations performed for the February 2012 event.

4.3.1 Synoptic analysis

The period preceding the 2012 winter cold spell is characterized by anomalous warm and dry conditions; the data of ISMAR-CNR archive shows that the previous quarter is characterized by only 31% of the 1981-2010 climatological precipitation amount. Accordingly Adriatic rivers runoff is also below the average on both the western (-25% the Po river) and the eastern coast and positive sea water salinity anomalies are recorded right before the event [Mihanović, 2013].

Close to the end of January a change in the large-scale circulation regime is observed from zonal to meridional and NCEP reanalysis clearly shows a drop of geopotential height for the whole period [Grazzini, 2013]. The synoptic setting that establishes is persistent as in a typical blocking situtation: a ridge stretches from Scandinavia to eastern Atlantic and allows cold continental air to enter in the Mediterranean basin directly as a Bora flow or by running along the Alps and through the Rhone Valley. The second path yields to the formation of consecutive mesoscale cyclones over the Ligurian Sea that move slowly southeasterly and activate a southern inflow over the Adriatic Sea as a consequence of the cyclonic circulation. This feature is typical of cyclonic Bora cases. The configuration keeps unchanged for days and severe weather conditions are already observed prior to the period analyzed in the simulation. For example the snow cover is higher than a meter over a wide area of Romagna before the second cold surge approaches [ARPA-SIMC, 2012a].
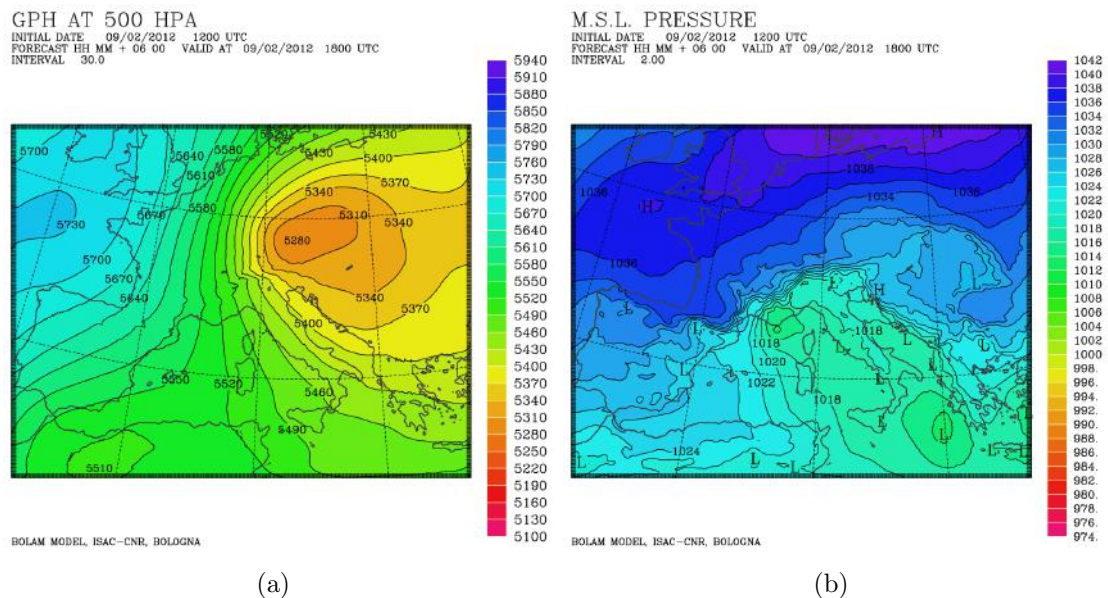

Figure 4.4: Geopotential height at 500 hPa (a) and mean sea level pressure (b), BOLAM forecast valid at 18 UTC on 09 February 2012.

4.3.2   Simulated fields

The CNTRL run for this event starts at 12 UTC on 9 February 2012. An anticyclone is settled over Scandinavia (where the 1040 hPa isobar appears) with its edges elongated from Spain to Russia (Fig. 4.4b). At 500 hPa the largest geopotential height values are located to the East with respect to the pressure at the soil and block the westerly flow (Fig. 4.4b). Thus a cold advection from the East is allowed to reach the Mediterranean basin associated with strong wind jets flowing along the southern border of the anticyclone. At 09 UTC on 9 February a significant pressure gradient is established across the Alps (Fig. 4.4b) and the wind, aligned to the isobars, is channelled along the Rhone Valley (Fig. 4.5b). A low pressure system develops off the coast of southern France while a Mediterranean cyclone, previously formed in the same way, leaves the domain towards Greece. At the same time a 10 hPa-gap is measured between the two flanks of the Dinaric Alps and the cold air damming is occuring.

The incoming easterly flow has a very cold core, up to $-19°C$ at 850 hPa (Fig. 4.5a) while higher values, positive too, are forecasted over the Mediterranean Sea.

(a)   (b)
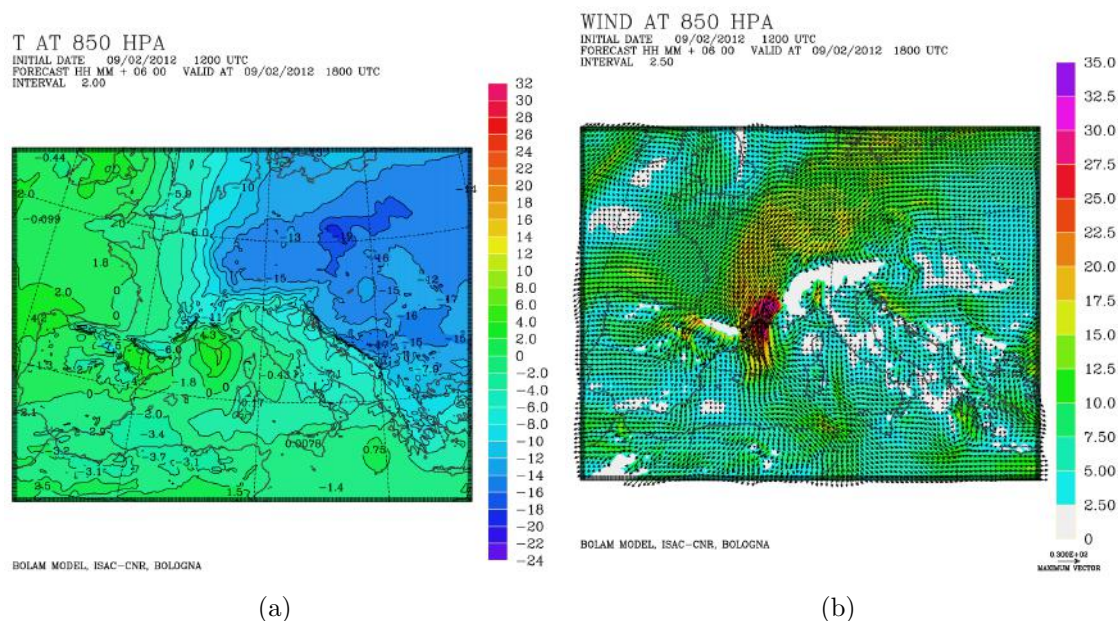
Figure 4.5: Temperature (a) and wind (b) fields at 850 hPa, BOLAM forecast valid at 18 UTC on 09 February 2012.

The simulated total precipitation field (both rain and snow) shows two distinct peaks of 172 mm and 130 mm in 45h over the Apennines in correspondence to the city of Rimini and Ancona, respectively (Fig. 4.6a). The northern peak is due mainly to precipitation occurred in the last day of simulation, between 12 UTC on 10 February and 12 UTC on

11 February, while the southern one occurs during the first 24 hours. Moderate snowfalls affects a wide area of the Emilia Apennine (a third lower peak of 75 mm of equivalent rain is predicted) and the sea as well.

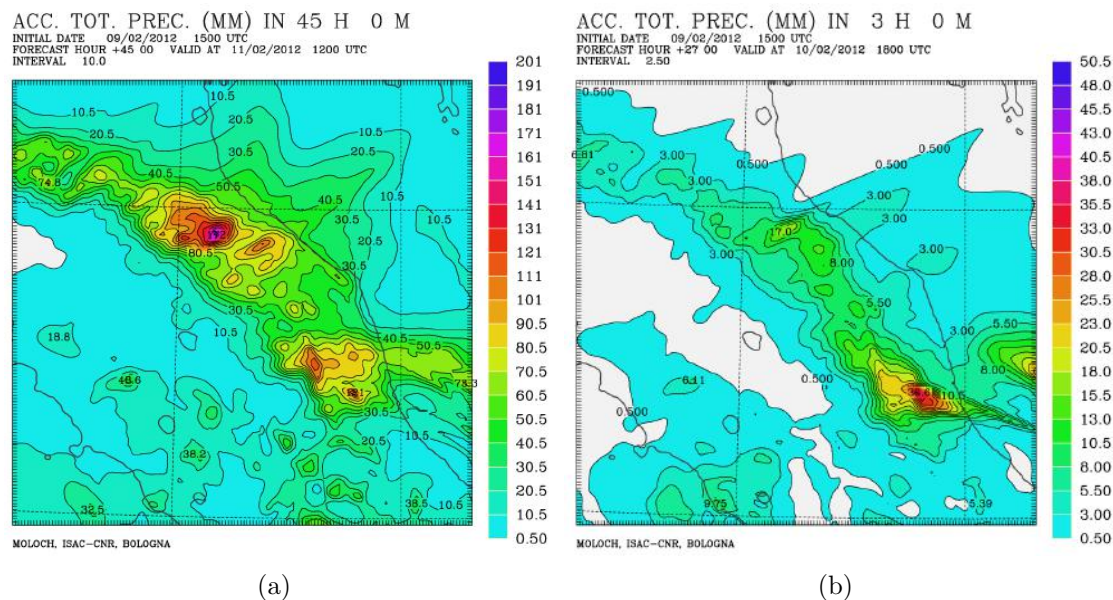(a)   (b)

Figure 4.6: Total accumulated precipitation forecast by MOLOCH in 45h (a) from 15 UTC, 09 February 2012 to 12 UTC, 11 February 2012 and in 3h (b) from 15 UTC to 18 UTC on 10 February 2012.

The low-level wind field, as simulated by MOLOCH, shows a weak northeasterly Bora until 10 February, 00 UTC, which is confined on the eastern side of the Adriatic basin. Along the Italian coast, moderate (up to 10 $m \cdot s^{-1}$) northwesterly winds blow south to Ancona (Fig. 4.7a). The flow is northwesterly above 850 hPa but as soon as the Mediterranean cyclone deepens it turns to southwesterly following the counterclockwise circulation. From 12 UTC on 10 February the Bora wind attains its maximum intensity at sea level and up to 850hPa in the northern part of the basin. The low-level southerly flow associated with the cyclone is predicted at sea level in correspondence to the fourth jet (Fig. 4.7b) where they melt and produce the narrow precipitation band over the sea observed in Fig. 4.6b. A remarkable vertical wind shear generates as the wind direction progressively turns from northeasterly to southwesterly. Looking together the precipitation pattern and the wind field (Fig. 4.6a and 4.7b) a correspondence can be inferred between the three rainfall peaks forecast inland and the three stronger jets reaching the coasts, the southernmost associated with the warm inflow.

Simulated air-sea heat fluxes show a pattern that is strictly correlated with that of wind speed. Higher values both for sensible and latent heat fluxes are attained along distinct bands that arise from the inner water of Dalmatia exactly at the heads of the jets

(Fig. 4.7c-d). On average latent heat fluxes values are higher than sensible heat fluxes: istantaneous heat losses up to 1000 $W \cdot m^{-2}$ are simulated locally.
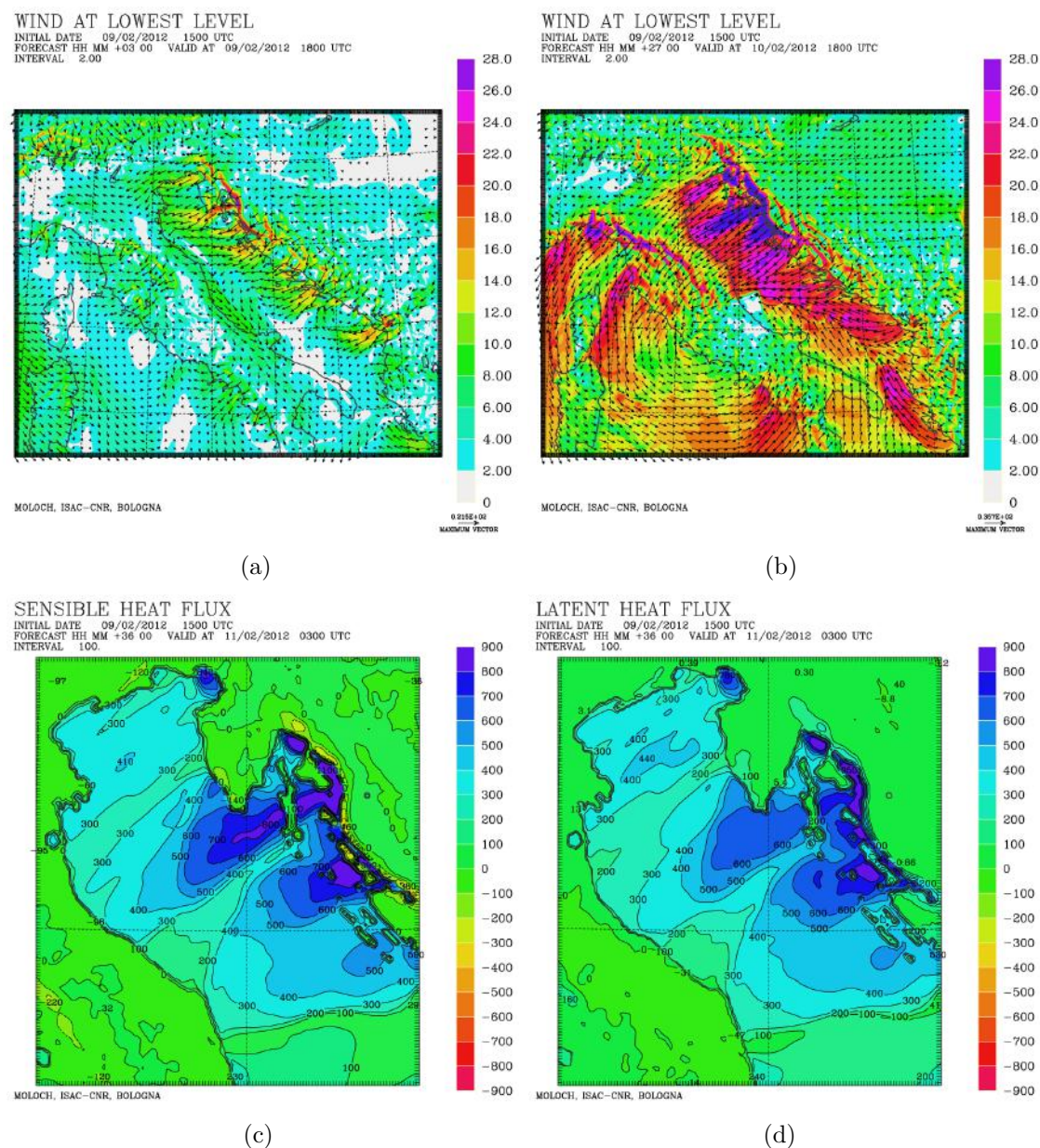

(a)

(b)

(c)

(d)

Figure 4.7: Wind field forecast by MOLOCH at 03 UTC on 09 February 2012 (a) and at 18 UTC on 10 February 2012 (b) at the lowest MOLOCH level ($\sim$ 72m). Sensible (c) and latent (d) heat fluxes forecast by MOLOCH at 03 UTC on 11 February 2012.

4.3.3   Comparison with observations

Several weather station networks have been queried to analyse the evolution of some surface meteorological variables namely temperature, mean sea level pressure, relative humidity, wind speed and direction and to compare them with the values simulated for the MOLOCH CNTRL run on the grid points. A large number of data belonging to ARPAV, ARPA SIMC, Marche and Abruzzo regional networks have been collected. It can be said that for this case the Bora outbreak is well-predicted by the MOLOCH model, especially if the analysis is focused on the northern part of the domain considered (mainly to Veneto). According to MOLOCH forecast, the first Bora gusts are expected to affect the Venetian plain by the evening of 9 February and the Po valley 2 hours later. In Fig. 4.8 the Concordia Sagittaria (VE) wind profiler data confirms that the low-level easterly flow starts to intensify at 19 UTC on 9 February. Data provided by radiosoundings performed at 00 UTC and 12 UTC daily at S. Pietro Capofiume (BO) are shown in Fig. 4.9: the Bora wind can be clearly identified from 00 UTC on 10 February.
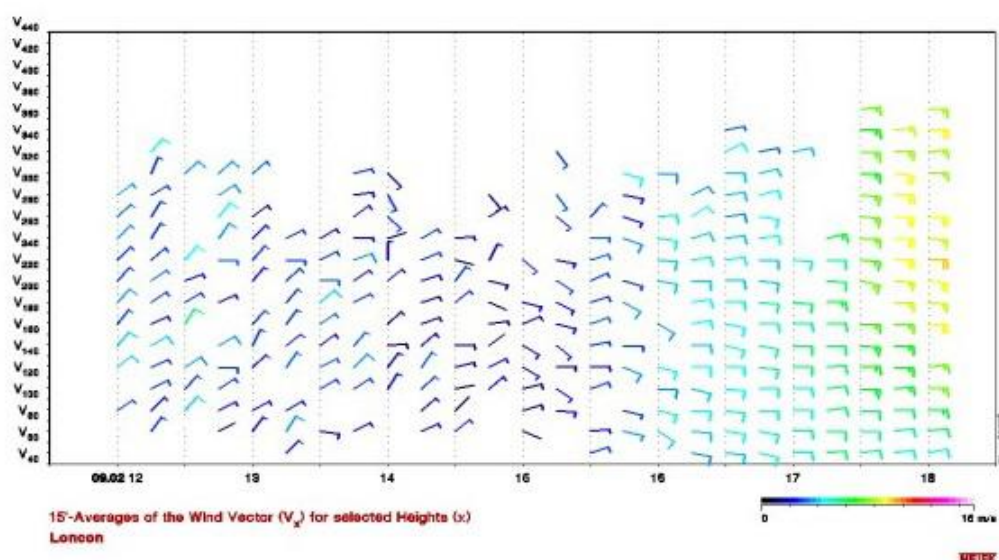
Figure 4.8: SODAR data at Concordia Sagittaria (VE) wind profiler (45.76 N, 12.84 E) from 12 UTC to 18 UTC on 09 February 2012. Source: ARPAV.

Although in general a good agreement is found between model simulation and observations, a couple of weather stations located more to the South is selected to show some errors in the forecast. Fig 4.10 shows that while temperature and wind speed are in good agreement: an increasing underestimation of the pressure and an overestimation of the relative humidity affect the first part of the simulation and this error is observed for some other stations located on the Adriatic coast. Wind speed and direction recorded and forecast in correspondence with other two weather station in central Italy are shown in
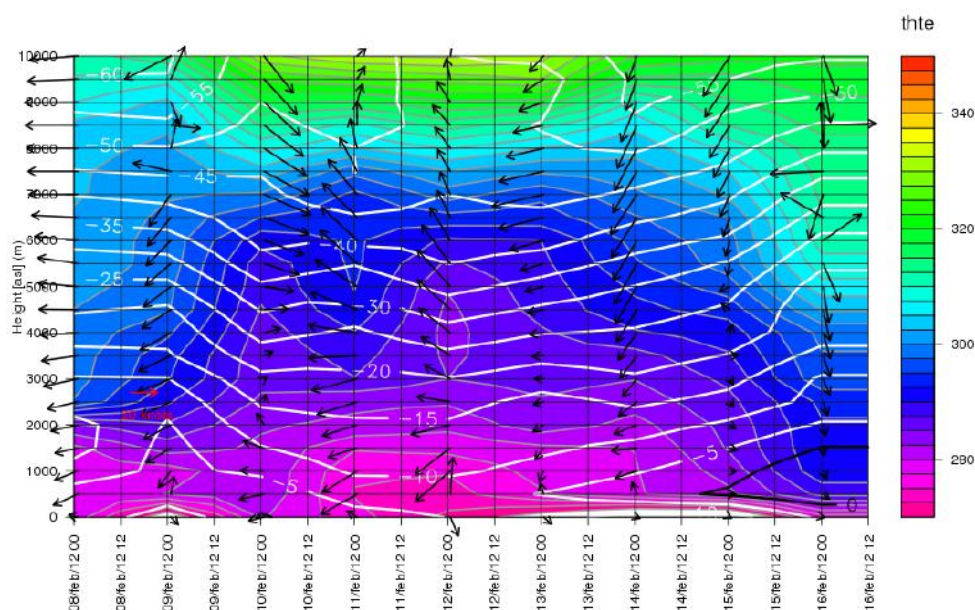
Figure 4.9: Radiosounding data at S. Pietro Capofiume (BO), (44.65 N, 11.62 E) collected from 12 UTC, 08 February 2012 to 12 UTC, 16 February 2012. Source: ARPA SIMC.

Fig. 4.11: at Porto Recanati (AN) an important northwesterly component is not properly simulated and at S. Benedetto del Tronto (AP) the Bora flow is overestimated in intensity, persistence and direction. This features are observed also for other weather stations in the surrounding areas while globally the wind field forecast can be considered satisfactory.

However these inconsistencies stem for the fact that MOLOCH expectation is that of a deeper cyclone displaced to the North so that the barrier wind south to Ancona can not occur or, at least, are weakened (that's why the NW component is hardly reproduced by the simulation at Porto Recanati). In that way the southernmost Bora jet is allowed to affect the coast (as forecast by MOLOCH at S. Benedetto del Tronto) while on the contrary calm wind is recorded.

Comparing observed and forecast precipitation, a good agreement is achieved even though the analysis of these data is affected by relevant uncertainty due to values exceeding instrument maximum capacities and to difficulties in getting reliable measurements by snow-gauges. A set of significant weather stations for which data have been quality-controlled is choosen to match the total snowfall recorded with the precipitation pattern simulated in Fig. 4.6. The wide area exceeding 100 mm of equivalent rainfall over Val Marecchia and South-Romagna Apennine includes weather stations that effectively attain snowfall of the order of one meter (Tab 4.3 - left column). A group of stations in the south to Marche experience total rainfall amounts around 50/60 mm (measured by warmed rain-gauges) and can be associated with the second peak (Tab 4.3 - right column).
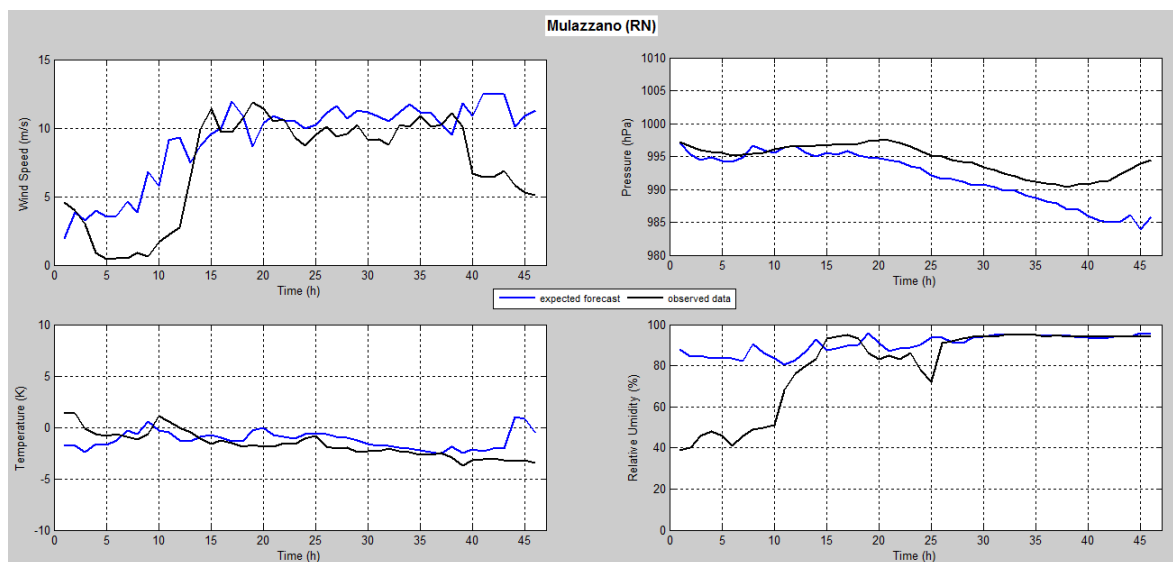
(a)
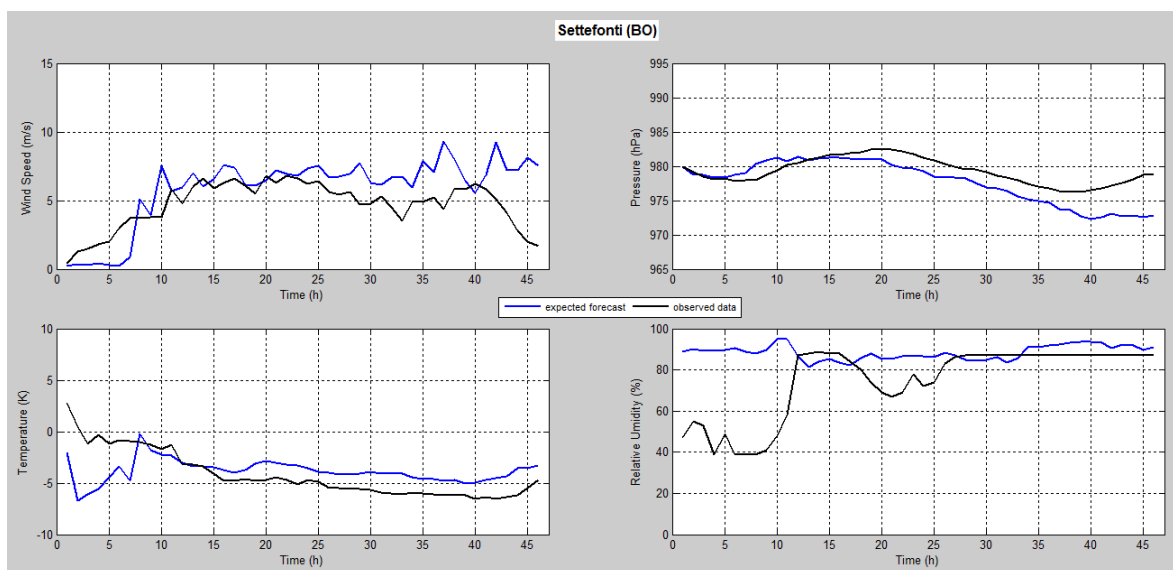
(b)

Figure 4.10: Comparison between MOLOCH forecast and observations for wind speed, temperature, m.s.l.p. and relative humidity at (a) Mulazzano (RN) and (b) Settefonti (BO) from 15 UTC, 09 February 2012 to 12 UTC, 11 February 2012. Source: ARPA SIMC.
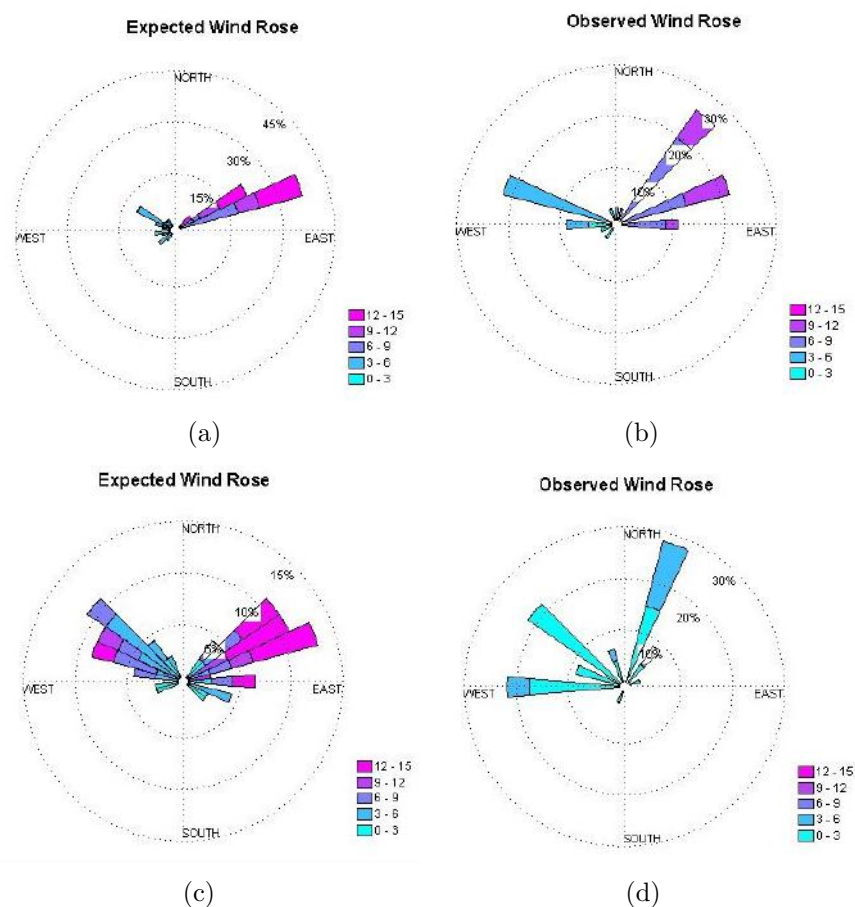
Figure 4.11: Comparison between MOLOCH forecast and observations for wind speed and direction at (a-b) Porto Recanati (MC) and (c-d) S. Benedetto del Tronto (AP) from 15 UTC, 09 February 2012 to 12 UTC, 11 February 2012. Source: C.F. Marche.

station	cm/48h	station	cm/48h
Monzuno (BO)	73	Serravalle di Carda (PU)	73
Santa Sofia (FC)	90	Urbania (PU)	122
Novafeltria (RN)	117	Ancona	44
Terzo di Carnaio (FC)	105	Ripatransone(AP)	63

Table 4.3: Total snowfall amount recorded in 48h (9-11 February 2012) at selected weather stations in Emilia Romagna (left column) and Marche (right column) regions. Shaded stations are located in the areas where MOLOCH forecast maximum rainfall. Source: [ARPA-SIMC, 2012c], [C.F.Marche, 2012b].

4.3.4 Sensitivity tests

Two sensitivity tests for the February case are performed varying the initial SST values, by adding and subtracting $2°C$, over the area displayed in Fig. 4.1. No significant differences are observed as regards the dynamics of the event (wind speed and direction, pressure and geopotential height patterns) except for heat fluxes that are higher in the SST+ simulation and lower in the SST- one (Fig. 4.12 to be compared with Fig. 4.6d). This behaviour is expected since the amount of heat lost by the sea depends on the air-sea temperature difference.

What is not clearly predictable is the effect of SST variations on rainfall and snowfall since other factors can play a role for example the incoming air stability and the boundary layer height on the sea (see Ch. 6 for further details). In Tab. 4.4 the total precipitation amount in 45h is evaluated for each sensistivity test over selected boxes (Fig. 4.3) as the sum of the mean hourly precipitation predicted by the model and a comparison in percentage terms is done. It turns out that an increase (decrease) of precipitation amount over Romagna and over the Adriatic Sea of the order of 10% is expected in response to an increasing (decreasing) SST. An opposite behaviour is observed over the central Apennines box.

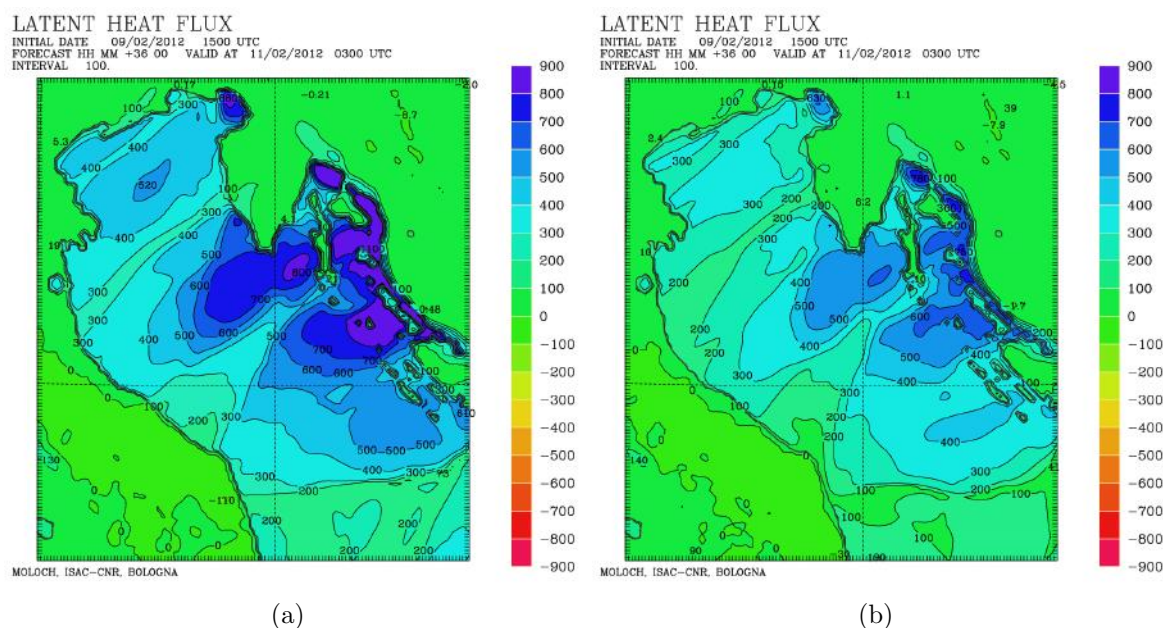(a)   (b)

Figure 4.12: Latent heat fluxes for SST+ (a) and SST- (b) sensitivity tests, MOLOCH forecast valid at 03 UTC on 11 February 2012. To be compared with Fig. 4.7d.

Further tests are carried out regarding heat fluxes: at first both latent and heat fluxes are lowered to zero over northern and southern Adriatic Sea (*nofluxN* and *nofluxS* codes)

by applying the mask in Fig 4.2 . Then since the largest sensitivity has been observed for the northern part of the Adriatic Sea, a further test is performed removing separately latent and sensible heat flux over that area only (*nolatN* and *nosenN* codes). Results in terms of precipitation fields are shown in Tab. 4.4: heat fluxes have a stronger impact with respect to SST as a drop of 60% in rainfall amount is predicted for *nofluxN* over the land, mainly due to the lack of latent heat since when only laten heat flux is removed (*nolatN*) almost the same value is observed. On the other hand, *nosenN* simulation induces a minor effect (the decrease is no more than 20% with respect to CNTRL).

The removal of all the fluxes on the southern part of the Adriatic Sea (*nofluxS*)produces a precipitation decrease of 16%, 33%, 16% respectively over Romagna, Central Apennine and Adriatic Sea.

If heat fluxes are set to zero, air-sea interaction is prevented and the Bora wind is allowed to pass over the Adriatic Sea mantaining its properties: colder temperature and drier air are expected over the Po Valley and in front of the Italian coast. After 30h from initial time a $6°C$ difference is observed over the Central Adriatic Sea between CNTR and *nofluN* simulations. Relative humidity also falls by 30% and this value is even more significant if considering that the maximum water vapour content of colder air is lower.

A further and more detailed analysis of the dynamical differences among the *noflux*-cases is proposed in Ch. 6 where cross-section are used to better understand what exactly happens above the sea.

February 2012

Romagna box			Central Apennines box			Sea box		
run	mm/h	var %	run	mm/h	var %	run	mm/h	var %
CNTRL	72.1		CNTRL	48.8		CNTRL	22.6	
SST+2	80.3	+11.6%	SST+2	43.5	-10.7%	SST+2	24.6	+8.5%
SST-2	63.2	-12.3%	SST-2	53.5	+9.8%	SST-2	19.2	-15.1%
nofluxN	29.8	-58.6%	nofluxN	19.4	-60.2%	nofluxN	18.9	-16.3%
nolatN	30.1	-58.3%	nolatN	31.9	-34.6%	nolatN	16.0	-29.2%
nosenN	57.8	-19.8%	nosenN	42.4	-13.1%	nosenN	36.4	+61%
nofluxS	60.4	-16.2%	nofluxS	32.5	-33.3%	nofluxS	19.0	-16%

Table 4.4: Sensitivity tests results on the precipitation field.

4.4   September 2012

This event is a clear example of cyclonic Bora. It has been part of the HyMeX SOP1 that aims to analyse HPE in the target area of Central Italy and a dedicated campaign (IOP-4) has been arranged with a flight, extra operational soundings and data collection. The cyclone attains high wind speed values yielding to several convective cells development and total rainfall amounts of more than 300 mm over 48h as recorded on the Gran Sasso massif. A typical feature of strong cyclonic systems is observed (Fig. 4.13): as the core deepens a cold air intrusion comes from upper levels. Globally the Central Italy is more affected than Emilia Romagna for this case.
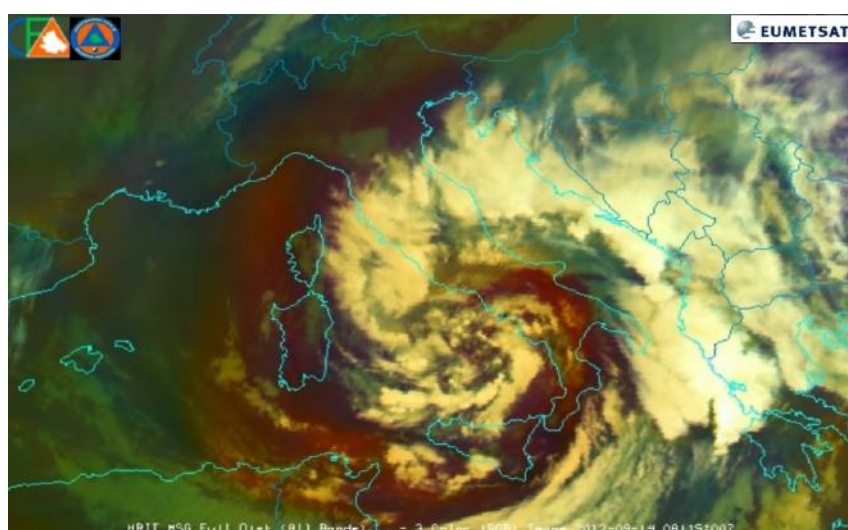
Figure 4.13: MSG airmass RGB image referred to 14 September 2012 at 08.15 UTC. Source: EUMETSAT.

event	initial time	fcst range	run code	description
			CNTR	control run
			SST+	SST +2 in the Adriatic Sea
			SST-	SST -2 in the Adriatic Sea
Sept 2012	13/09/2012 00 UTC	+45h	nofluxN	both fluxes removed in the N-box
			nolatN	latent flux removed in the N-box
			nosenN	sensible flux removed in the N-box
			nofluxS	both fluxes removed in the S-box

Table 4.5: List and codes of the simulations performed for the September 2012 event.

4.4.1 Synoptic analysis

Perturbed weather conditions on mid-September 2012 affects the Mediterranean basin as a whole. It is a time-window of severe weather over Italy where two HyMeX IOP are issued in a week, the first on 12 September related to deep convection over Friuli Venezia Giulia (IOP2) and the second, IOP4, related to the event simulated in this section.

Since early September, an anticyclonic pattern globally affected Southern and Central Europe and this prolonged warm and moist period leads to high temperatures and humidity values over Italy before the Bora outbreak occurs: at 06 UTC on 13 September, $+18°C$ are predicted over Sicily at 850 hPa (Fig. 4.14c). By 11 September a large-scale through moves from Scandinavia towards Germany and northern Italy (Fig. 4.14a). The associated cold front (thermal gradient more than 15° at 850hPa between incoming and pre-existing air) passes over the Alps and a lee cyclone forms over the Nortern Adriatic on 12 September and it is responsible for the high precipitation rates recorded in the North-East of Italy during IOP2. A second cyclone deepens between Sardinia and Corsica by 00 UTC on 13 September and follows the typical path of Mediterranean cyclones that is a southeasterly trajectory. It settles for a couple of days over Central Italy where it embeds the first cyclone before moving away.
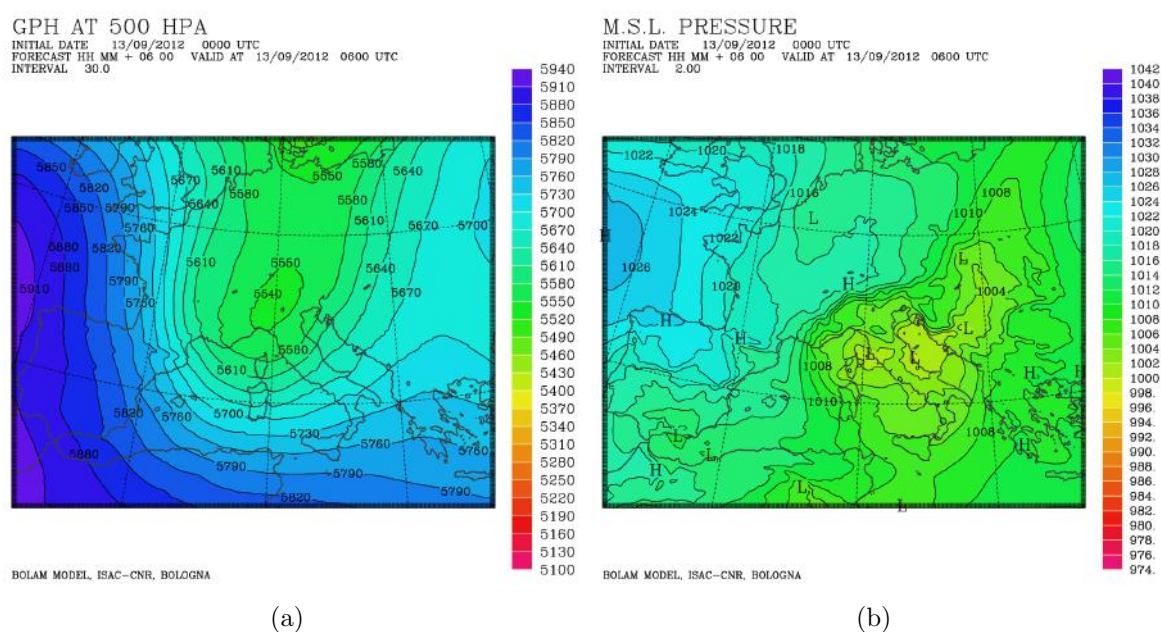

(a)   (b)

Figure 4.14: Geopotential height at 500 hPa (a) and mean sea level pressure (b), BOLAM forecast valid at 06 UTC on 13 September 2012.

4.4.2   Simulated fields

The simulation start on 13 September 2012: at 00 UTC the two cyclones are still separated and located on different flanks of the Apennines (Fig. 4.14b). Gradually a stronger cold air intrusion from the East (e.g. the Bora wind) is induced by the cyclonic circulation whilst in the previous days the westernmost path (northern Alps and Rhone Valley) was preferred for the flow to enter in the Mediterranean and large wind speed are still forecasted over southern France (Fig. 4.15b). At sea level no remarkable pressure gradient is observed between the Karst Plateau and the Adriatic Sea as typical with more easterly flows but it is enough to trigger the Bora wind possibly in response to a cold air damming occurring to the East of Dinaric Alps. During the following 48 hours persistent scattered convective precipitation affects the area close to the border between Marche and Abruzzo. Finally from 16 September onwards an high pressure ridge reinforces over Spain and the cyclone extinguishes.

(a)   (b)
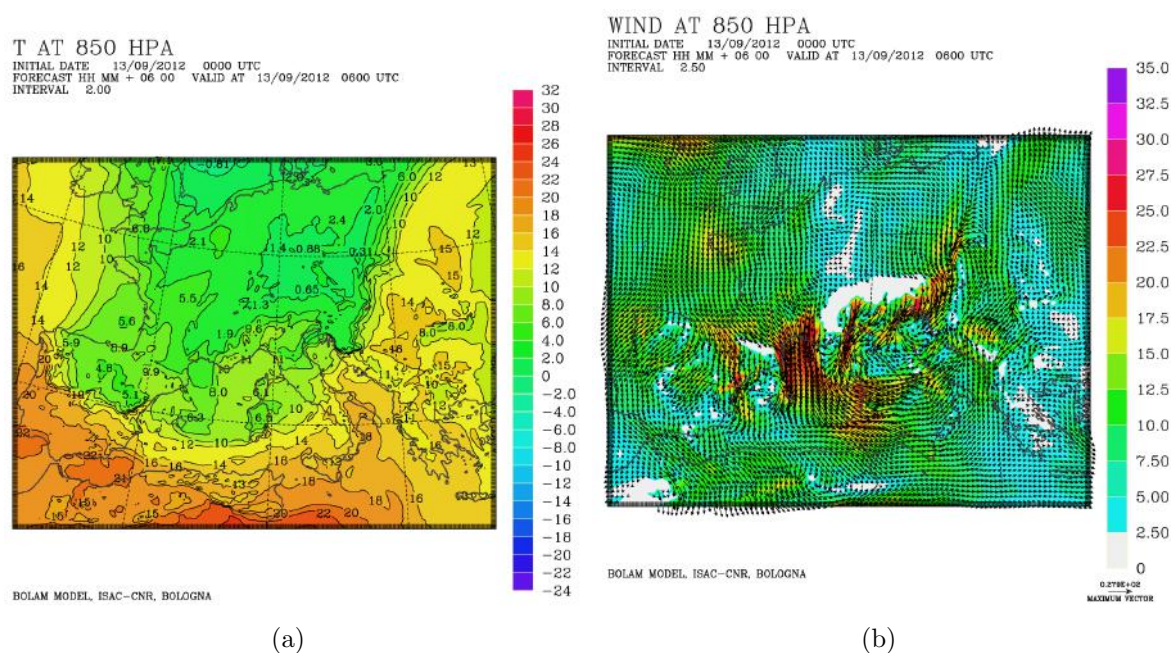
Figure 4.15: Temperature (a) and wind (b) fields at 850 hPa, BOLAM forecast valid at 06 UTC on 13 September 2012.

The 45h-accumulated rainfall map (Fig. 4.16a) clearly shows that the eastern side of the Apennines and the underlying plains are affected by heavy precipitation. Globally more than 100mm/45h are forecasted over an area approximately enclosed by Marche borders and large precipitations are simulated also over the sea. More specifically three distinct peaks exceeding 300mm/45h are simulated over the Apennines and a fourth

peaks is forecast offshore, south to Ancona. Intense rain rates are predicted as typical of convective phenomena: Fig. 4.16b shows this behaviour for the southern peaks for which more than 70% of precipitation is forecast in a 3h interval from 20 UTC to 23 UTC on 13 September.

(a)   (b)

Figure 4.16: Total accumulated precipitation forecast by MOLOCH in 45h (a) from 03 UTC, 13 September 2012 to 00 UTC, 11 September 2012 and in 3h (b) from 20 UTC to 23 UTC on 13 September 2012.

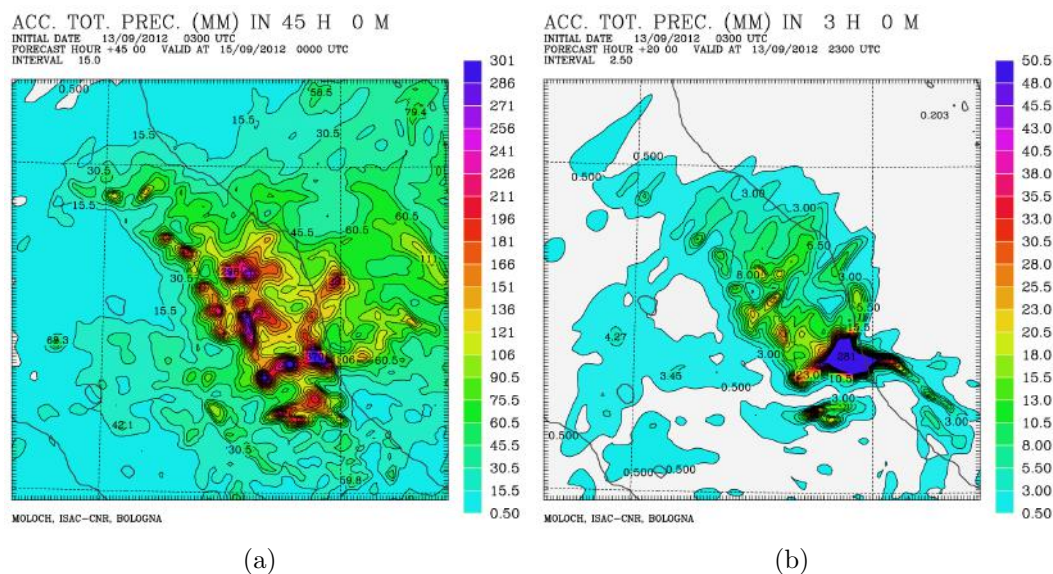Wind fields shown in Fig.4.17a-b are referred to 03 UTC on 14 September: three Bora LLJ are simulated at both 850 hPa and 950 hPa with a weaker additional jet, the southernmost, which is most of the time forced by the Adriatic cyclone whose effects on wind pattern are detectable below 850 hPa. As occurred in the February 2012 case, the presence of a low pressure system over Central Italy induces a counterclockwise circulation that merges with the Bora flow over the central Adriatic basin. The flow blowing above 850 hPa is mainly directed from the South-East at 00 UTC on 13 September over the whole Adriatic basin but it turns completely to the East from 12 UTC in the northern Adriatic where vertical wind shear forms without the appeareance of a jet pattern. It is worth noting that in the simulation the southernmost precipitation peak is located right in front of the coastal area where the fourth jet, and the warm moist southern inflow too, impinge.

As regards the temperature field a remarkable gradient is predicted between northern and southern Adriatic: fo example at 950hPa, at 11 UTC on 13 September, a temperature of $+11°C$ is associated with the main Bora jet (Senj jet, the third) while in correspondence
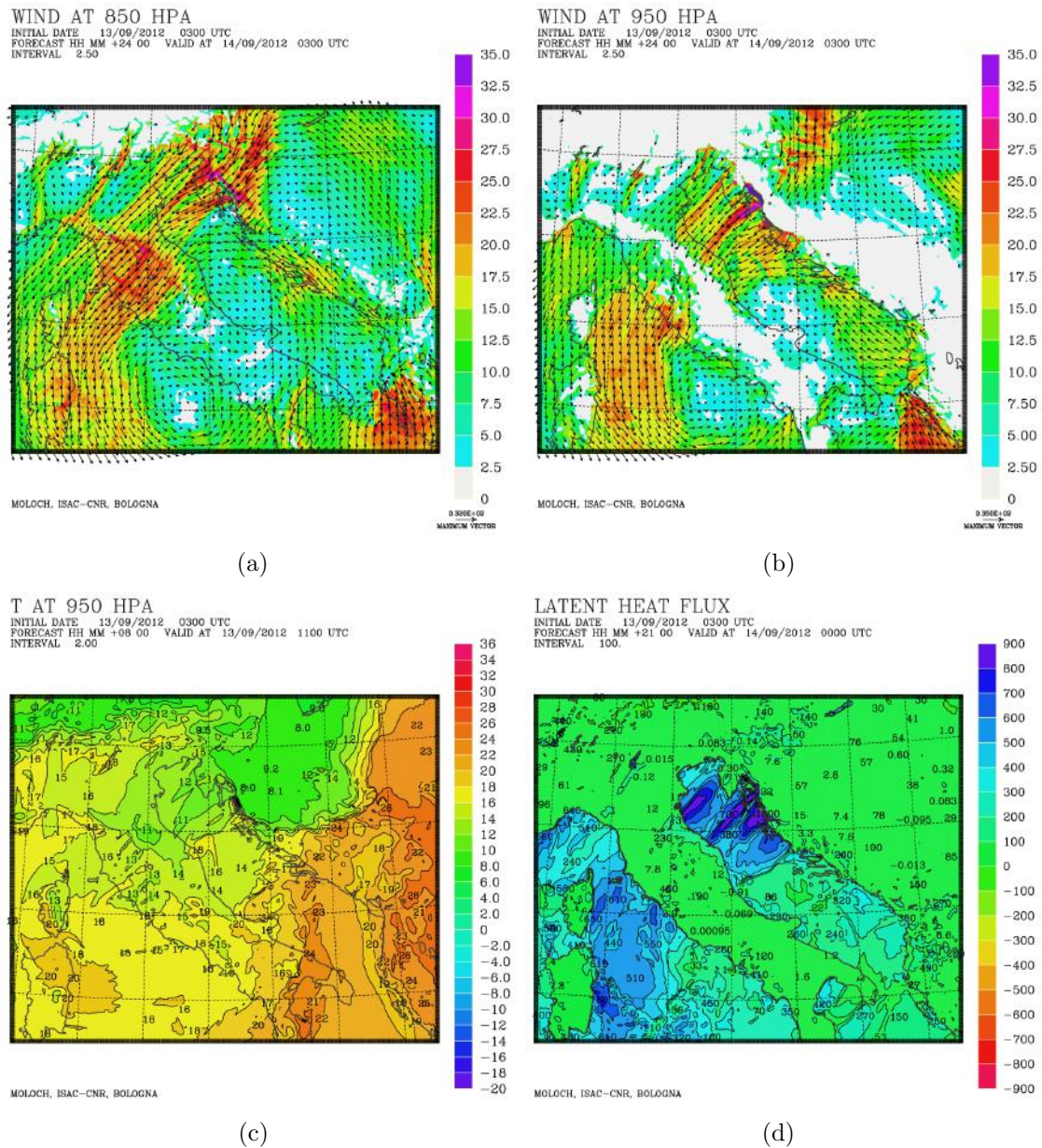
Figure 4.17: Wind field forecast by MOLOCH at 03 UTC on 14 September 2012 at 850 hPa (a) and at 950 hPa (b). Temperature field forecast at 11 UTC on 13 September 2012 at 950 hPa (c) and latent heat flux forecast at 00 UTC on 14 September 2012 (d).

to the cyclonic inflow entering from the South the predicted temperature is $+24°C$ (Fig. 4.17c). This difference reflects on air-sea heat fluxes that are larger where the Bora jets are simulated with narrow bands reaching locally 800 $W \cdot m^{-2}$ but approximate to

zero as the line that separates the area affected by the Bora wind from that affected by cyclonic circulation is crossed (Fig. 4.17d referred to latent heat). Finally for this case an SST decrease by $1°C$ between initial and final simulation time is predicted over the northern Adriatic.

4.4.3   Comparison with observations

The quality check of the MOLOCH forecasts for this event shows very good results. The forecast starts at 00 UTC on 11 November 2013 when the Bora flow is crossing the Dinaric Alps and the wind reinforces at all levels over the Adriatic basin with a very high wind speed values above 850 hPa. This agrees with the observations of the Concordia Sagittaria wind profiler (Fig. 4.18) which is located close to the northern Adriatic coast a hundred kilometers down to the foothills of Karst Mountains: an abrupt outbreak is recorded from midnight to 12 UTC on the same day and then a moderate easterly wind regime establishes.
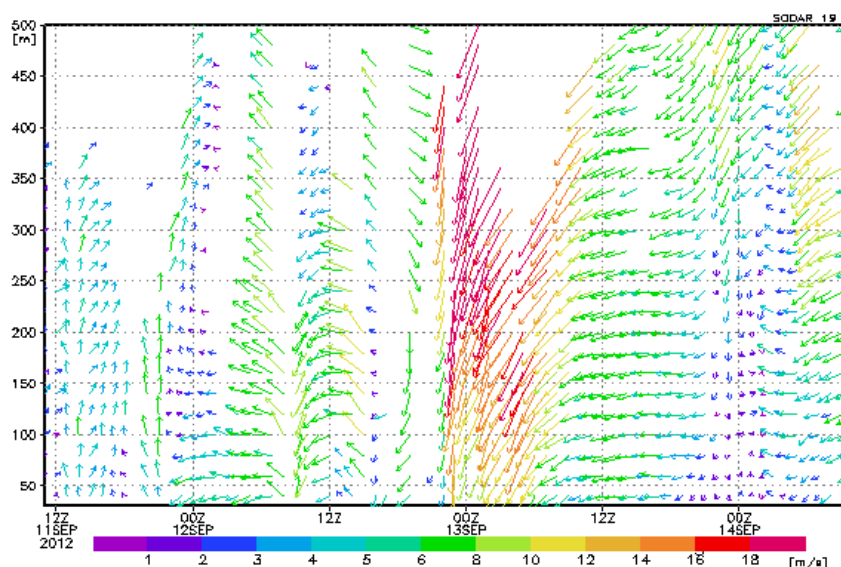
Figure 4.18: SODAR data at Concordia Sagittaria (VE) wind profiler (45.76 N, 12.84 E) for a 4-days time-span by the 11th September at 12 UTC. Source: ARPAV.

The mesoscale evolution is well-predicted by MOLOCH as turns out by several comparisons that have been done for a set of weather stations belonging mainly to Marche regional network and concerning temperature, relative humidity, pressure and wind. The graphs related to four different stations are presented in Fig. 4.19 and Fig. 4.20 to show the performances. These stations are chosen as to represent a wide areas ranging from the Po Valley, the Adriatic coast and up to the highest southern Apennine peak (Monte Prata, 1813 m).
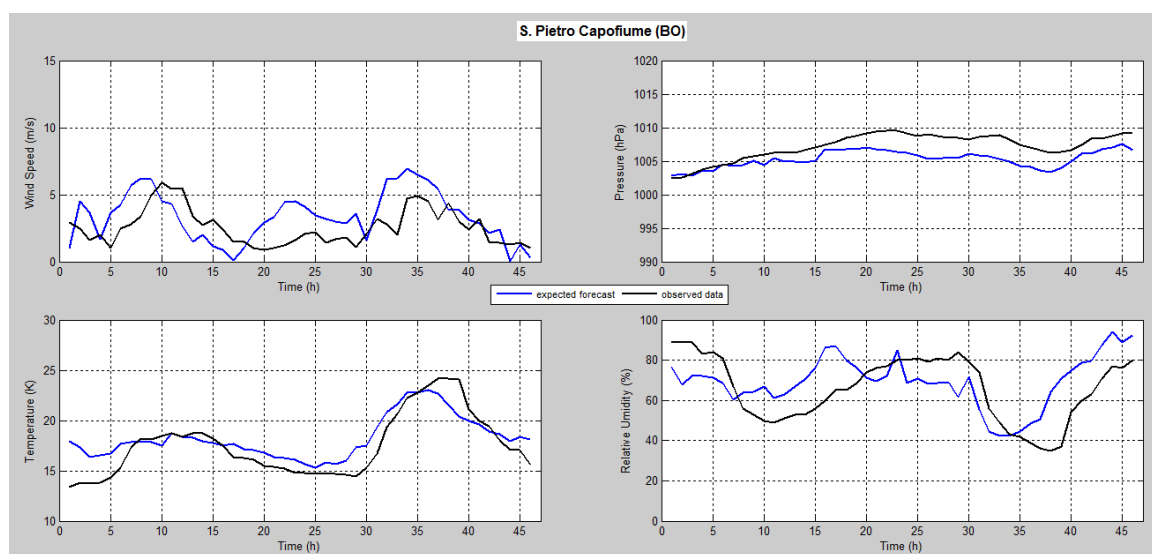
(a)
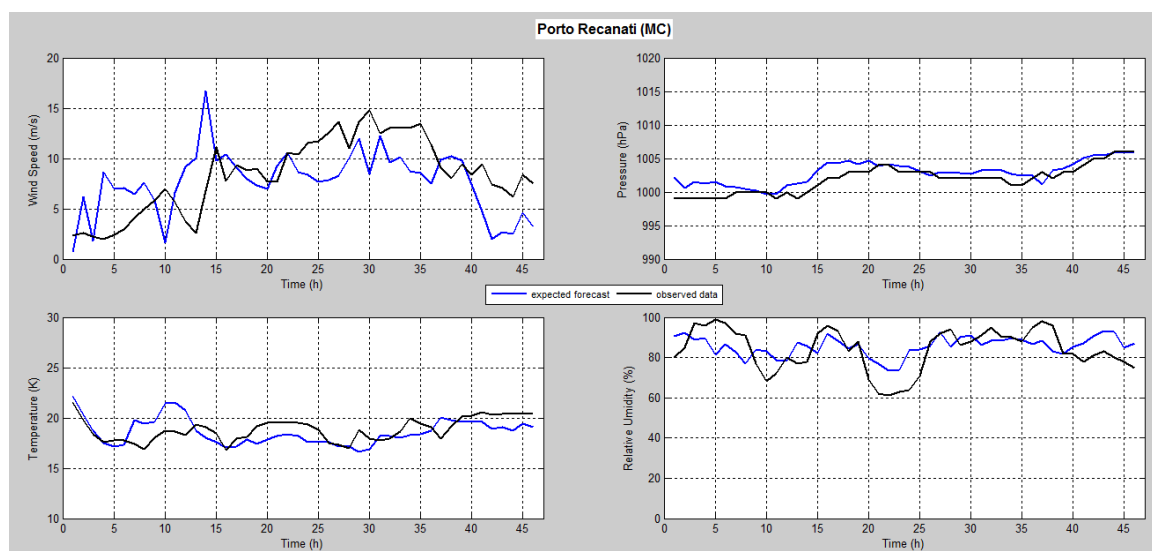
(b)

Figure 4.19: Comparison between MOLOCH forecast and observations for wind speed, temperature, m.s.l.p. and relative humidity at (a) S. Pietro Capofiume (BO) and (b) Porto Recanati (MC) from 03 UTC, 13 September 2012 to 00 UTC, 15 September 2012. Source: ARPA SIMC, C.F.Marche.

Simulated rainfalls affect mainly three areas (Fig. 4.16): the Gran Sasso massif, the Tronto river basin and the hills of southern Marche and maximum values in 45h reach about 250 mm, 370 mm and 290 mm, respectively. In Tab. 4.6 some rain-gauges located
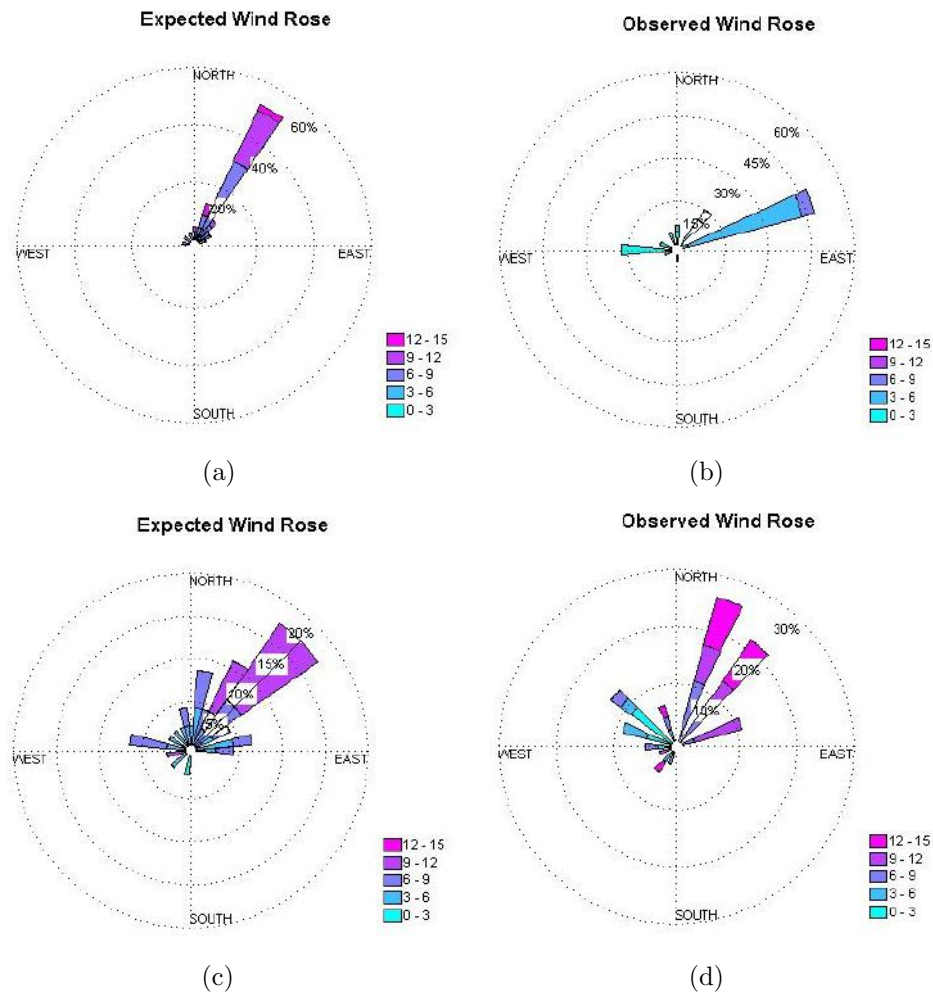
Figure 4.20: Comparison between MOLOCH forecast and observations for wind speed and direction at (a-b) Pesaro (PU) and (c-d) Monte Prata (AP) from 03 UTC, 13 September 2012 to 00 UTC, 15 September 2012. Source: C.F. Marche.

in these areas have been considered and the shaded ones located in the areas where MOLOCH predicts rainfall peaks. The values match except for that of Campo Imperatore where the observed value is 100 mm larger. Apart from individual peaks, an overview on the actual precipitation pattern is provided by interpolated maps in Fig. 4.21 for the 14th September.

| (a) | (b) |
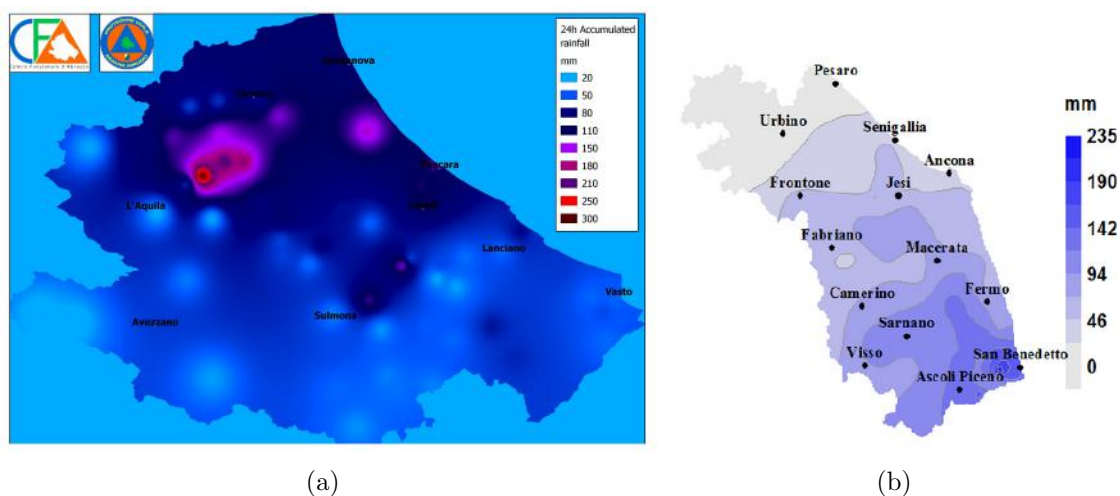
Figure 4.21: Interpolated data by Abruzzo (a) and Marche (b) Regional Agencies rain-gauges networks on 14 September 2012. Source: C.F. Marche and C.F. Abruzzo.

station	mm/48h	station	mm/48h
Camerino (MC)	171.2	Atri (TE)	199.2
Pintura di Bolognola (MC)	274.5	Giulianova (TE)	132.8
Monte Bove (MC)	210.6	Caramanico Terme (TE)	162.6
Ripatransone (AP)	245.6	Pescara	145.2
Ascoli Piceno	225.2	Campo Imperatore (AQ)	334.8

Table 4.6: Total rainfall amount recorded in 48h from 09 UTC, 13 September 2012 to 09 UTC, 15 September 2012 at selected weather stations in Marche (left column) region and from 00 UTC, 13 September 2012 to 00 UTC, 15 September 2012 in Abruzzo (right column)region. Source: [C.F.Marche, 2012a] and C.F. Abruzzo. Shaded stations are located in the areas where MOLOCH forecast maximum rainfall.

4.4.4   Sensitivity tests

The results of SST sensitivity tests for the September 2012 case are in line with those of the February case: the Romagna box experiences an increase in total rainfall of 10% with respect to the CNTRL run when a $+2°C$ perturbation is applied and an opposite reduction when the SST is lowered by the same amount (Tab. 4.7). An analogous tendency is observed for the Adriatic Sea box (+20% and -10% respectively). As for the previous case the box related to the Central Apennine behaves in a different manner and the total precipitation amount for SST+ simulation is 10% less then in the CNTRL run while SST- test does not produce remarkable effects in this area. It is worth noting that the values we are dealing with are significant: on average over the Central Apennines box, which is approximately 130x85 km wide, 130mm in 45h are forecasted.

On the other hand, the heat fluxes sensitivity tests show a larger impact than SST: -60% over land and -20% over the sea when both fluxes (*nofluxN*) are switched off. It is worth noting that the same impact can be attained by removing latent heat only (*nolatN*), while sensible heat fluxes produce a weaker impact on rainfall (*nosenN*). It turns out that latent heat fluxes over the Adriatic play a key role in determining the amount of rainfall over the Italian territory. Moreover an unexpected +26% is predicted over the Romagna box by the *nofluxS* simulation. The areas affected by heat fluxes removal are those indicated in Fig. 4.2.

This Bora event is characterized by the largest difference in lower levels temperature of *noflux*-tests run with respect to CNTRL run: at the lowest MOLOCH level this gap is up to 8° in the Central Adriatic for *nofluxN* test (Fig. 4.22) right in correspondence to the area affected by the strongest Bora jet (and largest fluxes indeed).

The *noflux* simulations results, for this event and for the February 2012 case, are analysed in more detail in Ch. 6.

September 2012

Romagna box			Central Apennines box			Sea box		
run	mm/h	var %	run	mm/h	var %	run	mm/h	var %
CNTRL	44.9		CNTRL	128.4		CNTRL	56.2	
SST+2	49.5	+10.2%	SST+2	114.9	-10.5%	SST+2	67.3	+19.7%
SST-2	39.8	-11.5%	SST-2	128.7	+0.2%	SST-2	50.9	-9.6%
nofluxN	18.7	-58.4%	nofluxN	43.4	-66.2%	nofluxN	46.5	-17.4%
nolatN	17.2	-61.7%	nolatN	48.3	-62.4%	nolatN	47.1	-16.2%
nosensN	37.3	-16.9%	nosensN	98.9	-23%	nosensN	55.1	-2%
nofluxS	56.6	+26%	nofluxS	122.3	-4.8%	nofluxS	54.6	-2.9%

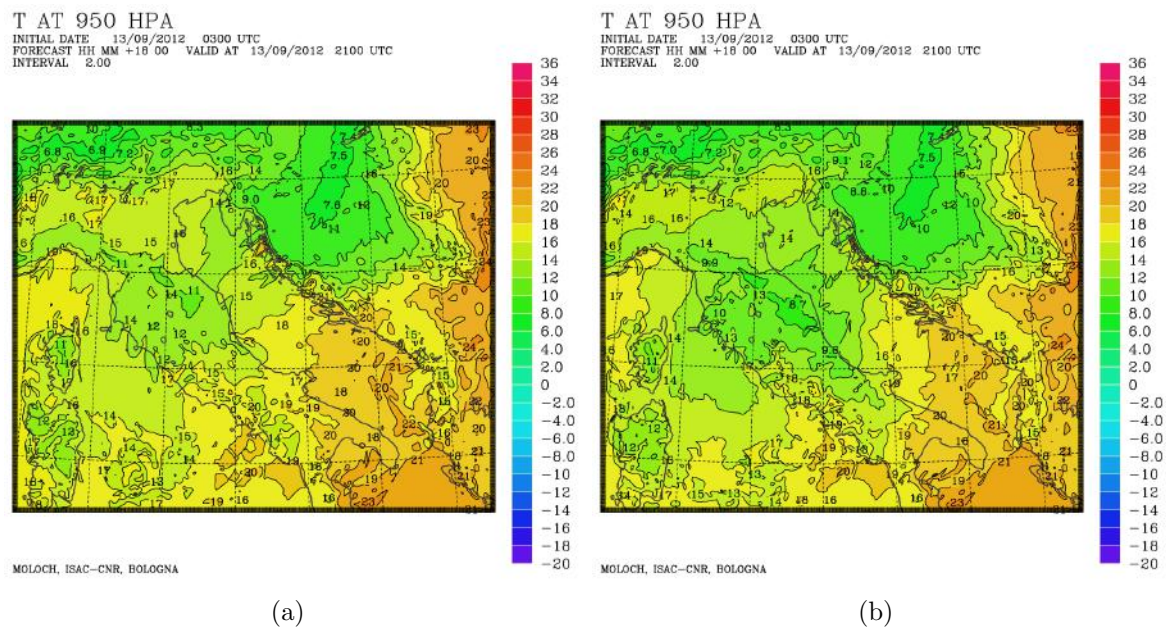Table 4.7: Sensitivity tests results on the precipitation field.

Figure 4.22: Temperature at 950 hPa for CNTRL run (a) and *nofluxN* run (b), MOLOCH forecast valid at 21 UTC on 13 September 2012.

4.5 November 2013

The November 2013 event strongly affects a large area yielding to local flood in Romagna and Marche coastal plains and to landslides in Umbria main river basins. Such adverse impact are not infrequent (similar effects were associated with an almost identical event occurred in May 2014) and are caused to the Bora impinging almost perpendicularly on the Central Apennines. The event is also significant for a remarkable storm surge associated with large wave height offshore [ARPA-SIMC, 2013b]. Moreover, in this case the slow-evolving synoptic pattern favours the persistence of severe weather conditions for more than 3 days, from 10 November to the end of 13 November. This cyclone is the third that crosses the Mediterranean Sea by the beginning of the month.

It originates as a cut-off low from a through located over Central Europe, crosses rapidly from the northern Adriatic to the Tyrrhenian Sea and becomes almost stationary in front of North Africa coast, driving the Bora flow towards the Adriatic Sea. Return period between 100 and 200 years have been estimated regarding total rainfall amount at specific rain-gauges [C.F.Umbria, 2013].

event	initial time	fcst range	run code	description
Nov 2013	11/11/2013 00 UTC	+45h	CNTR	control run
			SST+	SST +2 in the Adriatic Sea
			SST-	SST -2 in the Adriatic Sea
			nofluxN	both fluxes removed in the N-box
			nolatN	latent flux removed in the N-box
			nosenN	sensible flux removed in the N-box
			nofluxS	both fluxes removed in the S-box

Table 4.8: List and codes of the simulations performed for the November 2013 event.

4.5.1 Synoptic analysis

The synoptic forcing for the November 2013 case is particularly efficient in mantaining the Bora flow for a long time: differently from what occurred in the February and September 2012 cases, the cyclone trajectory displaced more to the South and the low pressure system remains for a couple of days in the South Tyrrhenian Sea favouring a stronger Bora inflow, both at the surface and at upper levels.

At 500 hPa a cut-off is settled between two anticyclonic ridges located at the edge of the domain over Spain and over Turkey. The development of the large scale disturbance along a meridional direction favours the stationarity of the cyclone in the Mediterranean basin (Fig. 4.23a) where it deepens, up to a pressure value of 990 hPa at the surface. A wide cyclonic circulation settles over Italy characterized by two main inflow paths: the first at the North of the Alps and the second connected to the Bora outbreak. A pressure gradient larger than 30 hPa in a spatial-range of few hundreds kilometers (from Austria to Central Italy) is predicted at sea level and consequently the wind speed shows high values in the whole area affected by the cut-off low: the Rhone Valley and the southern France, the northern Adriatic and the Central Tyrrhenian Sea. Wind speed exceeding 35 $m \cdot s^{-1}$ at 850 hPa are predicted over that areas for all the simulation period (Fig. 4.23b).

The isotherms at 850 hPa (not shown) and at 12 UTC on 11 November attain a value of $-6°\,C$ next to the Alps and of $+2°\,C$ in front of the North Africa coast.

(a)   (b)
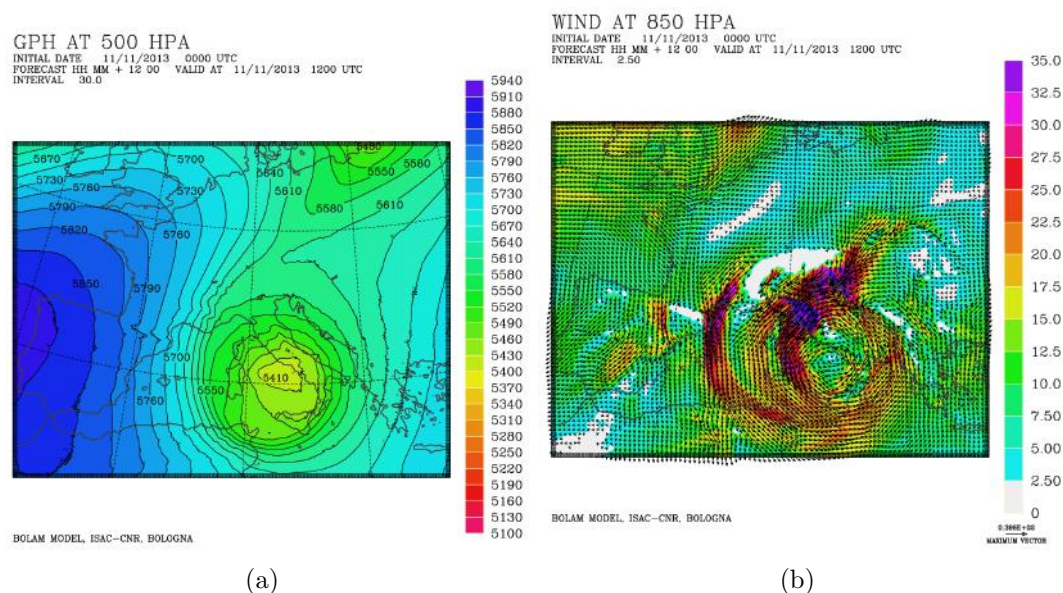
Figure 4.23: Geopotential height at 500 hPa (a) and wind field at 850 hPa (b), BOLAM forecast valid at 12 UTC on 11 November 2013.

4.5.2   Simulated fields

The simulation starts at 00 UTC on 11 November. The total precipitation amounts forecasted in 45h are shown in Fig. 4.24a: values in excess of 300mm are indicated over a long strip approximately superimposed to the highest orography, with individual peaks exceeding 500mm. The values rapidly decrease moving towards the coast especially in the northern half of the affected area while to the South more than 100mm/45h are still predicted over the coastal area. The precipitation field over the sea is characterized by a band oriented from the South-East to the North-West located at the border between Marche and Abruzzo right along the area affected by the cyclonic circulation where the Bora wind and the southern warm inflow converge. It is associated with moderate total amount in a short time-interval. It is important to note that this convergence pattern is observed for all the three cyclonic cases considered in the present work (Fig. 4.6b, Fig. 4.16b and Fig. 4.24b). Precipitations initially affects mainly the Romagna and northern part of Marche regions while in a second phase, during the evening of 11 November, the most intense phenomena are simulated over an area among Marche, eastern Umbria and northern Abruzzo. Fig. 4.24(b) which is referred to the interval 18 UTC - 21 UTC on 11 November clearly shows the typical precipitation pattern of the second phase of the event with severe condition to the South.

The wind field above the sea show the typical jet-pattern of Bora events: at the beginning 5 jets can be recognised but suddenly two of them merge (Senj and Bakar jets) and finally a four-jet pattern establishes by 21 UTC on 11 November (Fig. 4.25b).
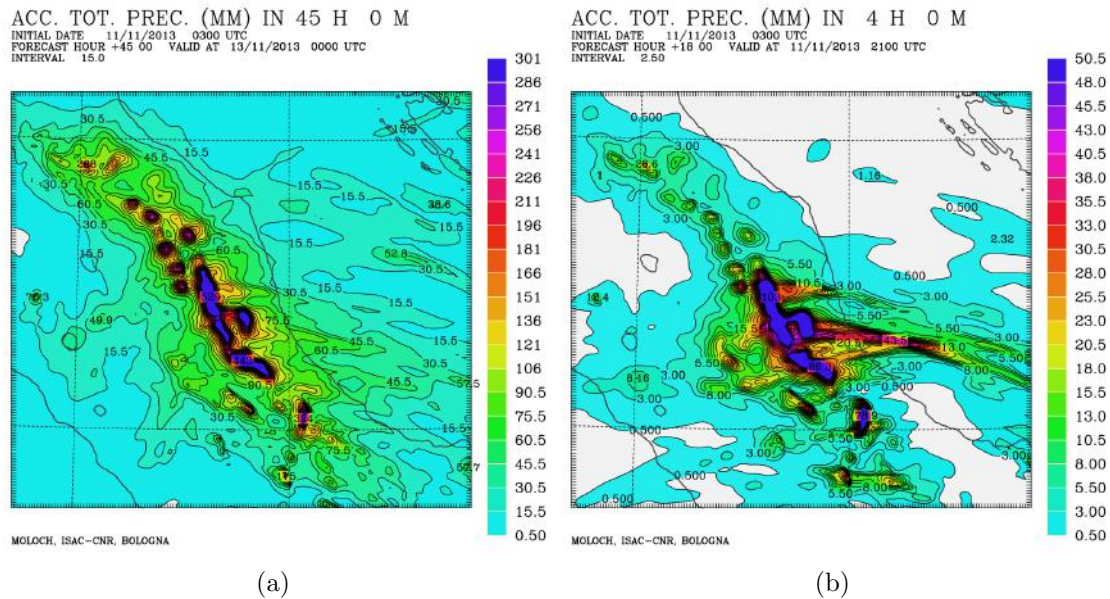
Figure 4.24: Total accumulated precipitation forecast by MOLOCH in 45h (a) from 03 UTC, 11 November 2013 to 00 UTC, 13 November 2013 and in 3h (b) from 18 UTC to 21 UTC on 11 November 2013.

At variance with the previous cases, Bora affects also the central part of the Adriatic, at least in the lowest 1000 m from the surface. The cyclone is centered in the southern Tyrrhenian Sea and the associated circulation is not able to confine Bora to the northern part of the Adriatic basin (whilst it changes at 850 hPa as in Fig. 4.25a). Only at 12 UTC on 12 November, when the Bora intensity decreases, the flow over the Adriatic Sea turns southeasterly at lower levels too.

The heat fluxes field shows the same features already seen for the previous cases. However the values are lower on average and latent heat fluxes attain 500 $W \cdot m^{-2}$ and sensible heat fluxes values 250 $W \cdot m^{-2}$ (Fig. 4.25c-d) at most.

(a)

(b)

(c)

(d)
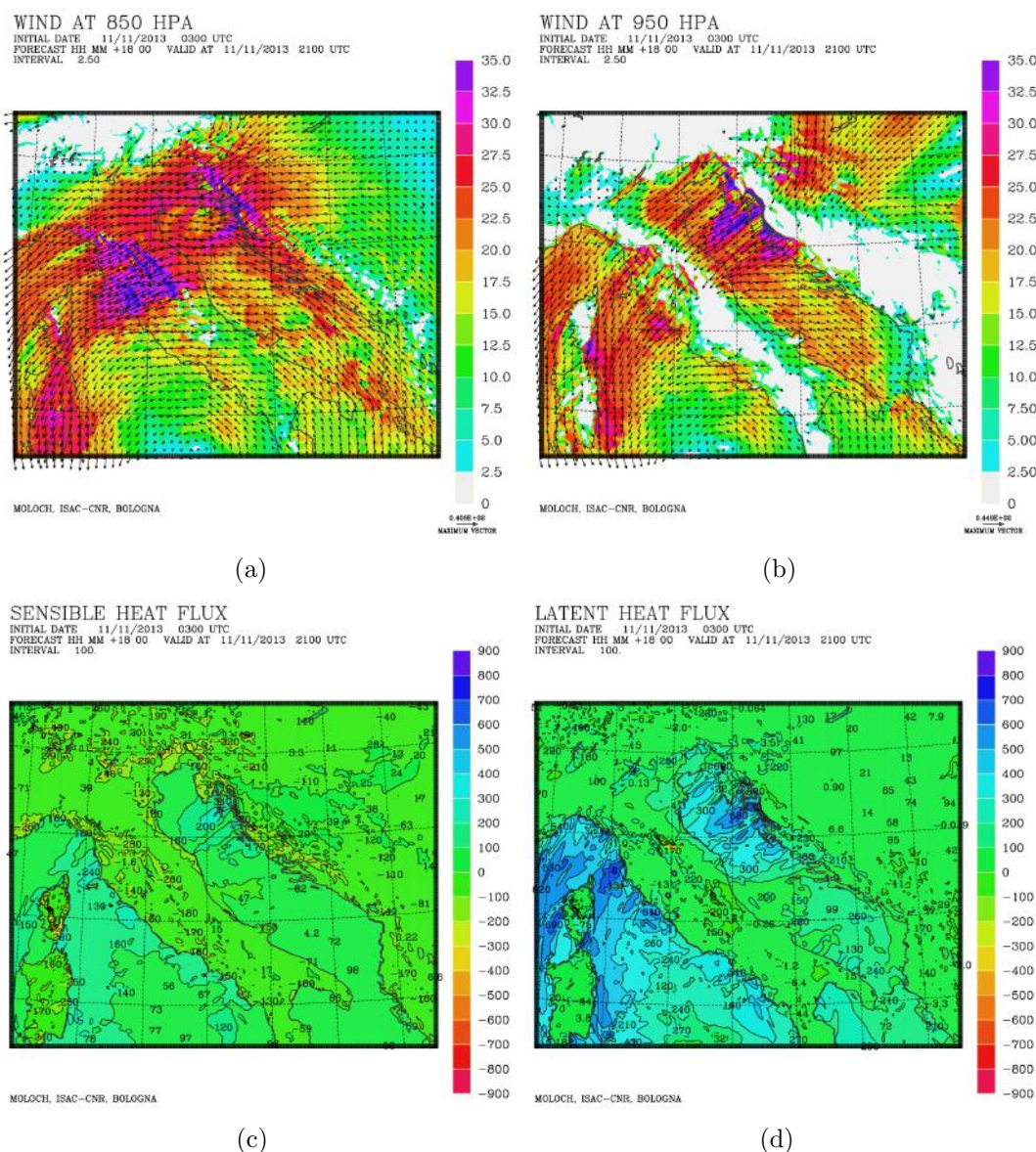
Figure 4.25: Wind field forecast by MOLOCH at 850 hPa (a) and at 950 hPa (b), sensible (c) and latent (d) heat fluxes, valid at 18 UTC on 11 November 2013.

4.5.3 Comparison with observations

The evaluation of the forecast performances for this case and for the next ones is done considering the precipitation field only. The simulated 45h-rainfall pattern (actually snowfall above 1800 m) is that in Fig. 4.24a and is characterized by larger values along the Apennines with several individual peaks and lower values on the coast. Interpolated

maps of rain-gauges data belonging to Marche and Umbria networks are used and confirm that largest values are recorded next to the mountains on both the western slopes in Umbria (Fig. 4.26(a)) and the eastern slopes in Southern Marche (Fig. 4.26(b)). A set of rain-gauges measurements is proposed in Tab. 4.9 where shaded station are located in proximity to the peaks predicted by the simulation: a great accordance is observed.

| (a) | (b) |
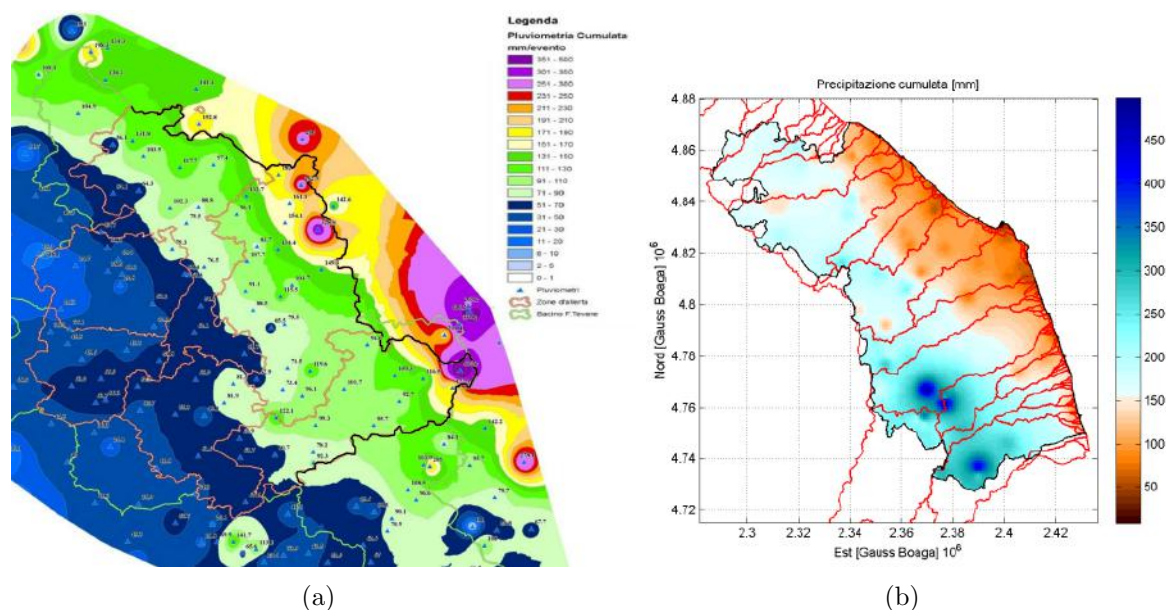
Figure 4.26: Interpolated data by Umbria (a) and Marche (b) Regional Agencies rain-gauges networks for the period 00 UTC, 10 November - 00 UTC, 13 November (Umbria) and 12 UTC, 11 November - 00 UTC, 13 November (Marche). Source: [C.F.Umbria, 2013], C.F. Abruzzo.

A radar reflectivity image referred to 11 November in the evening is shown in Fig. 4.27. The reflectivity peaks, that persist over the same area for several hours, matches with the northern precipitation peak simulated by MOLOCH over Romagna Apennine. The image is also significant for the clearly visible pattern of parallel narrow bands of larger rainfalls, perpendicular to the Apennines, that are typical of Bora cases.

station	mm/48h	station	mm/48h
Verghereto (FC)	99	Camerino (MC)	192.4
Novafeltria (RN)	90.6	Pintura di Bolognola (MC)	449.7
Gualdo Tadino (PG)	311.8	Fiastra Trebbio (MC)	441.4
Monte Cucco (PG)	248.4	Acquasanta Terme (AP)	398

Table 4.9: Total rainfall amount recorded in 48h (00 UTC, 11 November 2013 - 00 UTC, 13 November 2013) at selected raing-gauges. Source: [ARPA-SIMC, 2013a], [C.F.Umbria, 2013], [C.F.Marche, 2013]. Shaded stations are located in the areas where MOLOCH forecast maximum rainfall.
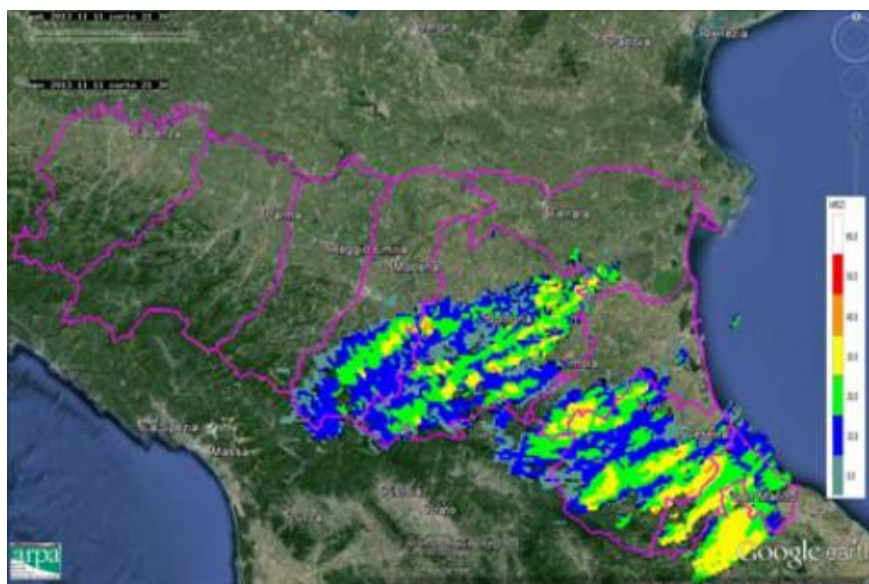

Figure 4.27: Radar reflectivity at 21.30 UTC on 11 November 2013 over Romagna. Source: [ARPA-SIMC, 2013b].

4.5.4 Sensitivity tests

The precipitation field for this case is more sensitive with respect to the two previous cyclonic cases to SST departures. Moreover it is also characterized by an unexpected behaviour regarding the SST- test. In particular the SST+ test is associated with a +18% of precipitation in the Romagna box (Tab. 4.10) and with a larger percentage increase in the sea box, where the average total rainfall jumps by 60% from 20mm to more than 30mm in 45h with respect to CNTRL run. Together with the increase over Romagna and Adriatic Sea, a minimal decrease is once again observed as regards the Central Apennines box (-3%).

The behaviour of Central Appenine box is controversial since precipitation decreases if SST is increased, but at the same time a strong increase in rainfall amount is predicted for the sea box. This feature has been observed for all the three cyclonic Bora cases and can be explained considering that the sea box is almost exactly located in front of the Central Apennine box (Fig. 4.3) and that a warmer sea may favor the convection that can deplete the water vapour above the sea, thus decreasing the moisture of the air column approaching the coast (Fig. 4.28). This phenomenon does not happen to the North where the atmosphere is more stable (note that the sea box also encompasses the warmer inflow induced by the cyclone) and the precipitation are mainly due to orographic lifting; in fact no precipitation is expected above the sea beyond the 43th parallel.

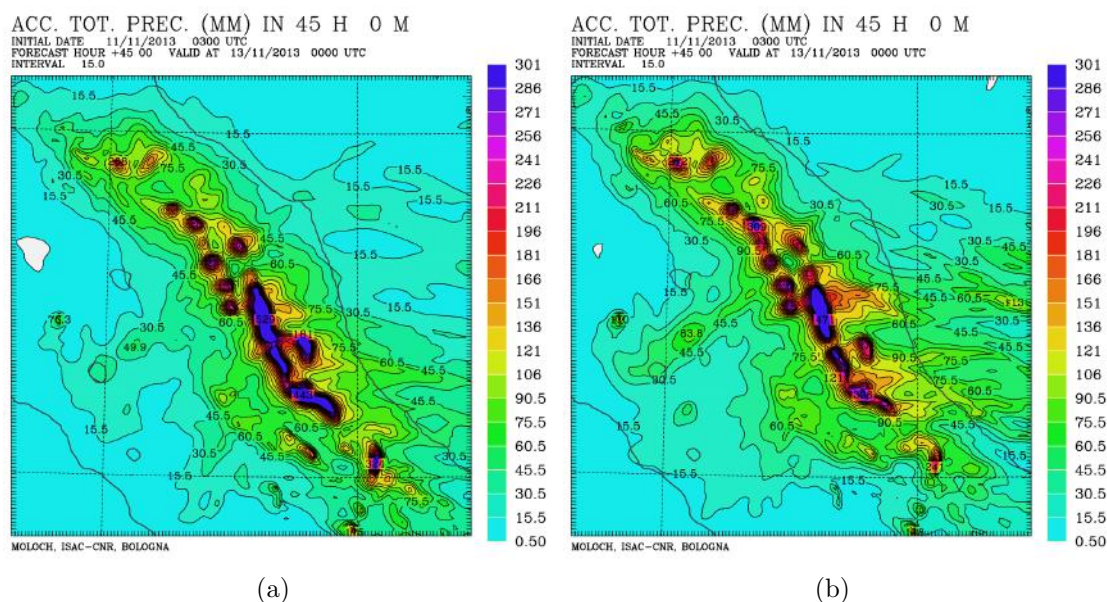(a)   (b)

Figure 4.28: Total accumulated precipitation in 45h for CNTRL run (a) and SST+ run (b), MOLOCH forecast valid from 03 UTC, 11 November 2013 to 00 UTC, 13 November 2013.

The SST- simulation, contrary to the other Bora cases discussed, still results in increasing rainfall amounts over both Romagna and Adriatic Sea boxes while no effect is expected for the Central Apennine box.

As regards heat fluxes sensitivity tests the November case confirms the fact that the removal of all the fluxes or the latent flux only has almost the same impact on the precipitation. In particular, as observed for the other cyclonic cases, the largest effects are simulated for the Romagna box (-30% for this case) and for the Apennines box (-15%) and the test without sensible heat flux (*nosenN*) induces a change that is less than the half of these values (Tab. 4.10).

Finally the *nofluxS* simulation does not produce any interesting features on the precipitation field neither it induces changes in the mesoscale pattern of northern Adriatic. Its effects have been unsignificant for the other cyclonic cases too thus it can be said that this specific test does not affect the area we are interested in and will not be further examined in Ch. 6.

November 2013

Romagna box			Central Apennines box			Sea box		
run	mm/h	var %	run	mm/h	var %	run	mm/h	var %
CNTRL	65.9		CNTRL	131.3		CNTRL	19.4	
SST+2	78.1	+18.5%	SST+2	127.6	-2.9%	SST+2	30.8	+58.8%
SST-2	71.7	+8.8%	SST-2	130.7	-0.5%	SST-2	22.1	+13.8%
nofluxN	45.4	-31%	nofluxN	112.2	-14.6%	nofluxN	18.9	-2.4%
nolatN	45.3	-31.3%	nolatN	114.2	-13%	nolatN	18.1	-6.7%
nosenN	55.6	-15.6%	nosenN	123.2	-6.2%	nosenN	19.1	-1.8%
nofluxS	66.8	+1.5%	nofluxS	124.5	-5.2%	nofluxS	19.4	0%

Table 4.10: Sensitivity tests results on the precipitation field.

4.6 December 2010

This case is not so impressive for Bora severity or possible wind speed record-values but it can be considered as an ordinary Bora event. The synoptic pattern is anticyclonic with intense wind clearly detectable over the whole Adriatic basin affecting Italy from the city of Trieste to Puglia coast. Differently from cyclonic cases the Bora flow is undisturbed since no cyclonic inflow occurs in Central Adriatic, vertical wind-shear does not develop and the convection above the sea is not favoured. Moreover a barrier wind jet, whose origin will be discussed, appears at the end of the forecast range.

What actually is remarkable regarding anticyclonic Bora events is that nearly all Italy, instead of the northern and central part only, experiences cold temperatures and snowfalls (Fig. 4.29).
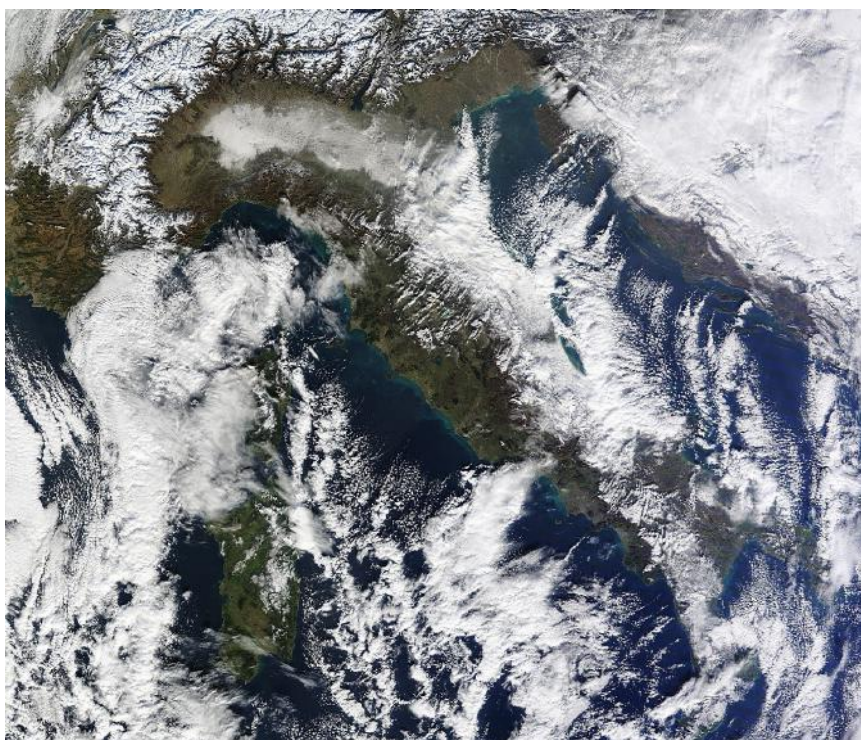

Figure 4.29: MODIS image of Italy on 16 December 2010 at 10.15 UTC.

event	initial time	fcst range	run code	description
Dic 2010	15/12/2010 00 UTC	+45h	CNTR	control run
			noflux	both fluxes removed on the sea

Table 4.11: List and codes of the simulations performed for the December 2010 event.

4.6.1 Synoptic analysis

The Atlantic blocking pattern is responsible for the mid-December 2010 cold spell. From the geopotential height at 500 hPa and the mean sea level pressure fields it can be inferred that the Azores High merges with an high pressure system over Greenland and allows a through to form to the East and to move from Scandinavia to more meridional latitudes. The descent results in a first pulse of cold air that enters into the Adriatic Sea as a Bora flow on the morning of 14 December and in a second pulse with a northerly trajectory the 17th that goes beyond the Alps and along their western side. A lee cyclon forms in the Tyrrhenian Sea and affects Italy in the following days.

At 500 hPa low geopotential height values, associated with a slight low pressure core at the surface, approch from the East (Fig. 4.30) while the cold inflow causes the isotherms over the Mediterranena Sea to be up to 5/6 degrees below zero at 850 hPa. The Adriatic Sea is affected by a steady easterly flow at the surface and at upper levels too, in the northern as well as in the southern basin (not shown). The specific timing of this event, with the Mediterranean cyclone that forms later with respect to the Bora outbreak, makes possible to have a 48 hours of continuous Bora flow.
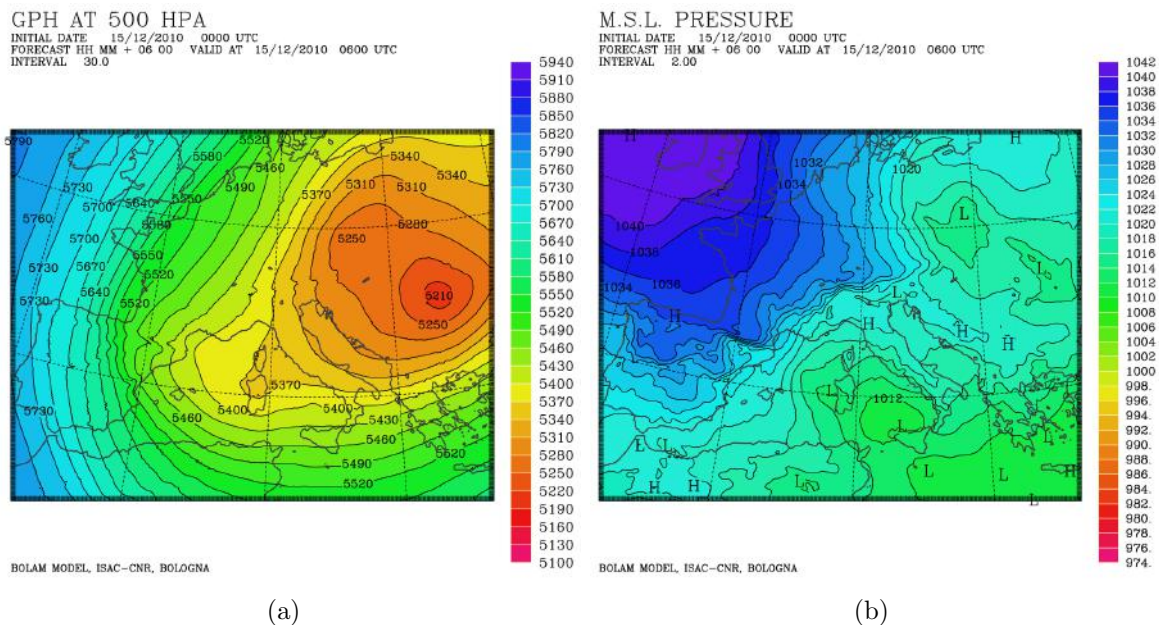

(a)   (b)

Figure 4.30: Geopotential height at 500 hPa (a) and mean sea level pressure (b), BOLAM forecast valid at 06 UTC on 15 December 2010.

4.6.2   Simulated fields

The forecast range for this case includes the phenomena related to the first outbreak: the simulation starts at 00 UTC on 15 December 2010. The precipitation amounts forecast for the December 2010 Bora outbreak are weak and distributed over a wide area that goes from Romagna to Abruzzo and encompasses the sea up to a hundred km offshore (Fig. 4.31). Four peaks exceeding 45mm in 45h are predicted over the mountains but most of the area experiences no more than 25 mm. The Apennines experiences quite all the forecast precipitation during the first 24 hours of the simulation, until 00 UTC on 16 December, while the coastal areas and the Romagna during the second day.
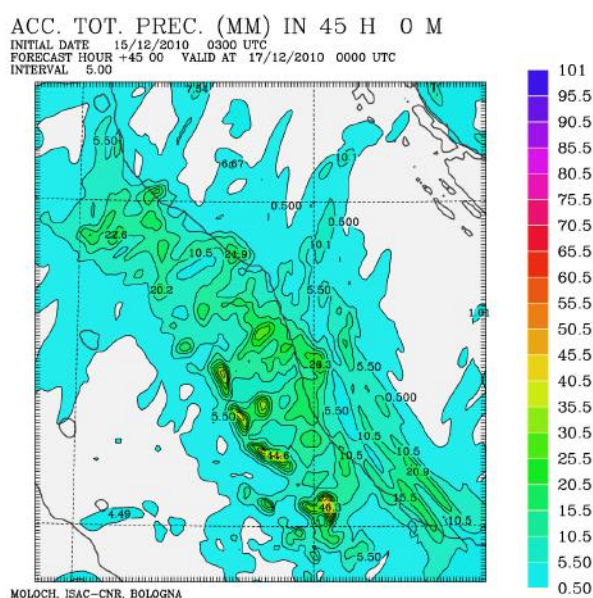

Figure 4.31: Total accumulated precipitation forecast by MOLOCH in 45h from 03 UTC, 15 December 2010 to 00 UTC, 17 December 2010.

Th wind field shows the typical jet-pattern: actually the Trieste jet is not forecasted while the southernmost jets, that were prevented to form in the cyclonic cases, are now better defined in the simulation even if not particularly strong. In the most intense phase, between 00 UTC and 12 UTC on 16 December, typical values are between 14 $m/cdots^{-1}$ and 20 $m/cdots^{-1}$ close to the eastern Adriatic coast only (Fig. 4.32a). By 12 UTC of the same day a sudden wind speed drop is forecasted and the wind turns to southeasterly in front of the Apennines (from lower levels to 850 hPa) as a barrier wind. The largest related wind speed are simulated at 950 hPa with mean values around 15 $m/cdots^{-1}$ (Fig. 4.32b).

At 850 hPa the forecasted wind flow is northeasterly and moderate over the northern Adriatic while at 700 hPa it turns slightly from the North (not shown). The wind is weak over the southern Adriatic and constant during all the period. It can be said that the

(a)

(b)

(c)

(d)
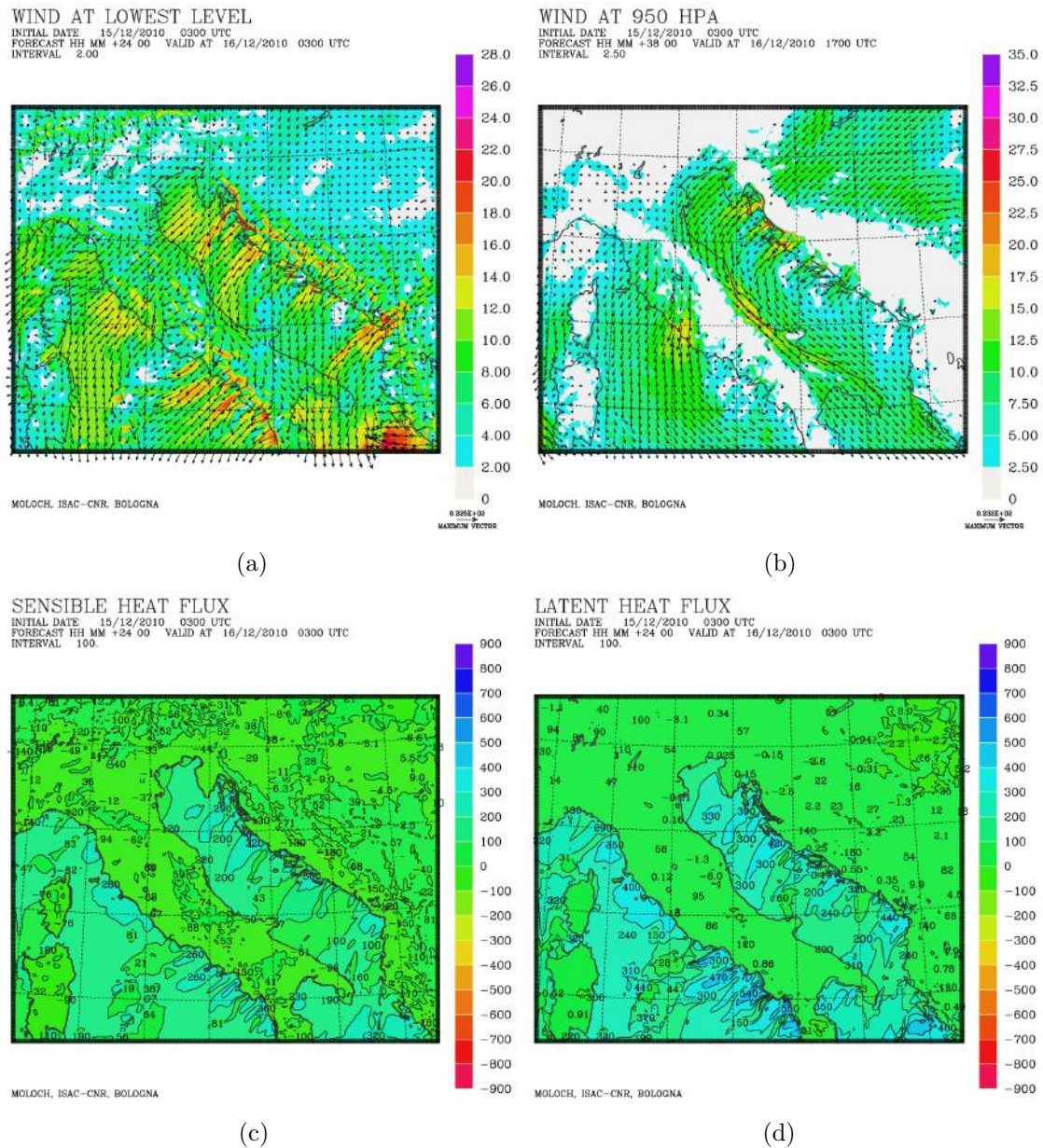
Figure 4.32: Wind field forecast by MOLOCH at lowest level ($\sim 72m$) at 03 UTC on 16 December 2010 (a) and at 950 hPa at 17 UTC on 16 December 2010 (b). Sensible (c) and latent (d) heat fluxes forecast by MOLOCH at 03 UTC on 16 December 2010.

48 hours considered for this Bora case are affected by a sort of transition period during which a weak northeasterly flow still persists over the Adriatic but is not supported at synoptic scale where the pattern is changing in response to a through descending from

Great Britain. This situation is likely to be associated with anticyclonic Bora pattern for the absence of a Mediterranean cyclone and for the steady Bora flow along the whole Adriatic basin.

The heat fluxes are not as relevant as in the cyclonic cases mainly because of weaker wind speed but larger values are forecasted over the southern Adriatic Sea, always in correspondence to the LLJ (Fig. 4.32). Latent heat fluxes still attains higher values (up to 400 $W \cdot m^{-2}$) than sensible heat ones.

4.6.3   Sensitivity tests

For the anticyclonic cases only one sensitivity test is performed (*noflux*), removing heat fluxes (both latent and sensible heat) over the whole Adriatic (Fig. 4.2). The SST sensitivity tests performed for the previous cases have shown that there is no impact on the mesoscale evolution and that the only detectable effect is a modification of total rainfall amount by a quantity that is, however, small-to-moderate. Moreover, considering the typical antyciclonic synoptic pattern, there is no reason why northern and southern Adriatic Sea would affect in a different manner rainfalls or snowfalls over Italy since the wind flow is steady, northeasterly and aligned over the whole basin and no other differences can be found latitudinally. Thus it is decided not to consider all the potential combinations of sensitivity tests as for the cyclonic cases.

The *noflux* test applied to the December 2010 case reveals how the absence of air-sea heat fluxes yields to impressive drops in the total precipitation amount forecast, by more than 94% for Romagna and sea boxes and by 84% for the Central Apennine box (Tab. 4.12). These values are significantly larger with respect to those obtained for the cyclonic cases whose reduction is from 20% to 60% thus they indicate that the role of air-sea heat fluxes is more important for anticyclonic Bora than for cyclonic Bora. Furthermore the air flow approaching Italy is predicted to be up to $4°C$ colder and up to 20% drier at 950 hPa than in the CNTR run especially to the South. The wind field is also modified over the Adriatic Sea where a general decrease in LLJ wind speed is predicted.

<div align="center">December 2010</div>

Romagna box			Central Apennines box			Sea box		
run	mm/h	var %	run	mm/h	var %	run	mm/h	var %
CNTRL	8.6		CNTRL	12		CNTRL	2.8	
noflux	0.3	-96.5%	noflux	1.9	-84.2%	noflux	0.1	-96.4%

Table 4.12: Sensitivity test results on the precipitation field.

4.7   December 2014

The event occurred at the end of 2014 is a clear example of an anticyclonic Bora pattern since the wind flow is intense all along the vertical profile and along the whole Adriatic coast. The area affected by intense precipitation is the central and southern Apennines windward side where moderate snowfall amount are recorded. The eastern flow lasts for several days, from 28 December 2014 to 02 January 2015.

As in the previous case, that of December 2010, this event does not stands out for severity but what is peculiar is the involvement of the southern basin. Moreover, among all the Bora events accounted in the present work, in this case we can talk about a possible ASE (see Ch. 2) since no moisture feeding is provided by outer sources but the Adriatic Sea itself and snowfalls peaks are observed in inland together with typical cloud-bands pattern (Fig. 4.33).
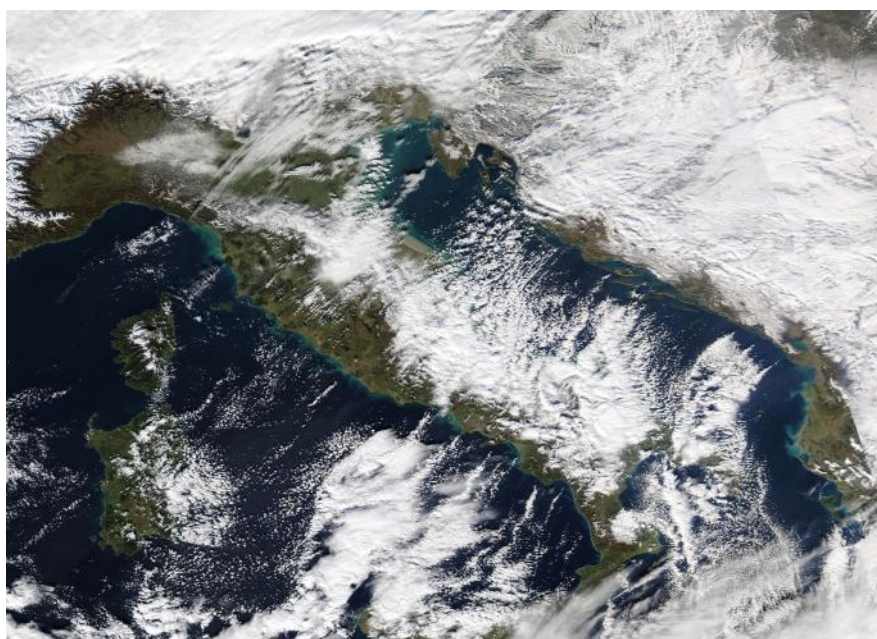

Figure 4.33: MODIS image of Italy on 30 December 2014 at 10.15 UTC.

event	initial time	fcst range	run code	description
Dic 2014	30/12/2014 00 UTC	+45h	CNTR	control run
			noflux	both fluxes removed on the sea

Table 4.13: List and codes of the simulations performed for the December 2014 event.

4.7.1   Synoptic analysis

The synoptic circulation for this event is characterised by the descent of a retrogressive wave from Russia towards the Egean Sea. This deep through is located at 500 hPa to the North-East of the Balcans where a cut-off is occurring while the surface low pressure core already stands over Greece (Fig. 4.34a-b). The whole system is longitudinally stretched because of a fast-moving high pressure ridge coming from the Atlantic Ocean (up to 1040 hPa at sea level) that is expanding North to the Alps and forces the synoptic circulation along the parallels.

Cold air (the core is at $-19°C$ at 850 hPa) comes from continental Eurasia, flows along the southern edge of the ridge and runs orthogonally into the Dinaric Alps from the North-East (not shown). Later on, the wind flow turns to easterly at all levels partially supported by the counterclockwise circulation of the low pressure system over the Egean Sea. At the end of the period considered, that is at 00 UTC on 01 January 2015, this cyclone progressively moves away and allows the Atlantic ridge to extend over Southern Europe in the following days.
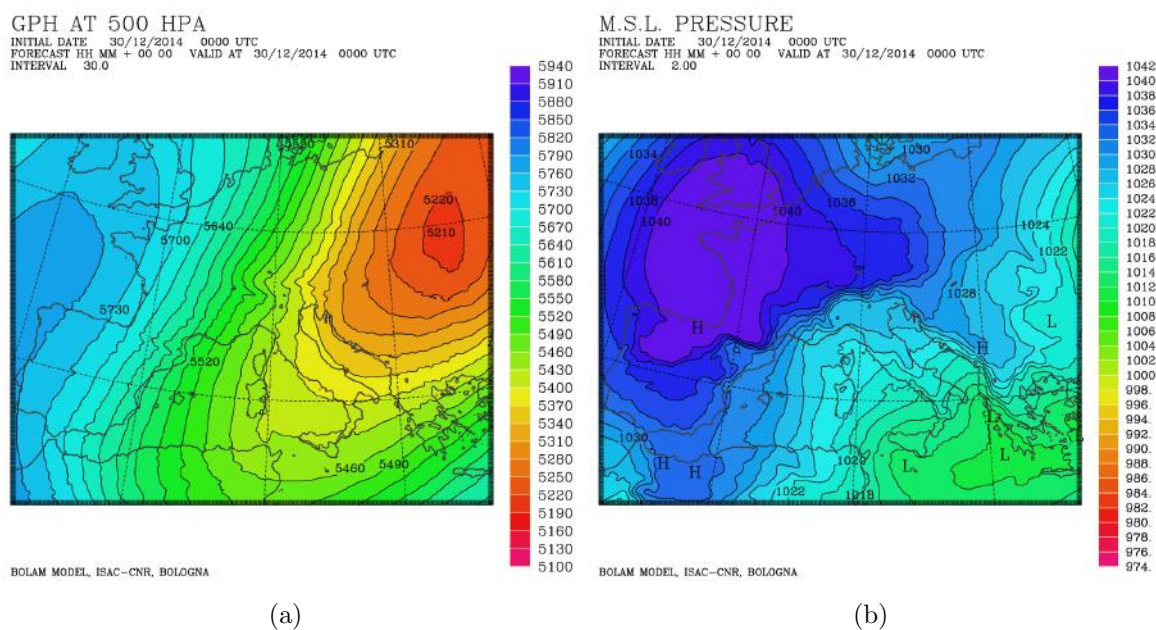

(a)   (b)

Figure 4.34: Geopotential height at 500 hPa (a) and mean sea level pressure (b), BOLAM forecast valid at 00 UTC on 30 December 2014.

4.7.2   Simulated fields

The simulation starts at 00 UTC on 30 December 2014. Also in this second anticyclonic case, the largest precipitation amounts are forecasted over the mountain areas (Fig. 4.35a). The precipitation field, mainly associated with snowfalls, shows a spotted pattern with peaks (168mm and 101mm in 45h) in correspondence to the Apennines crest. The model simulates the precipitation along narrow bands aligned with the LLJs as already pointed out in Sec. 4.7 and Fig. 4.33 with the maximum values at their end. In Fig. 4.35b a 6h-time interval has been isolated to better show this feature.

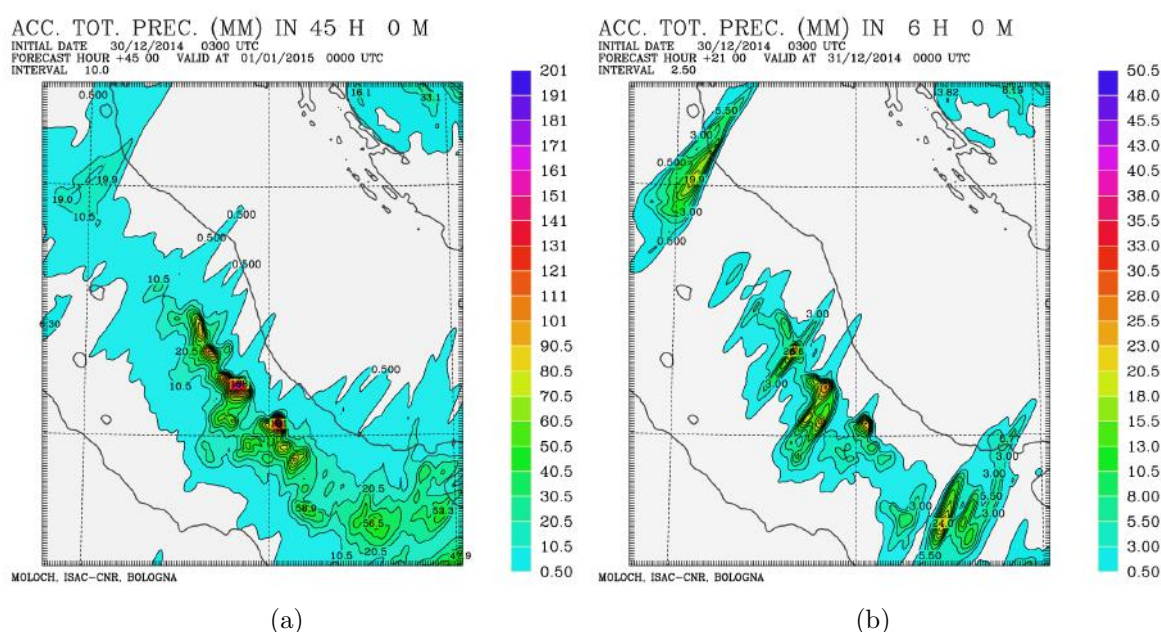(a)   (b)

Figure 4.35: Total accumulated precipitation forecast by MOLOCH in 45h (a) from 03 UTC, 30 December 2014 to 00 UTC, 01 January 2015 and in 6h (b) from 21 UTC, 30 December 2014 to 00 UTC, 31 December 2014.

This event affects the southern part of the Adriatic basin more than the northern one. The LLJs, also those that blow from the southern Dinaric gaps, are well-defined according to the simulation while at 850 hPa a northward wind-shift is forecast because of the forcing of the through on the large scale circulation of the South Mediterranean Sea (Fig. 4.36a). Up to 8 jets can be recognised (Fig. 4.36b), all those suggested in Sec. 2.4.2. The associated wind speeds are constantly larger than 20 $m/cdots^{-1}$ for most of the time downstream to the Dinaric Alps but only for the northern jets the wind speed remains almost unchanged across the Adriatic Sea up to Italy.

The Adriatic Sea surface experiences very large heat exchanges since in this case all

the basin is affected by a strong Bora wind. Largest values are attained all along the jet trajectories (Fig. 4.36c-d) and an impressive drop of SST by $2°C$ in 45h globally from the Po delta to the Otranto channel is forecasted.
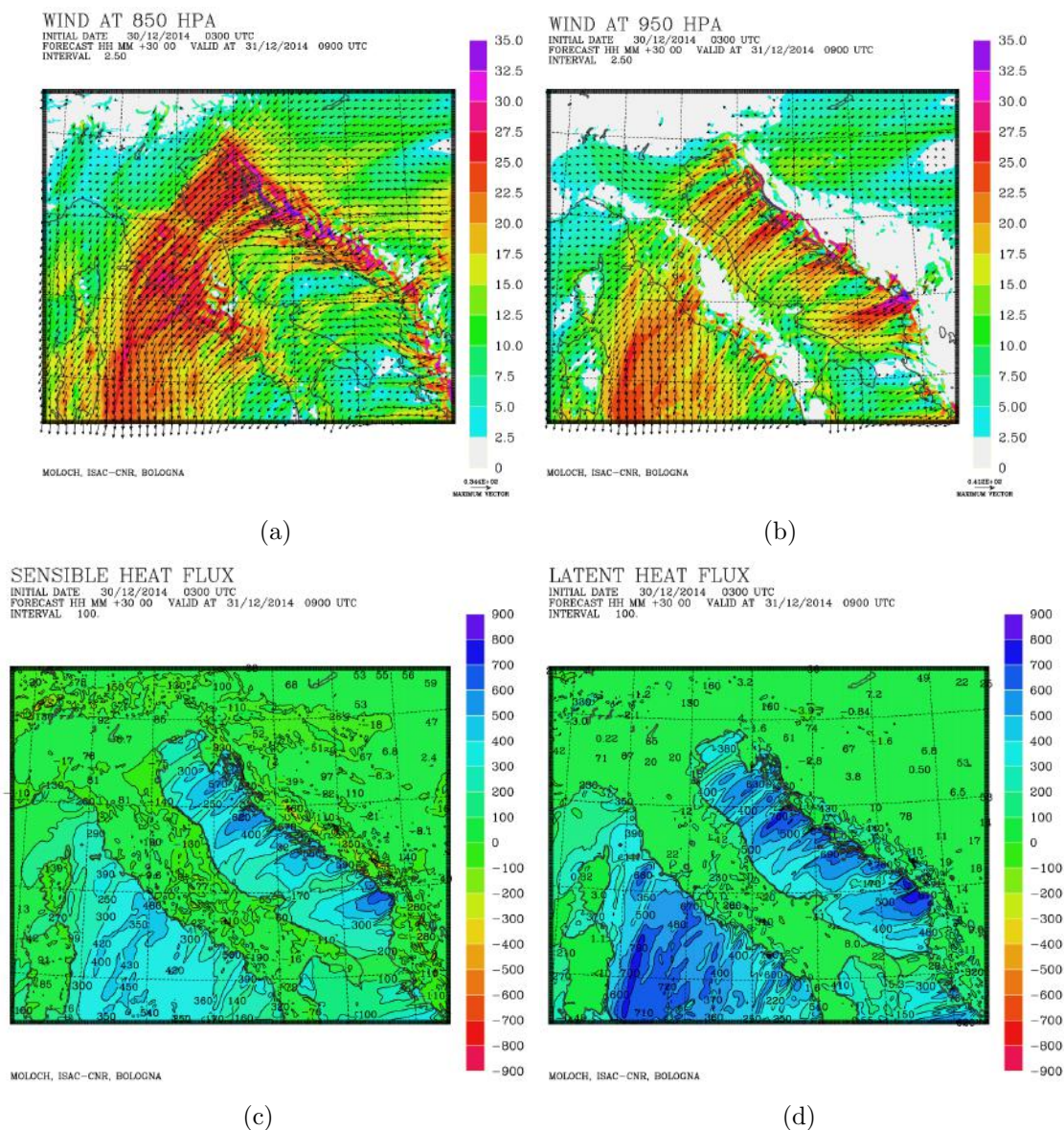

(a)

(b)

(c)

(d)

Figure 4.36: Wind field at 850 hPa (a) and at 950 hPa (b), sensible (c) and latent (d) heat fluxes, MOLOCH forecast valid at 09 UTC on 31 December 2014.

4.7.3 Sensitivity tests

The sensitivity test for the December 2014 case (*noflux* run) confirms the findings already dicussed for December 2010: the precipitation decreases to such an extent that in the Romagna box almost vanishes while the Central Appenines box experiences a fall by 78% with respect to CNTRL run (Tab. 4.14). No precipitation is predicted for the Adriatic Sea box both in CNTR run and in *noflux* run. A significant weakening of LLJ, on average about 5 $m/cdots^{-1}$ with respect to CNTRL run, is simulated (Fig. 4.37).

It is worth noting that for the anticyclonic cases, where no moisture feeding is provided by the cyclonic southern inflow, almost all the precipitation are due to orographic lifting in correspondence to the areas affected by strongest LLJ since, as the fluxes are setted to zero, the rainfall decrease is dramatic. In fact, and this is the second point, the LLJ weaken when heat fluxes are removed thus a crucial connection between them should be assessed (the issue is faced in Ch. 6).
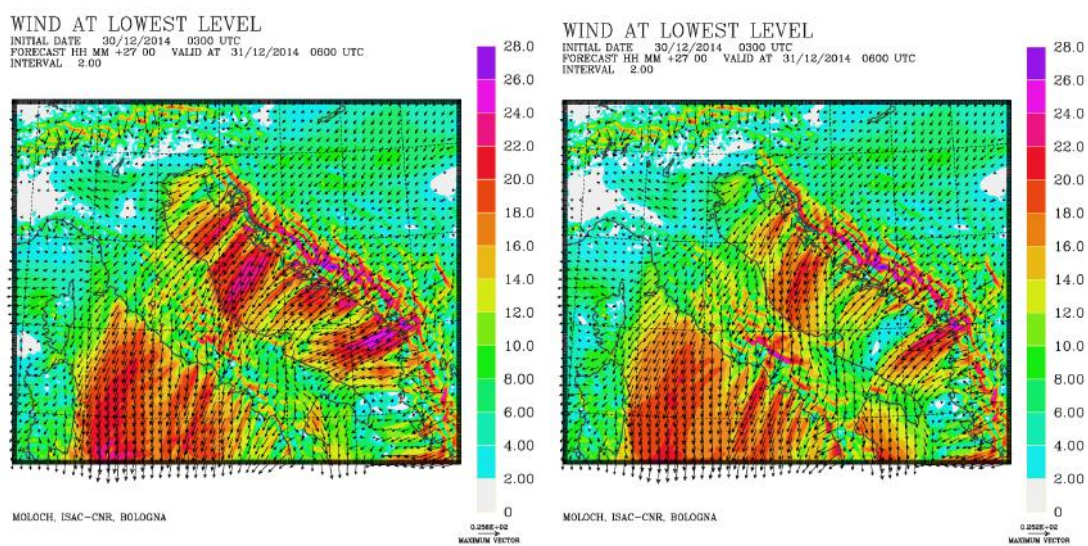

Figure 4.37: Wind field forecast by MOLOCH at lowest MOLOCH level ($\sim 72m$) for CNTRL run (a) and *noflux* run (b), valid at 06 UTC on 31 December 2014.

December 2014								
Romagna box			Central Apennines box			Sea box		
run	mm/h	var %	run	mm/h	var %	run	mm/h	var %
CNTRL	4.5		CNTRL	17.2		CNTRL	0	
noflux	0.1	-97.8%	noflux	3.8	-77.9%	noflux	0	/

Table 4.14: Sensitivity test results on the precipitation field.

Chapter 5

Profiles of water vapour fluxes and water balance

The sensitivity tests performed for each Bora case show that air-sea heat fluxes may have a remarkable impact on the precipitation over Italy and that the largest heat fluxes are observed in correspondence to the strongest wind speed bands. In this chapter the issue of a better characterization of the water vapour fluxes associated with the Bora wind above the Sea is faced. It was observed in Ch. 4 that the horizontal propagation of the LLJ over the Adriatic Sea may vary depending on several factors. The present chapter aims to analyse the water vapour flux structure along the sea: in Sec. 5.1 a focus on water vapour analysis and the diagnostic tools developed are described. In Sec. 5.2 along-coast water vapour fluxes profiles are presented while in Sec. 5.3 and 5.3.3 a complete atmospheric water balance is carried out over the Adriatic Sea.

5.1   Diagnostic tools for water vapour flux analysis

The wind modulation over the sea, the surface heat fluxes and the SST are mutually connected and vary one depending on the other via a feedback mechanism not yet fully understood. An important role is played by the SST input dataset since generally in NWP models, and MOLOCH is no exception, the SST field is allowed to change slowly because of constraints to deep sea temperature and to the parametrization scheme employed for the radiation fluxes (*slab model*). At the same time air-sea heat and momentum exchanges are double-acting: they strongly affect deep water mixing and Adriatic Sea circulation [Pullen et al., 2007] and they change the properties of the overhead air flow mainly raising the water vapour content and affecting the wind stress [Dorman et al., 2006].

The role of different water vapour sources (bottom fluxes or advection) is studied by means of two main diagnostic tools that have been developed:

- the evaluation of water vapour flux profiles, vertically integrated all along the Italian Adriatic coast;

- the computation of an atmospheric water balance over the Adriatic Sea.

In order to study the moisture flux evolution responsible for feeding heavy precipitation over the Italian shoreline and over the eastern-side of the Apennines, the evaluation of the water vapour flux crossing a virtual section which runs parallel to the coast is the keypoint. This kind of analysis will give information about the total amount of water vapour moving inland towards the Apennines. However, it does not provide information about the sources of moisture. The characterization of moisture flux for convective cases is the focus of a series of works on severe episodes occurred over France [Nuissier et al., 2008], [Ducrocq et al., 2008], [Duffourg and Ducrocq, 2011]. The authors show that the moisture feeding the heavy precipitation systems is provided by evaporation occurred over the Mediterranean Sea and over more distant ocean surfaces, depending on the synoptic conditions established the days before the event. Moreover it is shown from a similar study regarding Friuli-Venezia-Giulia, that rainfalls better correlate with the mean SST over the entire Mediterranean Sea than with the northern Adriatic only, supporting the idea that moisture coming from a large area is needed for the heaviest precipitation to occur [Manzato, 2007].

The computation of column integrated water vapour fluxes along the eastern coast of Italy is used to obtain information in addition to what can be deduced directly from the model outputs. The plots of the values obtained for each grid point all together along the coast, spanning over different heights and over the entire forecast range, give an overall view of the time and spatial evolution of the moisture inflow associated with the mean easterly wind component over the sea.

As previously pointed out, this is not enough for a full comprehension of the flux dynamics because informations about what happens before the water vapour impinges on the coast are still lacking and a second tool, more useful in this sense, is developed. It provides a water budget over selected volumes over the Adriatic basin, by means of properly defined boxes, taking into account all the terms that can play a role in water content transport. A similar study was carried out in California with the aim of investigating the three-dimensional changes in water vapour fluxes associated with an "atmospheric river" [Smith et al., 2010]. A water budget approch was also applied to a box that encompasses Switzerland to find a connection between water vapour fluxes and the extreme precipitations and floods that occured in that area in August 2005 [Koffi et al., 2013].

This kind of analysis, applied to Bora cases over the Adriatic Sea, has not been done yet. As part of this work, the atmospheric water balance and the vertically integrated vapour fluxes computation help to focus to those local situations that deserve particular attention. For example they are helpful in positioning cross-sections and in the selection of specific periods for comparisons among different events.

5.2 Water vapour profiles along the coast

It has been explained that is crucial to have various data about the easterly flow to better characterise the wind component that directly affects the Italian coast.

The water vapour flux vertically integrated up to a prescribed altitude is computed for each grid point of the model along the Adriatic coast. The first grid point over the Adriatic sea is selected for this purposes, identified by a land-sea mask value greater than 0.8. The selected coastal profile goes from Venice to the Gargano promontory (see the right side from Fig. 5.1 to Fig. 5.4).

The formula implemented in MOLOCH for the water vapour flux computation is

$$WV = \sum_{i=1}^{ztop} wr_i \cdot \rho_i \cdot z_i \tag{5.1}$$

where wr is the rotated wind intensity, ρ is the water vapour density, z is the thickness of each vertical layer and $ztop$ is the top level. The equation is dimensionally-consistent since the results are expressed in $[kg \cdot m^{-1} \cdot s^{-1}]$ that is a linear istantaneous flux.

The wind field is rotated on the MOLOCH grid and wr is computed as the wind component perpendicular to the direction of the Apennines. Although the northern Apennines present a slightly different orientation with respect to southern Apennines, a mean direction for the whole orographic chain (tilted by 30° with respect to the meridian) is considered.

The flux is computed summing over all the MOLOCH vertical levels up to the prescribed elevation.

A textual data file is created by MOLOCH and re-arranged with Matlab to produce graphical outputs. Two different types of graphs are presented:

- comparison among water vapour flux profiles referred to the same time but for different altitudes of the top level;

- comparison among CNTRL run and *noflux* runs at specific times.

In Fig. 5.1 and Fig. 5.2 the graphs belonging to the first type are presented. They are referred to significant time instants when the strongest Bora flow is simulated, typically in the first part of the forecast range.

The typical multiple wind-jet pattern can be recognised in the northern part of the Adriatic basin for the cyclonic cases also in the moisture flux along the Italian coast: a three-jet structure is clearly visible for the February case (Fig. 5.1a), two jets are distinguished for the September case (Fig. 5.1b) and four jets characterize the November case (Fig. 5.2a). Among the jets the southernmost attains the largest water wapour fluxes values: this is clear for the February and November cases but not so well-defined for the

September one for which the two jets are almost equivalent. The largest flux values are related to the autumn cases: the southermost September jet exceeds 350 $[kg \cdot m^{-1} \cdot s^{-1}]$, the southernmost November jet is characterized by a value of 600 $[kg \cdot m^{-1} \cdot s^{-1}]$ while the February one attains 150 $[kg \cdot m^{-1} \cdot s^{-1}]$.

The separation between the northern and southern Adriatic water vapour fluxes regimes is marked in all the cyclonic events by a drop in the water vapour fluxes values south of the last jet by more than half the jet value. The flux progressively raises moving southward and reaches another maximum.

A similar feature characterizes all the cyclonic events: the contribution to the water vapour fluxes associated with the northern Bora wind jets is mainly confined to the first 1500m-2000m and very low contributions come from the upper levels. On the other hand, in the southern part of the Adriatic basin, typically south of 43° N, an opposite situation is observed: the largest contributions are those above 3000m and the flux in the first layers up to 500m is nearly negligible. For the November case this pattern is not so defined and contributions above 3000m still counts for the Bora flow but a decrease in the importance of lower layers can be noticed to the South.

Recalling that the Bora wind is merged with the warmer cyclonic circulation flow in correspondence to the southernmost jet, a possible explanation for the observed behaviour is the following: the fact that the southernmost jet attains the largest value of the profile confirms the hypotesis that a large part of the water vapour content comes from the South (from the southern Adriatic or from the Mediterranean Sea) and that the transport of moisture from large distances by the cyclonic circulation is effective. Moreover the observed drop in water vapour fluxes is located in correspondence to the low pressure core and the southernmost maximum observed south of the minimum is connected to the southwesterly flow around the cyclone (since wind intensity is computed, the fluxes crossing the section from different directions always provide for a positive flux). It is worth noting that in the area affected by the Bora wind most of the contribution to the flow comes from lower levels (mainly up to 1000m), while the flow associated with the cyclonic circulation in the southern Adriatic is characterized by higher moisture content in the upper levels, typically above 3000m.

Finally, as regards anticyclonic Bora, only the December 2014 case (which is more significant with respect to the December 2010 one) is presented in Fig. 5.2b. The jet pattern is clearly visible and up to 8 jets (see Fig. 4.35b for comparison) are recognised. The pattern is different since the Bora wind affects uniformly all the Adriatic basin: the contribution up to 1000m is constant all along the coast, no drop occur and no significant water vapour flux is predicted above 5000m for the southern jets, while a significant upper-level component characterizes the flow to the North.
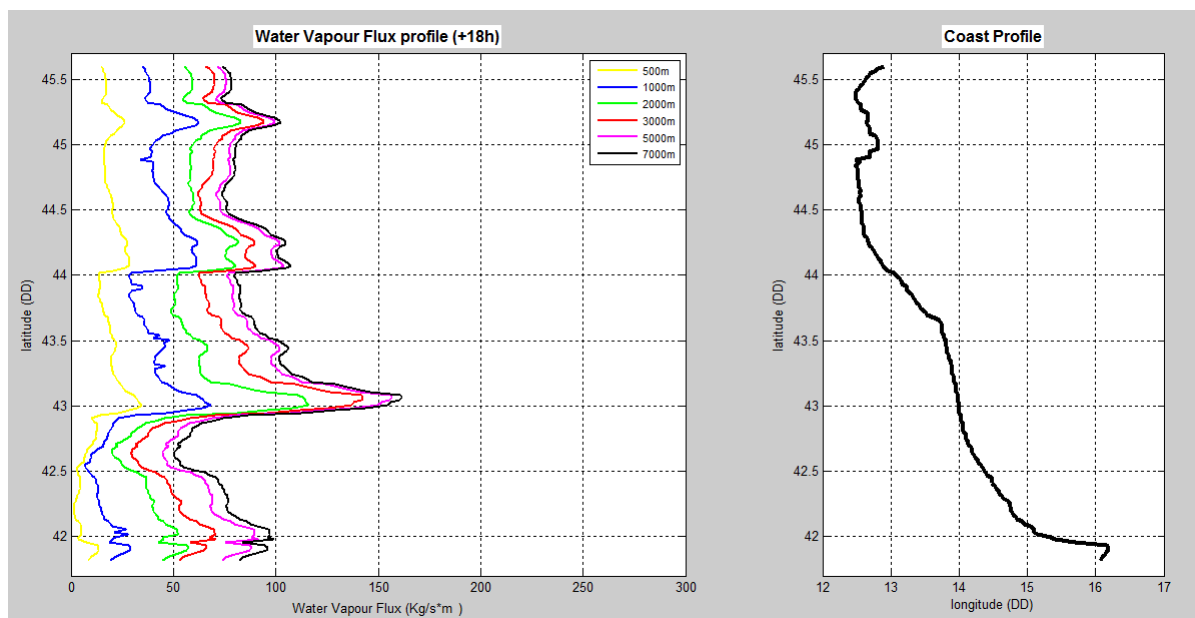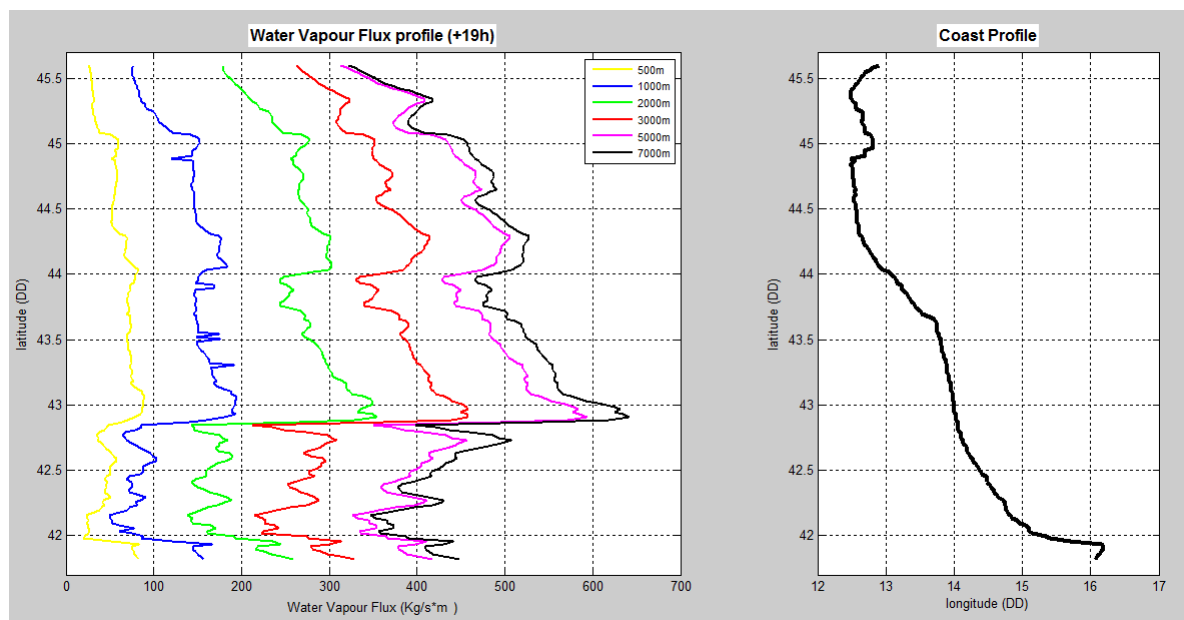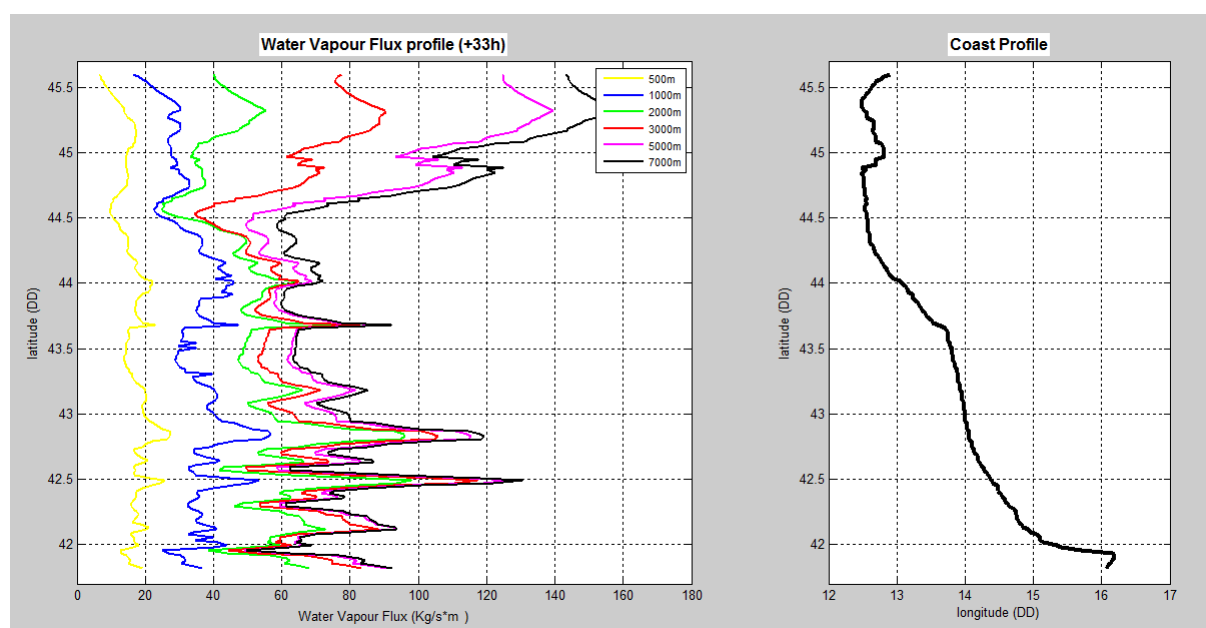
(a)
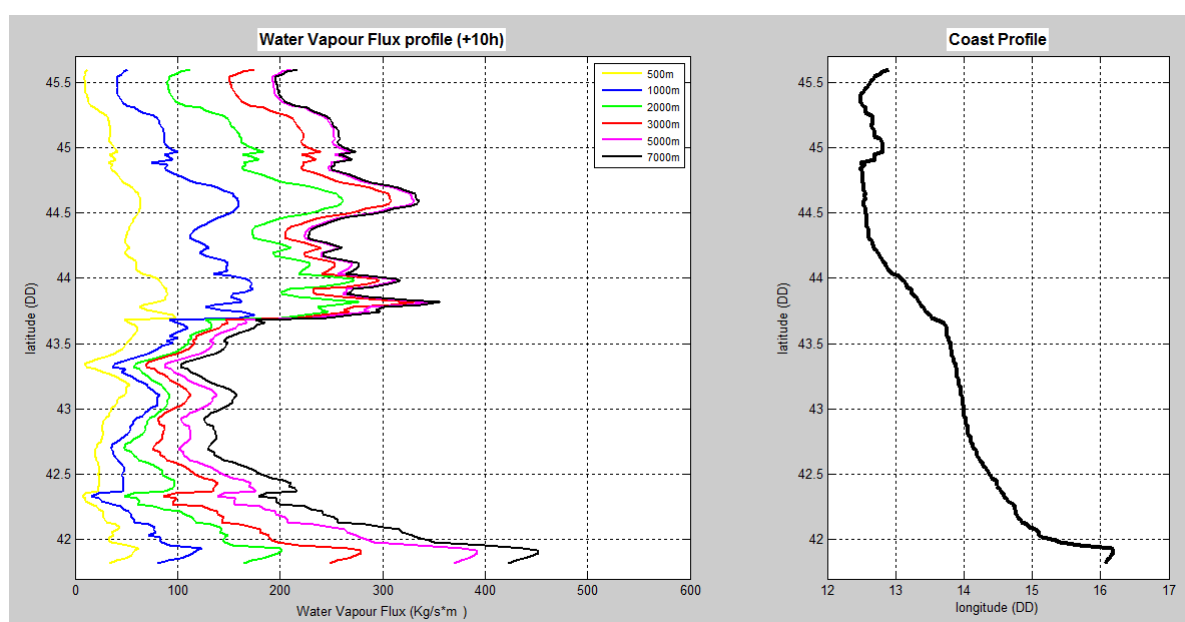
(b)

Figure 5.1: Water vapour flux profiles along the Italian coastline computed up to different heights at 09 UTC on 10 February 2012 (a) and at 13 UTC on 13 September 2012 (b), MOLOCH forecast.

(a)

(b)

Figure 5.2: Water vapour flux profiles along the Italian coastline computed up to different heights at 22 UTC on 11 November 2013 (a) and at 12 UTC on 31 December 2014 (b), MOLOCH forecast.

In Fig. 5.3 and Fig. 5.4 the comparison among water vapour profiles for the CNTRL run and the *noflux* runs are shown for the February 2012 and September 2012 cases. The top level is set at 2000m.

The *noflux* profiles show weaker flux values than the CNTRL profile for nearly all the forecast range. Intemediate flux values between the *nofluxN-nolatN* and the CNTRL ones are predicted for the *nosenN* test (sensible heat fluxes removed). The jet pattern is no more clearly recognisable at the specific time instant, in the CNTRL run as well, except for the southernmost jet whose peak attains the largest values of the profile. This peak is forecast also for the *nosenN* profile while *nofluxN* and *nolatN* have globally minor fluctuations.

This behaviour is consistent with the results obtained in the sensitivity tests in Ch. 4 for the precipitation field, where the largest decreases in total rainfall amount with respect to CNTRL simulation are predicted for *nofluxN* and *nolatN* runs and the impact of *nosenN* run is lower. This suggests that the removal of air-sea latent heat fluxes strongly modifies the water vapour content approaching Italy and prevents persistent severe precipitation to occur. Actually a water vapour flux decrease can be due to lower water vapour content or to lower wind speed (see Eq. 5.1). The atmospheric water balance over the Adriatic carried out in the next sections will account for this twofold issue.

South of the 43th parallel an inversion between the profiles occurs: the CNTRL run fluxes are lower than the *noflux* ones. This feature is common to all the cyclonic cases. Fig. 5.3b-c and Fig. 5.4b-c show the MOLOCH wind field forecast at 950 hPa for CNTRL and *nofluxN* runs at the time corresponding to the computation of the water vapour fluxes shown in Fig. 5.3a and Fig. 5.4a. It can be noted that, in the *nofluxN* runs, northwesterly barrier winds are predicted along the eastern-side of the Apennines with moderate wind speed (up to 20 $m \cdot s^{-1}$ for the February case). Moreover the surface low pressure core associated with the cyclone is shifted to the East with respect to CNTRL runs and is located above the Sea. The largest water vapour flux values for the *noflux* cases are thus connected with the apperence of the barrier wind which gives a positive contribution to the flux. The CNTRL run profiles values on the contrary decrease in that area because weak winds are predicted there as the cyclone is settled exactly over the coastline.

In Fig. 5.5 the comparison between CNTRL run and *noflux* runs profiles for the anticyclonic cases are shown. The main feature is that the simulations with removed heat fluxes (both sensible and latent heat for these cases) totally loose the jet pattern and no peaks are predicted for the water vapour fluxes at the coast. On the other hand, a weakening of LLJs was already noticed for the *noflux* simulations by the MOLOCH sensitivity tests output. This behaviour, that is common to cyclonic cases too, suggests that vertical heat fluxes at the Sea surface, horizontal water vapour fluxes at the Italian coast and total precipitation amounts recorded on the Apennines are strictly connected.
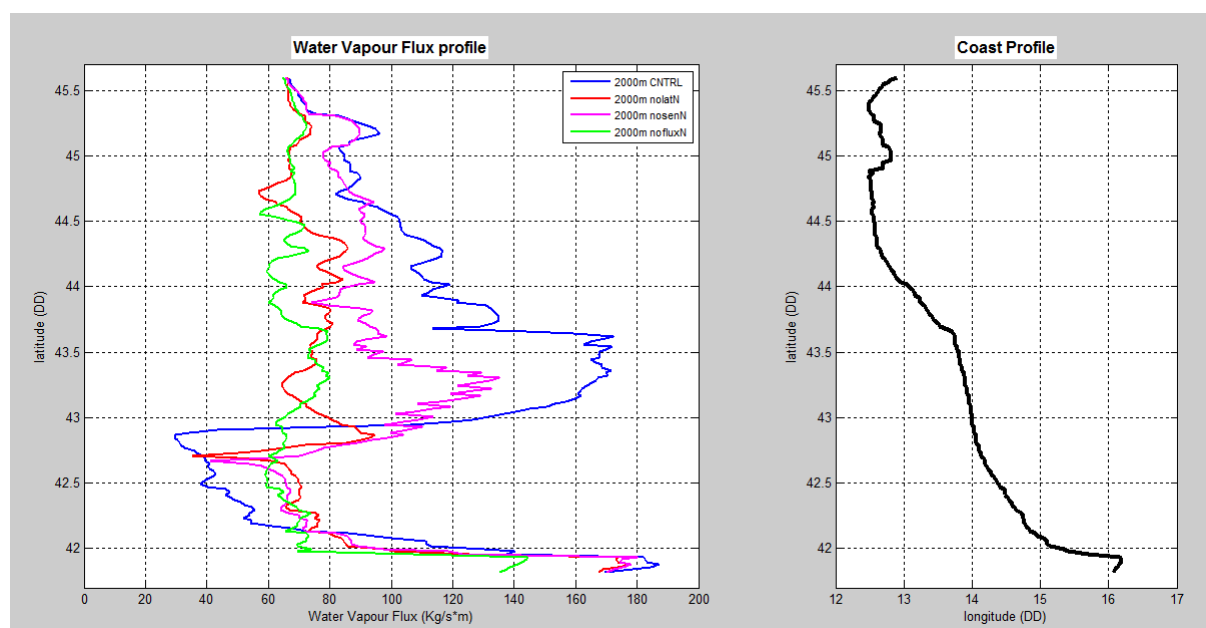
(a)
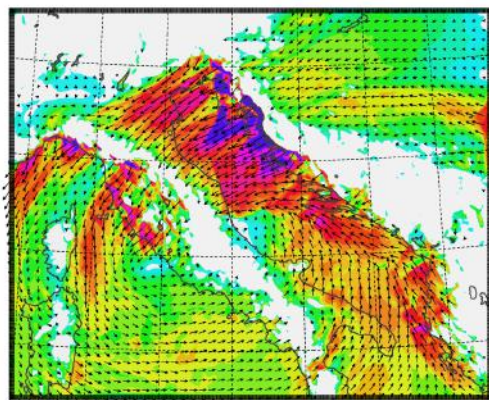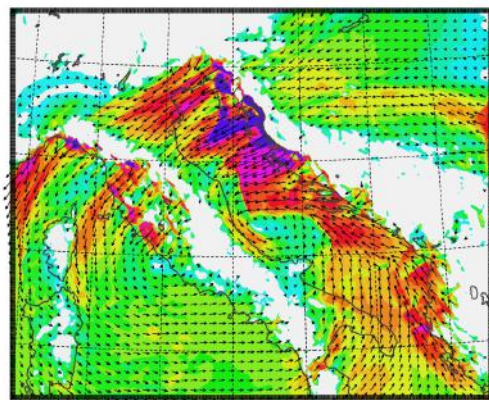
(b)   (c)

Figure 5.3: Comparison of water vapour flux profiles along the Italian coastline up to 2000m between CNTRL run and *noflux*-runs at 21 UTC on 10 February 2012 (a) and corresponding MOLOCH forecasts for 950 hPa wind field for the CNTRL run (b) and the *nofluxN* run (c)
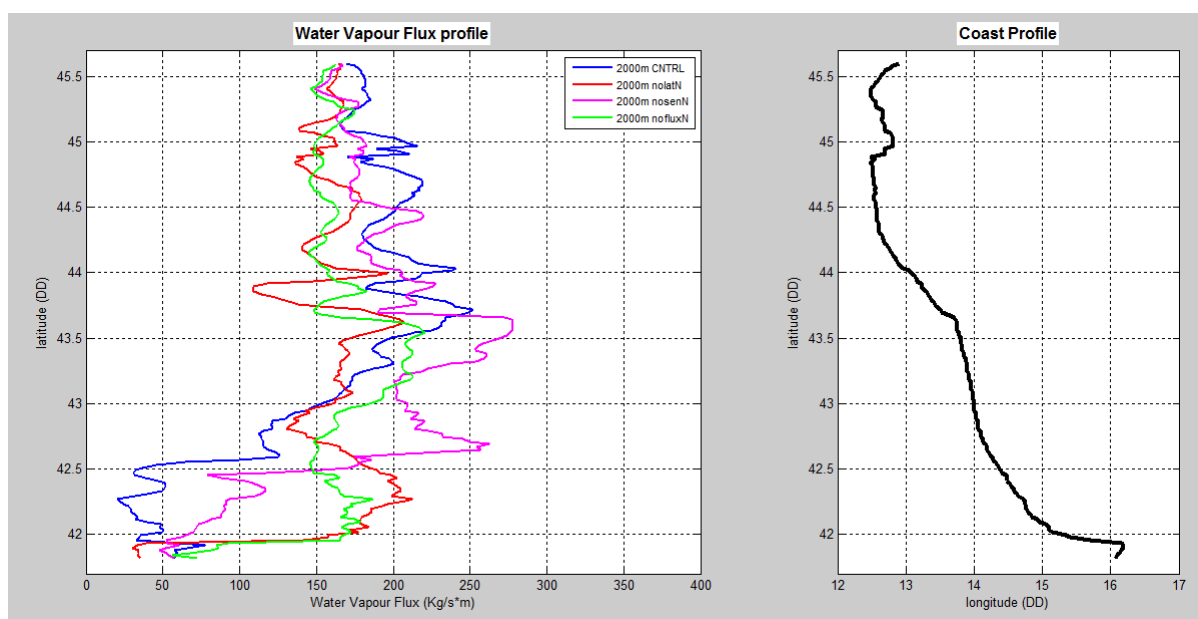
(a)

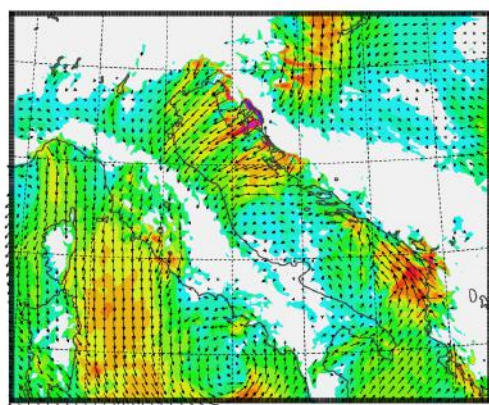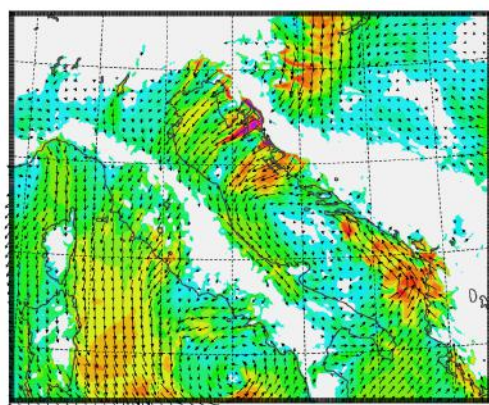(b)   (c)

Figure 5.4: Comparison of water vapour flux profiles along the Italian coastline up to 2000m between CNTRL run and *noflux*-runs at 09 UTC on 14 September 2012 (a) and correspondinf MOLOCH forecasts for 950 hPa wind speed for the CNTRL run (b) and the *nofluxN* run (c)
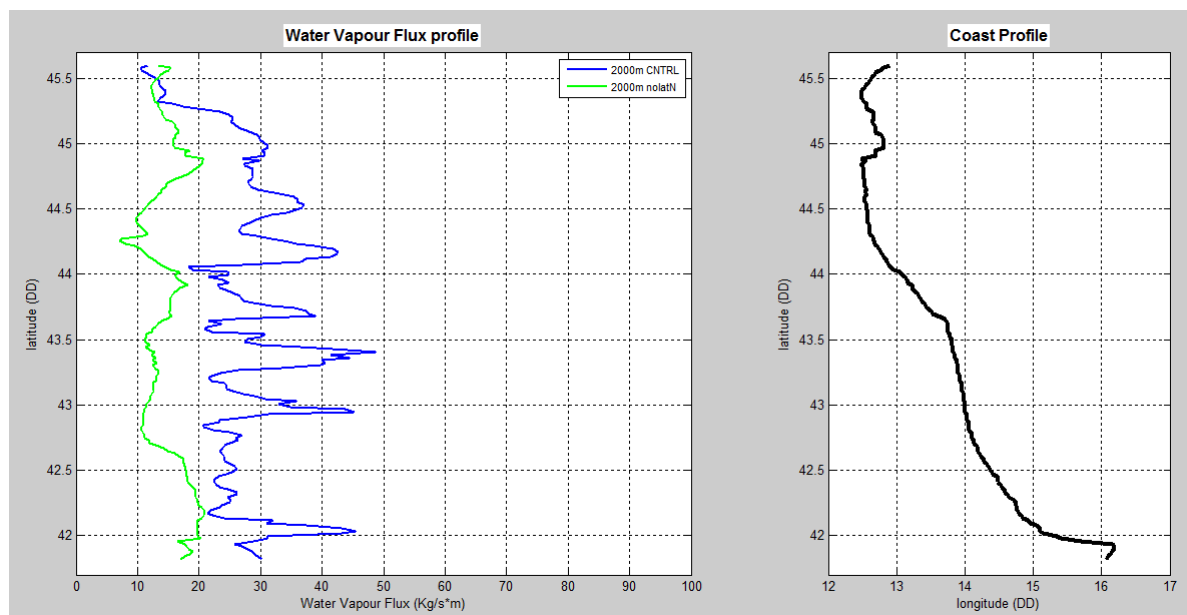
(a) December 2010
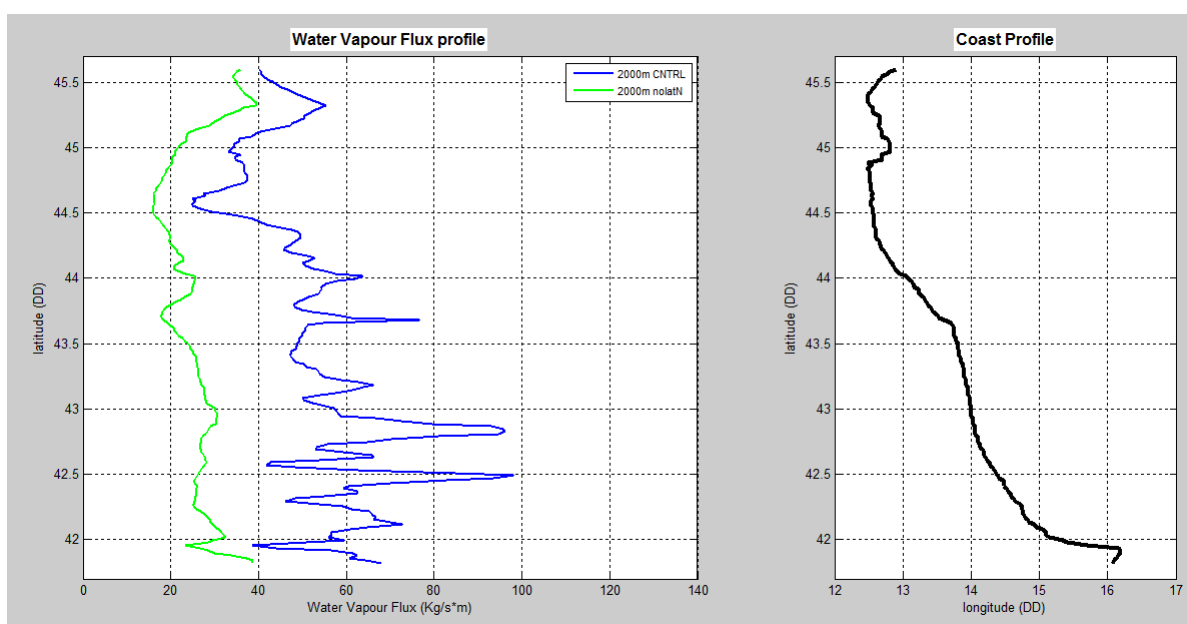
(b) December 2014

Figure 5.5: Water vapour flux profile along the Italian coastline forecast by MOLOCH at 18 UTC on 15 December 2010 (a) and at 12 UTC on 31 December 2014 (b).

5.3 Atmospheric water balance

5.3.1 The "Adriatic box"

In order to compute the water balance over the Adriatic Sea, a 3d-rectangular box is arranged with the bottom face attached to the sea surface and the top face above the troposphere. Different boxes are considered depending on the specific Bora case (Fig. 5.6). The choice of the key areas and the dimension of the boxes is done in order to:

- include the sea surface areas where largest heat fluxes are simulated;

- include the areas where largest wind speed and LLJs are simulated (that often coincides with the previuos case);

- arrange the eastern side normal to the Bora wind and the western side parallel to the Apennines and to the coast in order to intercept the flow feeding the rainfall inland;

The bottom face of the box is defined on the MOLOCH grid by keeping constant the number of grid-points for the shorther and the longer side of the rectangle, respectively.

Each contribution to the water balance entering or exiting from the box is properly computed as specified in Sec. 5.3.2 and the results are converted to be expressed in energy units (Watt). Thus the values obtained are intended as total values measured across the box. Not only water vapour but all the other hydrometeor species are considered for the fluxes computation: for example advected and falling precipitation takes into account both rain, snow, hail and graupel together with cloud water, cloud ice and precipitable water. The different atmospheric water species are considered also in the Integrated Water Vapour (IWV) content computation inside the box. Thus the balance can be referred as an energy balance or equally as a mass balance of the atmospheric water or, as we call it hereinafter, simply water balance.

As a general rule, positive flux values mean that the flow is entering in the box while negative values indicate outgoing flow. This means that the Bora northeasterly flow crossing the box provides a positive contribution on the eastern box surface and a negative contribution on the western section.
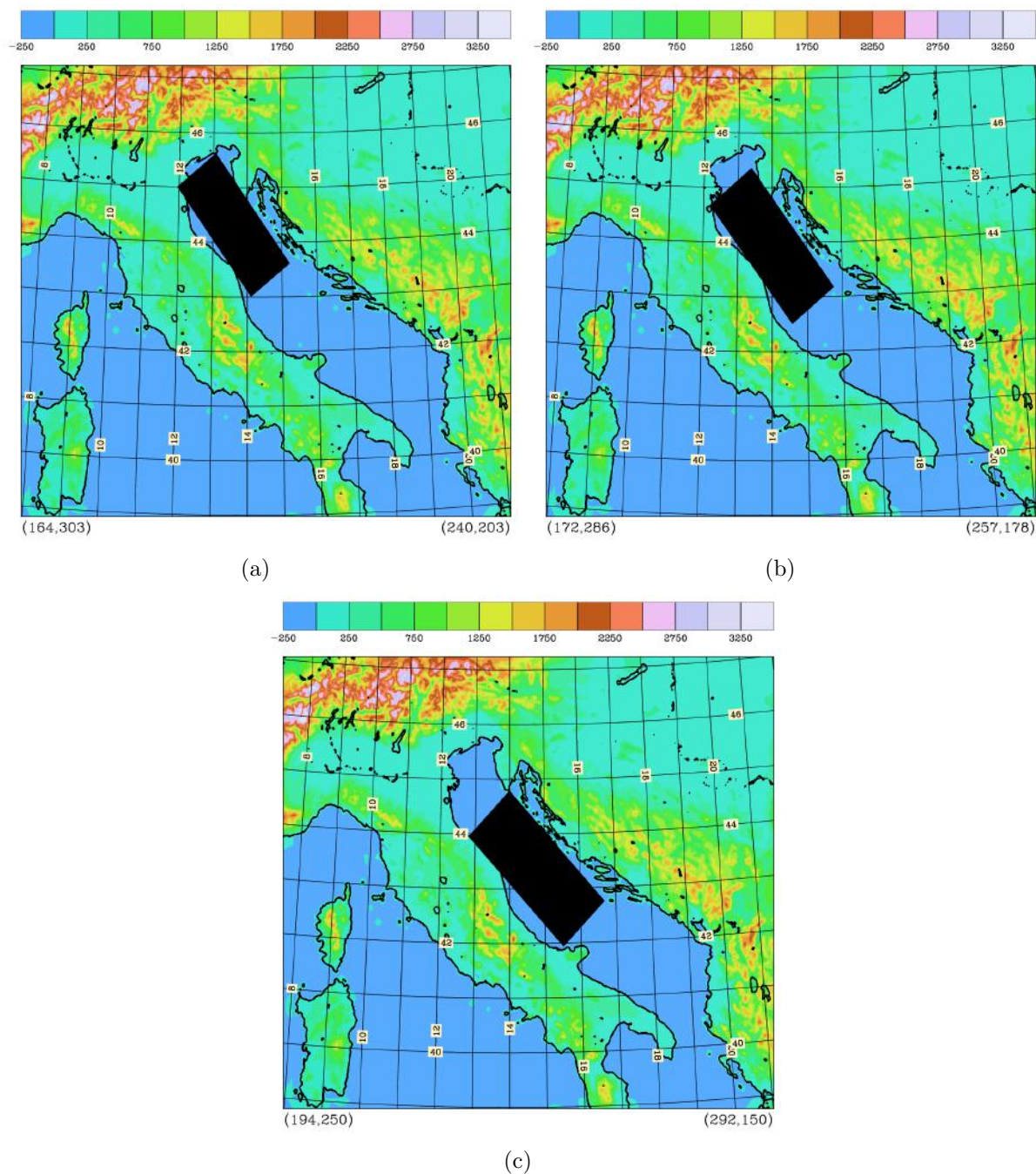
(a)

(b)

(c)

Figure 5.6: Atmospheric boxes defined for the water balance computation: February case (a), September and November cases (b), December cases (c)

5.3.2 Balance computation

Each balance component is computed starting from the different variables provided by MOLOCH. It is necessary to make istantaneous and cumulated values uniform and to normalise the values computed on the different areas of the box. It is supposed that an hourly interval is enough to properly compute the balance: actually the phenomena occuring inside the box can have shorter typical time-scale but the balance is supposed not to vary considerably. Recalling that $W = J \cdot s^{-1} = kg \cdot m^2 \cdot s^{-3}$ a consistency check is done for each term presented in the following paragraphs.

Lateral sections

Istantaneous water fluxes across each of the four lateral sections, extracted from the MOLOCH output are interpolated over vertical sections with a bilinear interpolation routine. The water flux is converted into energy units multiplying by the vaporization latent heat. The obtained value is multiplied again by the section area (A_{sec}) and normalised by the number of horizontal and vertical grid points of the cross-section ($npts \cdot nlivz$).

$$F_{lat} = \sum_{n=1}^{npts} \sum_{m=1}^{nlivz} q_{n,m} \cdot \rho_{n,m} \cdot v_{n,m} \cdot L \cdot A_{sec} \cdot \frac{1}{npts \cdot nlivz} \quad (5.2)$$

where q is the specific humidity, ρ is the air density defined as $P \cdot R_d^{-1} \cdot T_V^{-1}$, v is the normal wind component and L is the vaporization latent heat $L = -2.5 \cdot 10^6 \ J \cdot kg^{-1}$. As pointed out at the beginning of Sec. 5.3 q is defined by the sum

$$q = q_{cw} + q_{ci} + q_{pw} + q_{ip1} + q_{ip2} \quad (5.3)$$

including the contribution of advected precipitation (different water species: q_{pw} is precipitable water, q_{ip1} is snow and q_{ip2} is graupel) and cloud water/cloud ice (q_{cw} and q_{ci}, respectively) across lateral sections. This constribution is essential in order to have an exact balance since relevant amount of precipitation are predicted also at the box borders.

Bottom side

Two components are computed at the bottom side: an upward positive contribution from air-sea latent heat fluxes at the surface (Eq. 5.4) and a downward term that accounts for the loss due to precipitation (Eq. 5.5). Both latent heat flux and precipitation amount are provided directly by MOLOCH variables *cqflux* and *totpre*, respectively: rainfall is multiplied by L to be converted into energy. They are both cumulated values over hourly time-intervals, thus a conversion into instantaneous values is required. Normalisation by the number of grid points of the section ($npts$) is also required.

$$F_{bot}^{\uparrow} = \sum_{n=1}^{npts} \frac{cqflux_n}{3600} \cdot A_{sec} \cdot \frac{1}{npts} \quad (5.4)$$

$$F_{bot}^{\downarrow} = \sum_{n=1}^{npts} \frac{totpre_n}{3600} \cdot L \cdot A_{sec} \cdot \frac{1}{npts} \tag{5.5}$$

Top side

The top boundary of the box is set at 12 km so that no relevant water vapour content (and flux) is expected to be found in the atmosphere. The assumption is reasonable since at such an altitude, that corresponds to about 200 hPa, the specific humidity q is very low and no significant atmospheric water flux is expected.

Integrated Water Vapour balance

The balance obtained by the terms related to the six faces of the 3d-box has to match with the IWV tendency computed inside the box volume and the agreement between the two terms is a measure of the accuracy of the total balance. The IWV over an air column is provided hourly in the model output for each grid point in $kg \cdot m^{-2}$ thus, as previously done, a normalisation, a conversion into energy unit and into instantaneous values is needed.

$$F_{IWV} = \sum_{n=1}^{npts} iwv_n \cdot L \cdot \frac{1}{3600} \cdot A_{sec} \cdot \frac{1}{npts} \tag{5.6}$$

We are interested in the IWV hourly variation thus the time-derivative of IWV by the finite difference between two time-steps is taken

$$\frac{dIWV}{dt} = \frac{IWV(t_+) - IWV(t_-)}{\Delta t} \tag{5.7}$$

where t_- and t_+ are two consecutive time instants ($\Delta t = 1h$).

5.3.3 Results

Three kinds of graphs are produced:

- a graph showing the total balance to evaluate the closure of the budget;

- a graph showing the components of the budget to evaluate the relative contribution of each term;

- a graph focusing on the western section to highlight the outgoing flow that impinges on the Apennines; (the western section is parallel to the mountains and the water content that passes across it is clearly connected to the precipitation to the West)

A 44h time-range is considered since the initial simulation instant is meaningless for the hourly cumulated values. The IWV hourly differences are centered in the middle of the interval while the istantaneous values are plotted hourly. To better evaluate the closure of the total balance the IWV differences values are inverted so that the IWV and the fluxes balance superimpose in the figures. Figures from 5.7 to 5.11 show the three graphs for each Bora case: total balances, separated components and the focus on the western section.

Total balance graphs
The total balance is characterized by a good closure for all the five Bora cases considered except for few significant differences observed between the IWV variations (purple lines in the (a)-panels) and the fluxes balance across the six faces (black lines) in correspondence to peak values. The closure of the balance is not completely attained where the trend shows large fluctuations and this is true especially for the periods characterized by large precipitation, as can be noticed for the February 2012 case and at the end of December 2010 forecast-range. Indeed, the December 2014 case, for which the bottom downward term due to precipitation fallout is negligible, shows the best result.

The balance of the four lateral sections together (NSWE, green lines in the (a)-panels) is negative for the anticyclonic cases and nearly close to zero with long periods characterized by positive values for the cyclonic events. The separated components graphs will provide an explaination for this behaviour.

The bottom upward term connected to air-sea latent heat fluxes (red line in the (a)-panels) is rather constant during the forecast range around the value of $1 \cdot 10^{13} W$ for the February 2012, September 2012 and December 2010 cases and up to $2 \cdot 10^{13}$ for the November 2013 and December 2014 cases for which actually the MOLOCH simulations already predicted the largest heat fluxes values over the sea among all the Bora cases considered (Ch. 4). The water content loss due to precipitation (blue line in the (a)-panels) is clearly higher for the cyclonic cases since heavy rainfall are simulated also over the sea, while for December 2010 and December 2014 cases, precipitation is almost negligible.

It is shown that the IWV evolution in the box agrees quite well with the total flux balance, thus indicating a suitable closure of the water balance. However, some discrepancies appears and may be ascribed to the following reasons:

- numerical errors in the interpolation of the model variables on the lateral cross-sections;

- the comparison among istantaneous values (those the of lateral sections) and integral values (those of the bottom face);

- the fluxes across the sections are computed hourly but an higher frequency is desirable;

- the fluxes across the top side are neglected;

Separated components graphs

In the separated component graphs the contribution of each face is shown individually while the bottom fluxes (both upward and downward) are summed up in the term *bottom balance* (red line in the (*b*)-panels). The dominant terms (both entering or exiting) in absolute values and the relative impact of each face with respect to the others can be discussed looking at this kind of graph.

In particular the contribution of the northern section (green lines in the (*b*)-panels) results the least important. For the cyclonic cases this contribution is negative, which means that an outgoing flux is established. The opposite situation is observed for the anticyclonic cases. A possible explanation is that, as already seen by analysing the wind fields at different isobaric levels, the cyclonic cases are characterized by a pronounced vertical wind shear and the prevalent wind direction over 850 hPa is basically from the South or the South-East over all the Adriatic basin. The anticyclonic cases on the contrary show a more regular wind pattern with the Bora wind that blows constantly from northeasterly thus it enters the box from the North or even flows parallel to the shorter box lateral sections (as in December 2014 case for which northern and southern sections have negligible flux values).

This behaviour is confirmed by the southern section trend (yellow lines in the (*b*)-panels). This section is crossed by the southerly flow associated with the cyclonic circulation. Large positive contributions (of the order of $1 \cdot 10^{14} W$) are provided by the cyclonic cases and the value increases during the event as the cyclone deepens and the cyclonic circulation reinforces.

In the February 2012 case the southern contribution equals the eastern one, associated with the Bora wind flow, for a 10h-period while the September 2012 and November 2013 cases attain lower but significant values with respect to the total flux entering the box. On the contrary, the anticyclonic cases are characterized by negative contribution from the southern section or, as in December 2014, by a slightly positive one.

The eastern (purple lines in the (*b*)-panels) and western (light blue) sections are those associated with the largest contributions. The flow is clearly an inflow from the East and an outflow from the West section with almost opposite trends. For the September 2012 and November 2013 cases the eastern section contribution reaches $3 \cdot 10^{14} W$ while typical values for the anticyclonic cases are one order of magnitude lower. The outflow across the western section is typically larger in absolute value with respect to that entering from the East because it gains water vapour from heat fluxes at air-sea interface and from the southern inflow associated with the cyclone. It is worth noting that for the cyclonic cases the prevalent term increasing the western outgoing flow is the southern inflow while the bottom fluxes are more important for the anticyclonic cases.

It has been decided to plot the third graph with the western section separated from the others to highlight this crucial feature that states a significant difference between the two kind of Bora occurrences.

West-section focus
The western section contribution (black lines in the (c)-panels) is compared with the
bottom upward and downward terms and the net balance of the remaining lateral sections.
Its sign is turned from negative to positive to simplify the interpretation. For the cyclonic
cases almost all the outgoing westward flow is balanced by the inflow from the other
lateral sections (green lines in the (c)-panels) which is mainly composed by the eastern
contribution and, secondly, by the southern one. For the anticyclonic cases almost a
third of the water content crossing the western section comes from heat fluxes at the
bottom (red lines in the (c)-panels). While their values are almost unchanged, the relative
contribution of bottom fluxes increases for the December cases since the water flux cross-
ing the lateral box boundaries is an order of magnitude lower with respect to cyclonic cases.

The role of air-sea heat fluxes turns out to be fundamental in enhancing the water
content of the air approaching the Italian coast when an anticyclonic Bora pattern is
established. For the cyclonic cases, on the contrary, what is critical is the atmospheric
water supply coming from the south. In general, the outgoing flux at the western section
is larger for the cyclonic cases that are those associated with more intense precipitations.

To sum up, it has been observed that the precipitation field over the Italian coastline
and Apennines is strongly sensitive to air-sea heat fluxes over the Adriatic Sea. A
remarkable decrease of rainfall is predicted when surface heat fluxes are suppressed
over the sea in the sensitivity tests for both cyclonic and anticyclonic Bora cases. The
water vapour profile analysis along the coast shows that also the horizontal water vapour
flux over the sea moving towards the Apennines decreases for these cases and that its
propagation front is no more characterized by alternated jets and wakes.
On the other hand, the atmospheric water balance computed over the sea suggests
that the contribution to the balance due to latent heat exchanges between the sea body
and the atmosphere (bottom face of the box) is residual with respect to the advection
terms across the lateral sections, at least for the cyclonic cases. It follows that air-sea
heat fluxes effects on precipitation must be explained by a dynamical mechanism and not
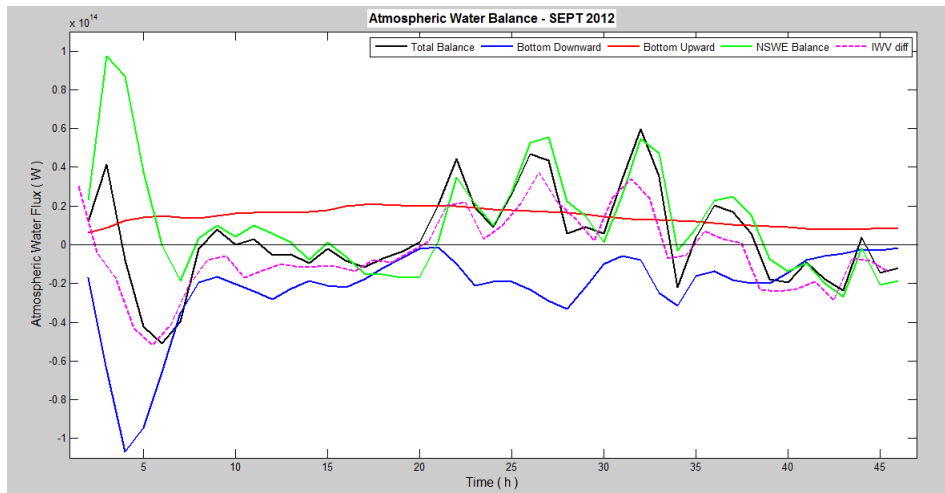by hsimple mass-balance.
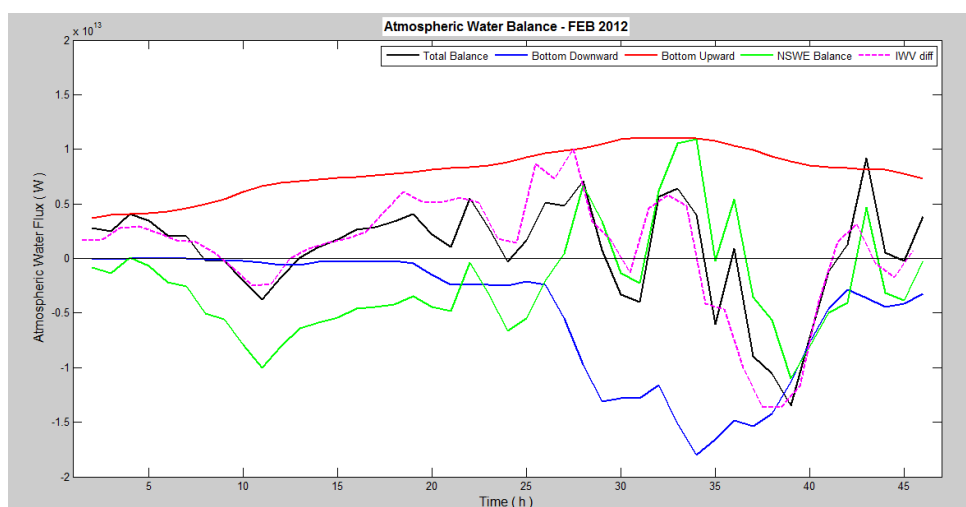
(a)
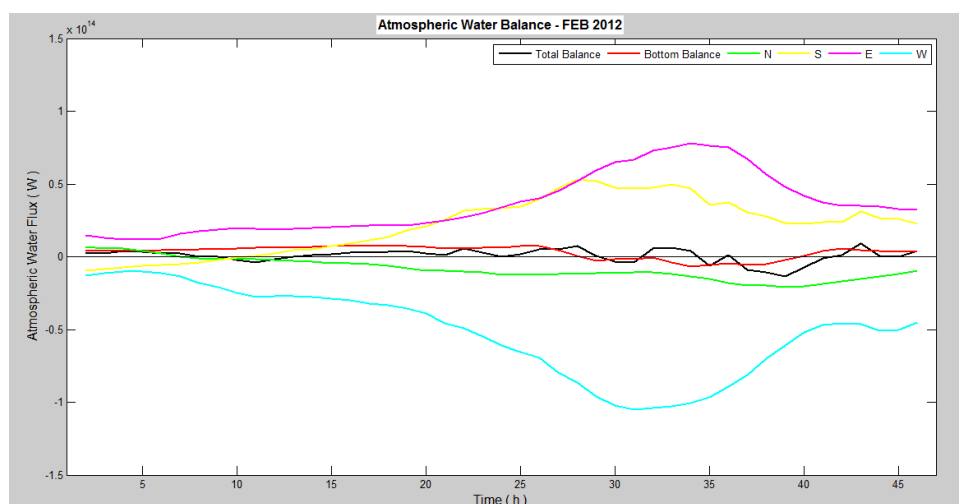
(b)
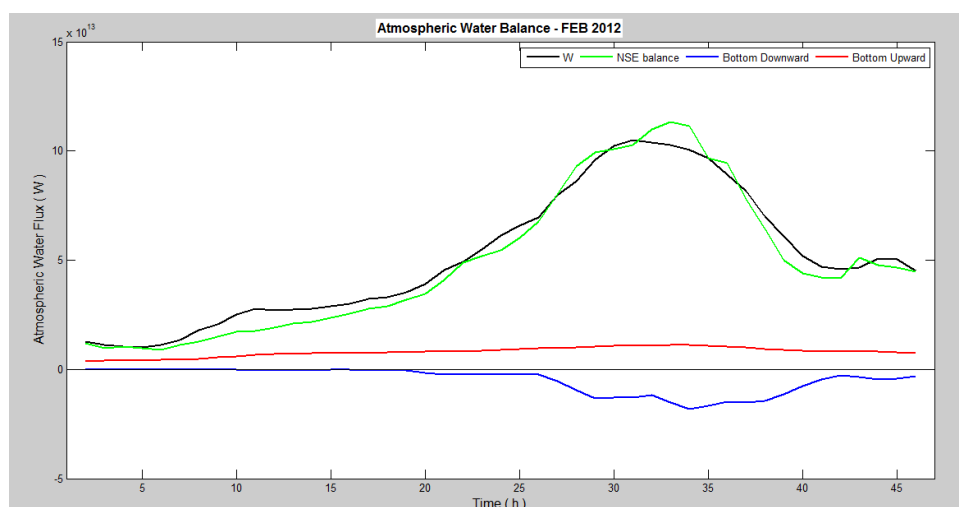
(c)

Figure 5.7: Atmospheric water balance for the February 2012 case: total balance (a), separated components (b) and focus on the western section (c).

(a)

(b)

(c)

Figure 5.8: Atmospheric water balance for the September 2012 case: total balance (a), individual components (b) and focus on the western section (c).

(a)

(b)

(c)

Figure 5.9: Atmospheric water balance for the November 2013 case: total balance (a), individual components (b) and focus on the western section (c).

(a)

(b)

(c)

Figure 5.10: Atmospheric water balance for the December 2010 case: total balance (a), individual components (b) and focus on the western section (c).
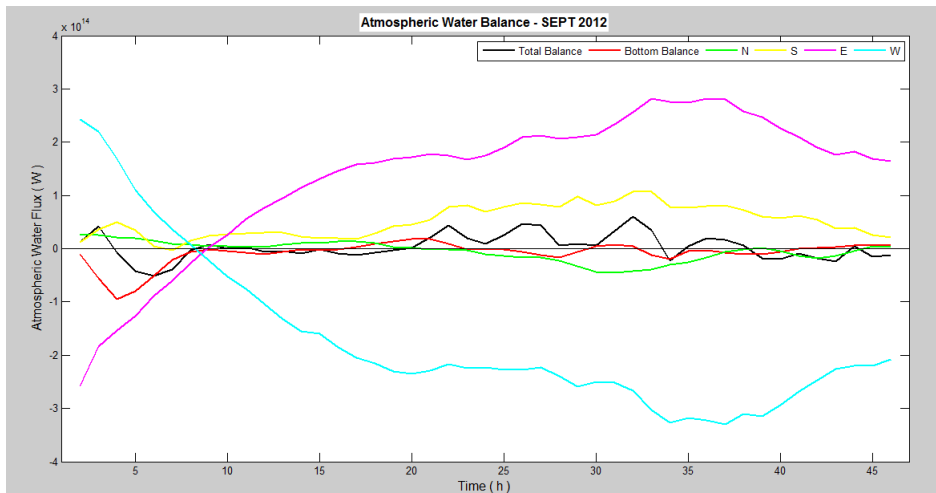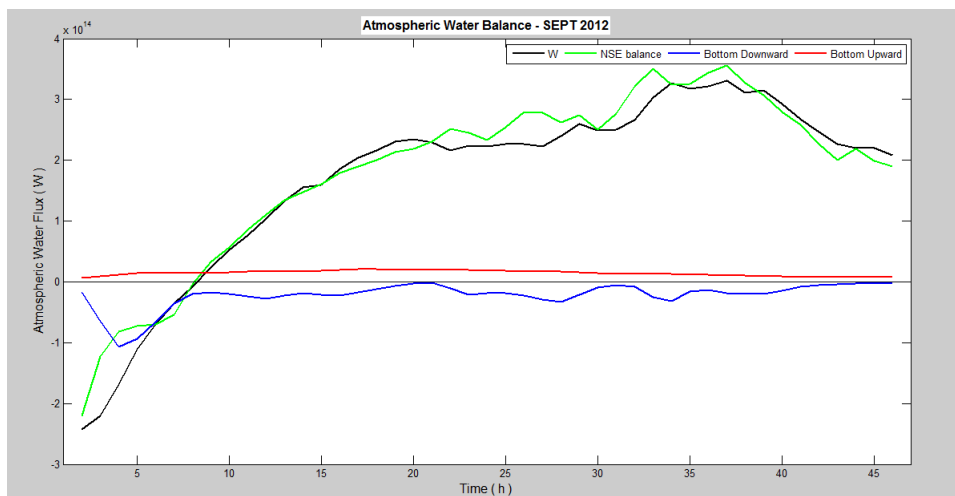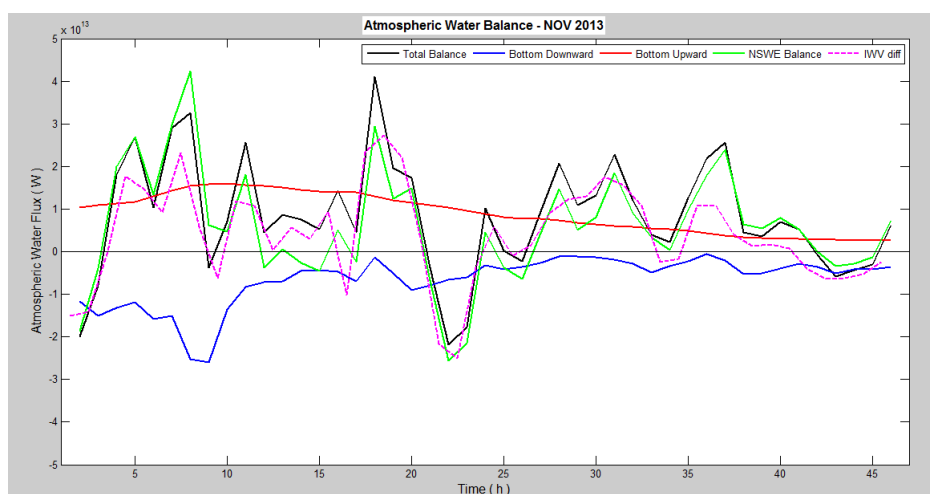
(a)
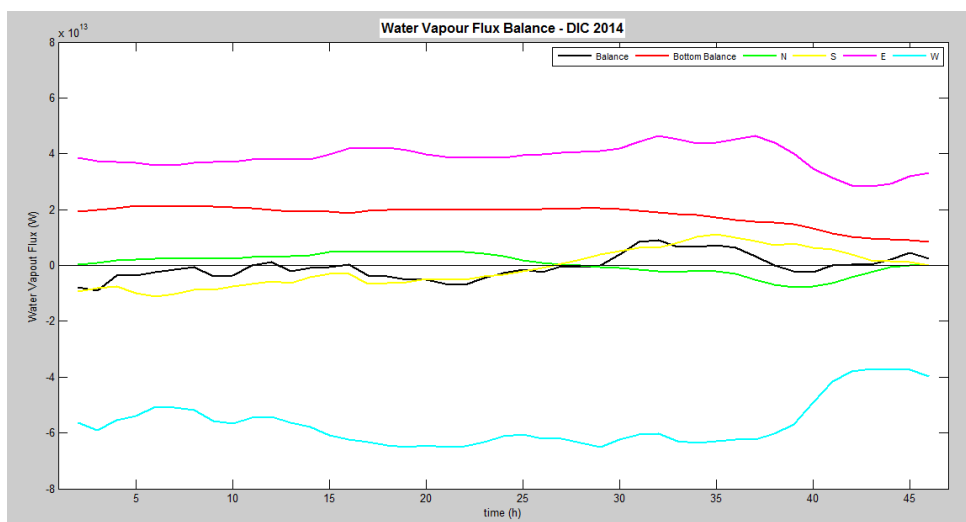
(b)
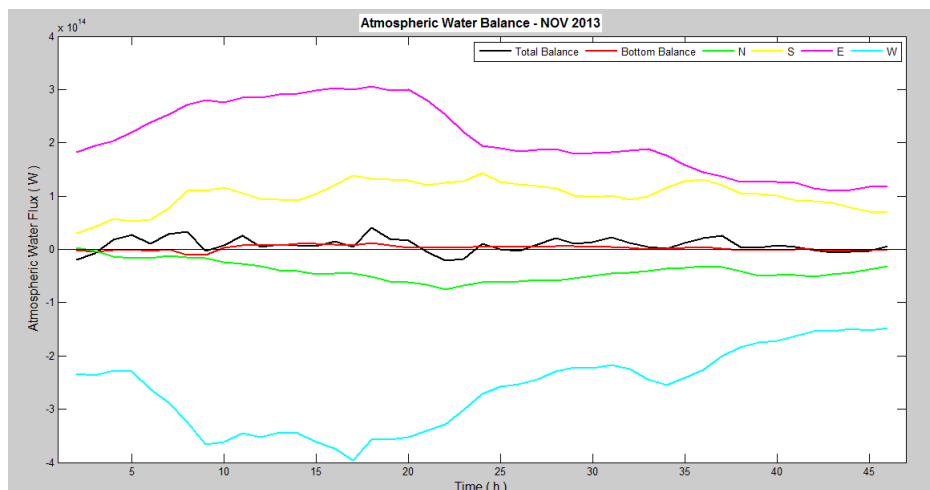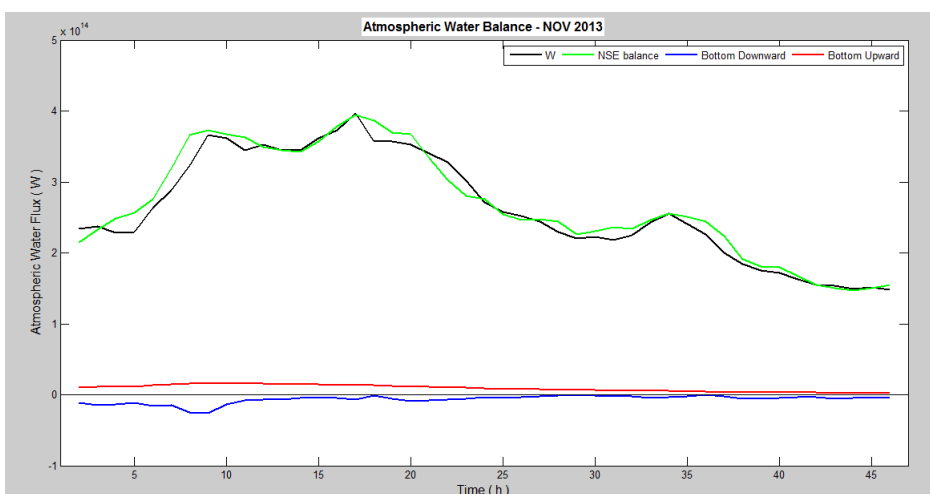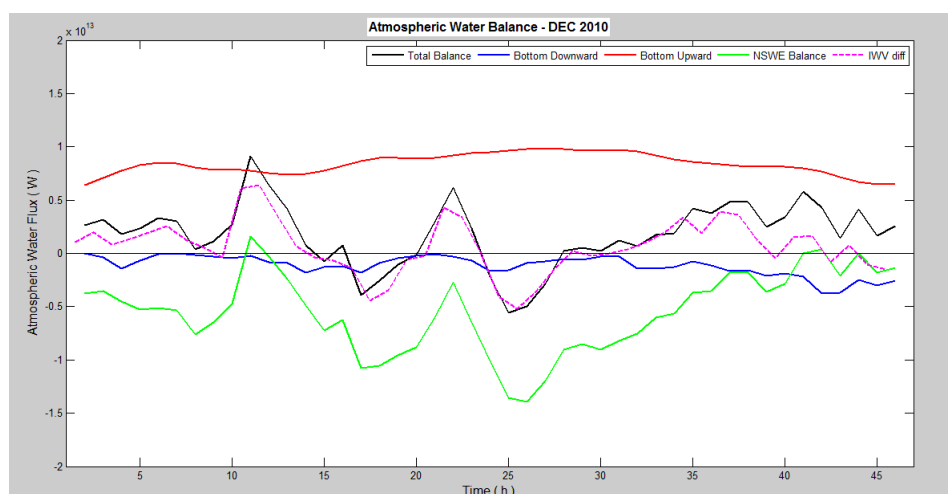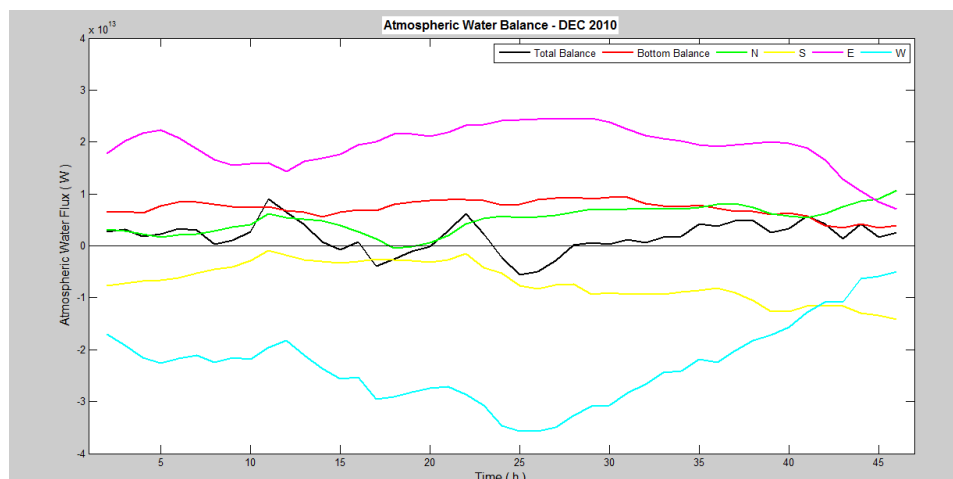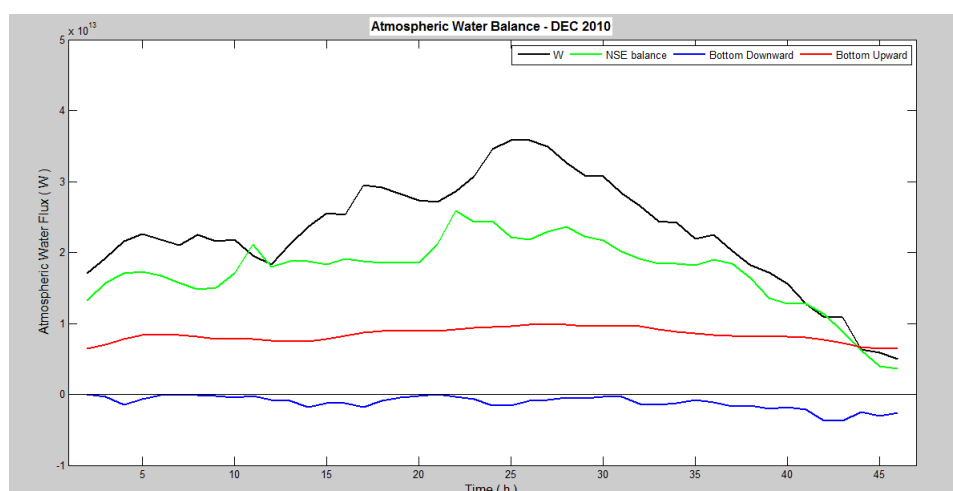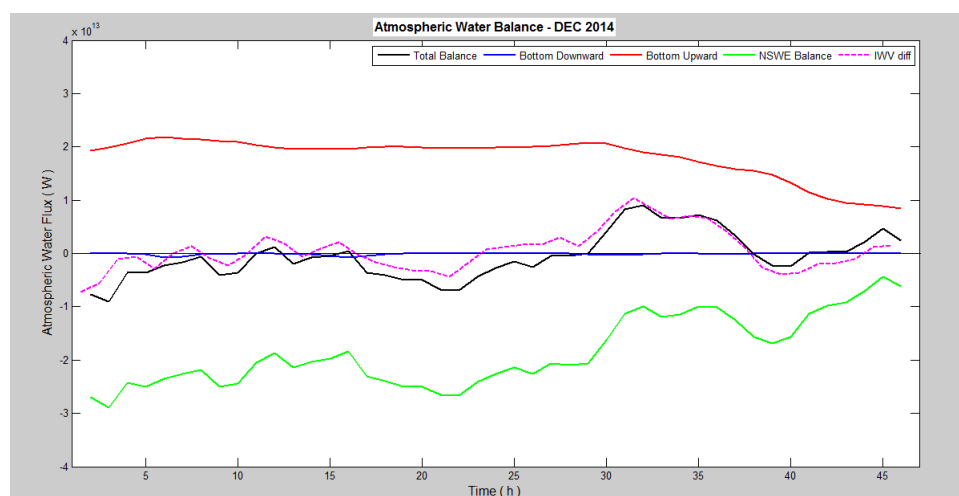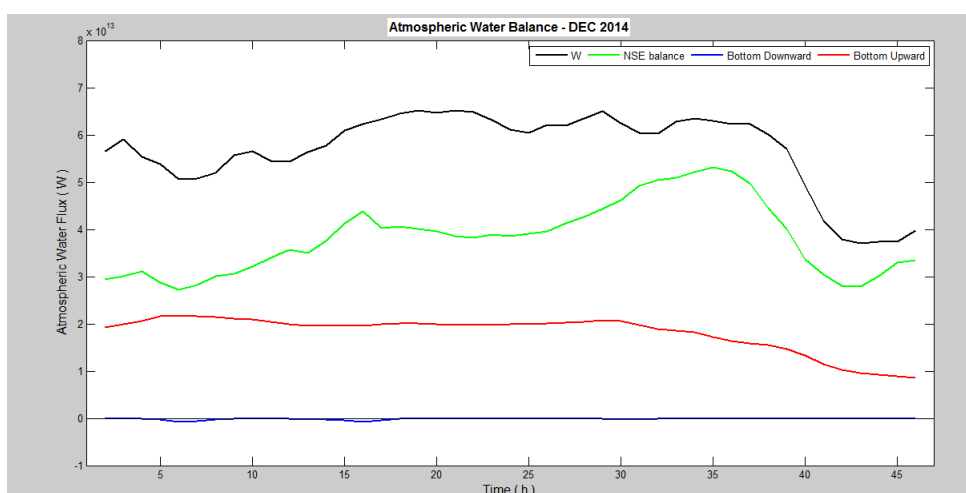
(c)

Figure 5.11: Atmospheric water balance for the December 2014 case: total balance (a), individual components (b) and focus on the western section (c).

Chapter 6

Focusing on dynamics of cyclonic Bora: results of numerical experiments and discussion

This chapter faces the open question illustrated at the end of Ch. 5, that is to identify dynamical processes, associated with surface heat fluxes, affecting wind and precipitation patterns during Bora cyclonic events. The discussion is focused on the February 2012 and on the September 2012 cases that are considered as the most relevant to the issue. In Sec. 6.1 the evolution of significant variables is inspected on different cross-sections located perpendicularly and parallel to the Bora jet trajectories. The sensitivity of MOLOCH simulated fields to modified orography is tested in Sec. 6.2 in order to better understand the dynamical role of orographic forcing. Final remarks are presented in Sec. 6.3.

6.1   Cross-sections

In order to assess the role of dynamical processes taking place in the atmospheric lower levels above the Adriatic Sea, the evolution of different meteorological variables simulated by MOLOCH are examined on specific cross-sections arranged in prescribed key-areas.

Three different locations are considered for the cross-sections:

- cross-sections over the sea, in the middle of the Adriatic;

- cross-sections located approximately along the Italian coastline;

- cross-sections parallel to the Bora wind jets.

The aforementioned three types of cross-sections will be referred hereinafter as to across-sea, along-coast and along-jet cross-sections.

The position of the across-sea cross-section is common to all the Bora cases analysed in this chapter, while the along-coast and the along-jet cross-sections vary depending on the specific Bora case, in order to probe the most significant regions. In Fig. 6.1 the different locations of the cross-sections that will be considered is shown.

The top level of each cross-section is prescribed at 3000m (with 50 vertical levels). The cross-sections located over the sea and along the Italian coastline are almost parallel each other and perpendicular to the Bora wind. For the third cross-section type a path along the strongest wind jet is considered.
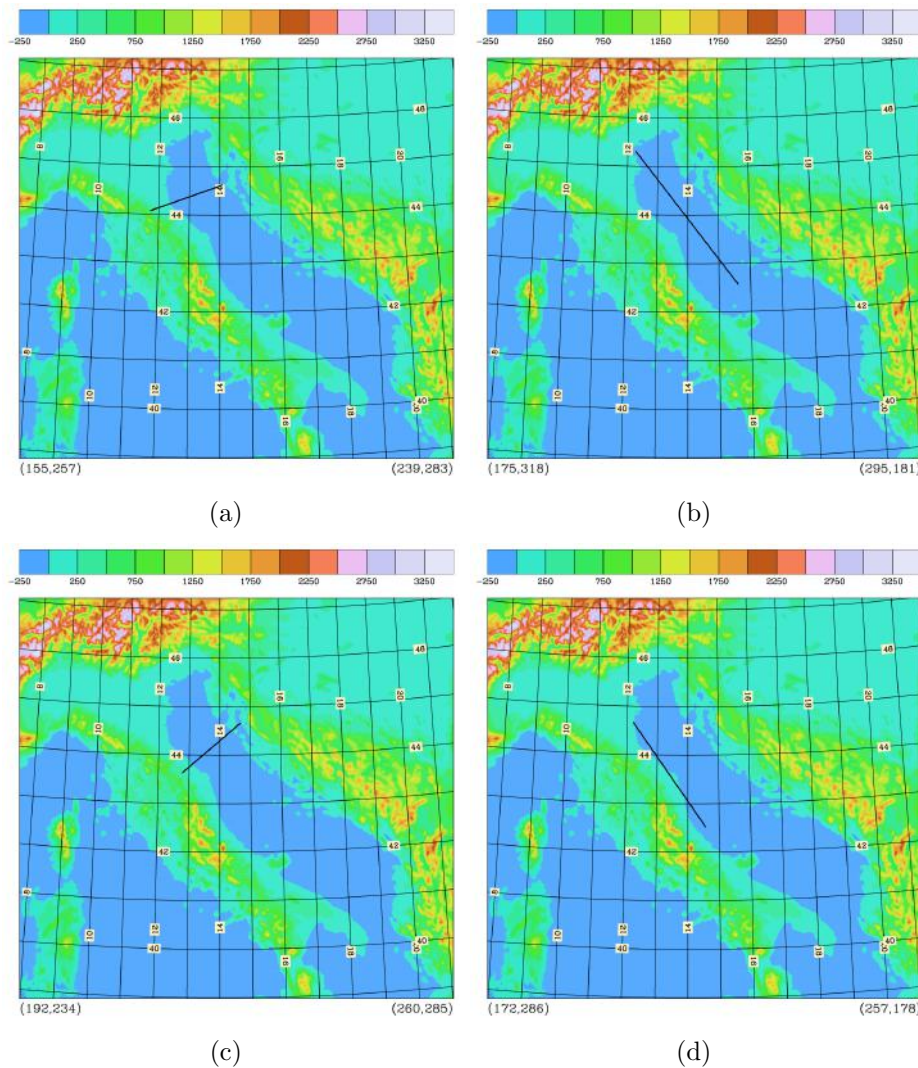

Figure 6.1: Cross-section positions: along-jet for the February case (a), across-sea for both cases (b), along-jet (c) and along-coast (d) for the September case.

6.1.1 Case of February 2012

The cross-sections for the February Bora event are shown at 09 UTC on 10 February 2012. The Bora wind is entering the most intense phase and moderate-to-heavy precipitation is affecting the Appenines and the Adriatic western coast. For these reasons this can be considered as a key-instant to examine the flow dynamics leading to severe weather condition over the Adriatic as a whole.

In Fig. 6.2a the across-sea cross-section is shown for the CNTRL run: the color scale is related to air temperature (in Celsius) while solid lines indicate the wind speed (in $m \cdot s^{-1}$) perpendicular to the section. Negative values mean that the flow is blowing towards the cross-section from the East. Higher temperature are observed to the South-East than to the North-East portion of the cross-section, both at sea level and up to 3000m. The wind speed contour lines mirror the jet pattern already observed in the MOLOCH output: four distinct areas characterized by larger negative (northeasterly) wind speed (highlighted by thick lines) can be recognised between the sea level and 1000m with the largest contour line for each area touching the surface. The wind speed gradually decreases above 1000m along all the cross-section. Finally, positive wind speed values above 2000m and higher surface temperatures are represented at the southern edge of the cross-section.

In Fig. 6.2b the same cross-section at the same time is shown for the *nofluxN* test. Temperature below-zero is predicted all along the cross-section also at sea level except for the southernmost part. The most interesting feature, however, is that the largest wind speed areas (highlighted by thick lines) are confined to a few hundred meters above the sea level while the surface is affected by much weaker wind than in the CNTRL run.

Two main differences between CNTRL run and *nofluxN* run deserve to be discussed in more detail. First of all the surface temperature is up to $5°C$ colder in the *nofluxN* run, mainly at the surface, but significant differences can be found up to 1000m. This feature has been already noted as a result of the sensitivity tests (Ch. 4) and it is almost obvious since air-sea heat exchanges are not allowed in this simulation. The second difference, that is more important, is that the four areas affected by the most intense wind are shifted to the upper levels in the *nofluxN* cross-section. Since this aspect can be hardly recognised by looking at individual cross-section, Fig. 6.2c provides the wind speed differences between CNTRL run and *nofluxN* run. Positive differences mean larger wind speed in the *nofluxN* run (the convention is that the wind speed entering the cross-section from the East is negative).

The wind speed difference between CNTRL run and *nolatN* run (not shown) is characterized by a pattern similar to CNTRL-*nofluxN*, while the CNTRL-*nosenN* difference (Fig. 6.2d) shows a weak wind speed decrease under 1000m but no significant increases are predicted at specific areas as in the previous cases.

The analysis of the cross-sections discussed above confirms that the Bora wind-jets cores are not located at the surface in the *nofluxN* and *nolatN* simulations due to a smaller

momentum mixing in the more stratfied cases, in which surface fluxes are inhibited. The higher temperature and the positive wind speed values above 2000m predicted at the southern edge of the across-sea cross-section are associated with the cyclonic circulation which carries warm air from the South-West. As mentioned in the water vapour profile analysis, this flow is mainly confined to upper levels, at least in the first part of the Bora outbreak.

The fact that the maximum wind speeds are attained at different altitudes in the CNTRL run and in the *noflux*-runs suggests to better examine the properties of the PBL. In order to analyse the PBL profiles over the sea the along-jet cross-section is considered. The along-jet cross-sections in Fig. 6.3 show the relative humidity field (color scale) and the Cloud Liquid Water Ice (CLWI) content: in the CNTRL run (Fig.6.3a) a moist layer with relative humidity values around 70% is predicted above the sea and the drier Bora flows over it in the eastern part of the section between 500m and 1000m. Values close to saturation are observed over the mountains due to orographic uplift. In the *nofluxN* (Fig.6.3b) the atmosphere up to 1000m is characterised by low relative humidity (around 50 %). A similar situation is predicted also in the *nolatN* simulation (Fig.6.3d) with relative humidity values even lower (30% in the eastern part of the cross-section). On the contrary, the *nosenN* cross-section (Fig.6.3c) shows a saturated layer 500m thick all over the sea and over the Appenines as well.

This findings suggest that the removal of air-sea heat fluxes or latent heat flux over the Adriatic Sea produces a Marine Boundary Layer (MBL) characterised by drier air. On the other hand, the removal of sensible heat flux produces a wetter layer above the sea surface. The boundary layer extends up to 1000m (500m) for *nofluxN* and *nolatN* (*nosenN*).

In order to better investigate the vertical stability of the PBL, potential temperature (θ) is considered on the along-jet cross-section. Fig. 6.4 shows θ distribution on the section for CNTRL run (*a*-panel) and *nofluxN* run (*b*-panel), while equivalent potential temperature, θ_e, is shown in the *c*-panel for *nosenN* since in this case the first 500 meters above the sea surface are characterized by saturation. The *nolatN* cross-section is not shown since it is very similar to the *nofluxN* one. The atmospheric stratification is larger in the *nofluxN* run cross-section than in the CNTRL one, where a small area next to the coast shows an inversion of θ-values. Lower θ-values up to 1500m in the *nofluxN* cross-section are due to lower absolute temperature values. In the *nosenN*, the θ_e-pattern shows a thicker inversion at the coast and inland where the Bora flow starts to lift over the Apennines. The inversion of θ_e is a sign of instability and the fact that the *nosenN* run is characterised by a more unstable layer next to the coast can explain the different impact that has been observed on the precipitation field: in the sensitivity tests of Ch. 4 it is shown that the run with removed sensible heat flux produces a decrease of total rainfall amount that is half the values simulated for the *nofluxN* and the *nolatN*.

(a)

(b)

(c)

(d)
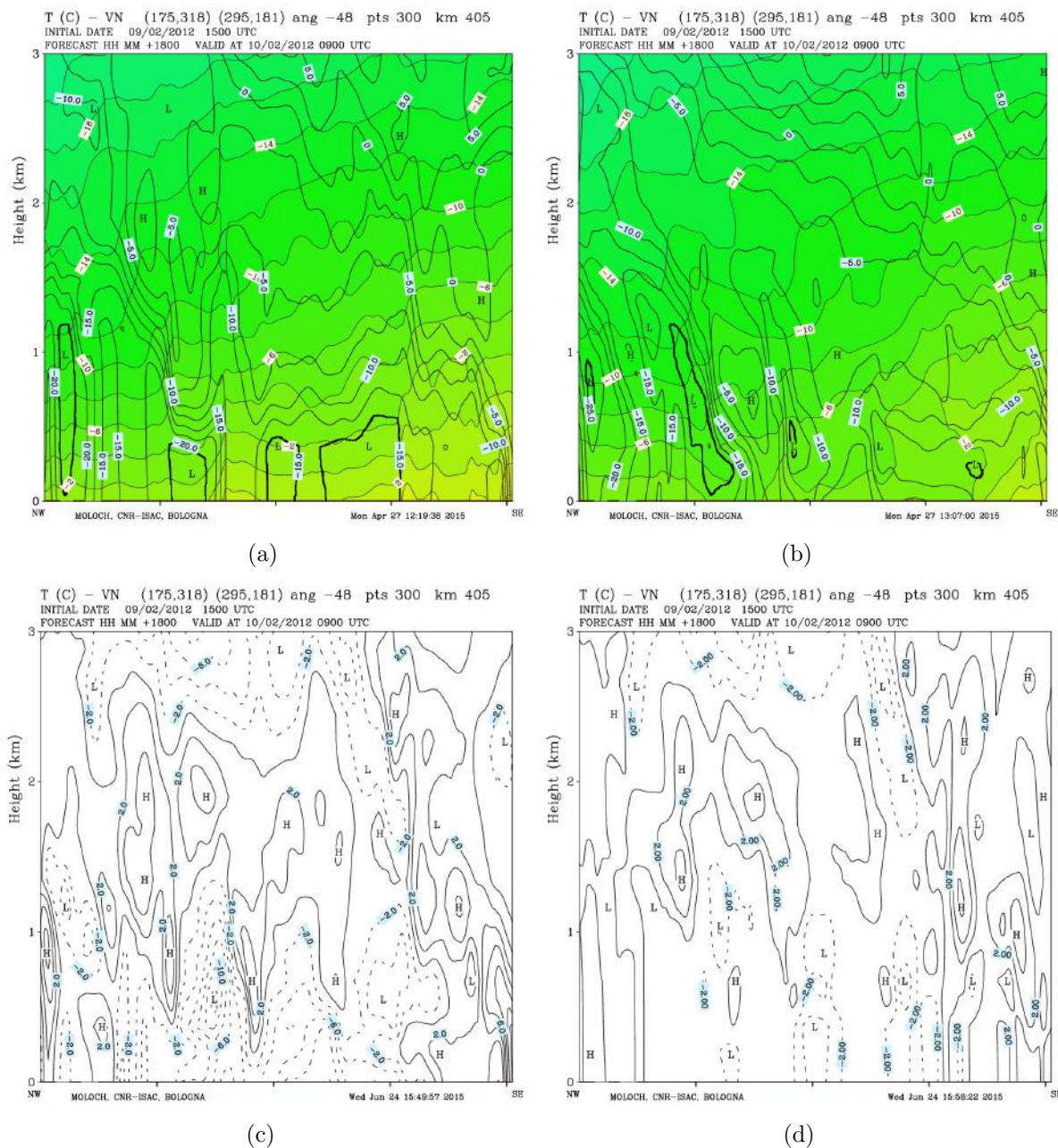
Figure 6.2: Temperature and normal wind forecast by MOLOCH on the across-sea cross-section for CNTRL run (a) and *nofluxN* run (b). CNTRL-*nofluxN* (c) and CNTRL-*nosenN* (d) wind speed differences. Continuous (dashed) lines refer to positive (negative) differences. Valid at 09 UTC on 10 February 2012.
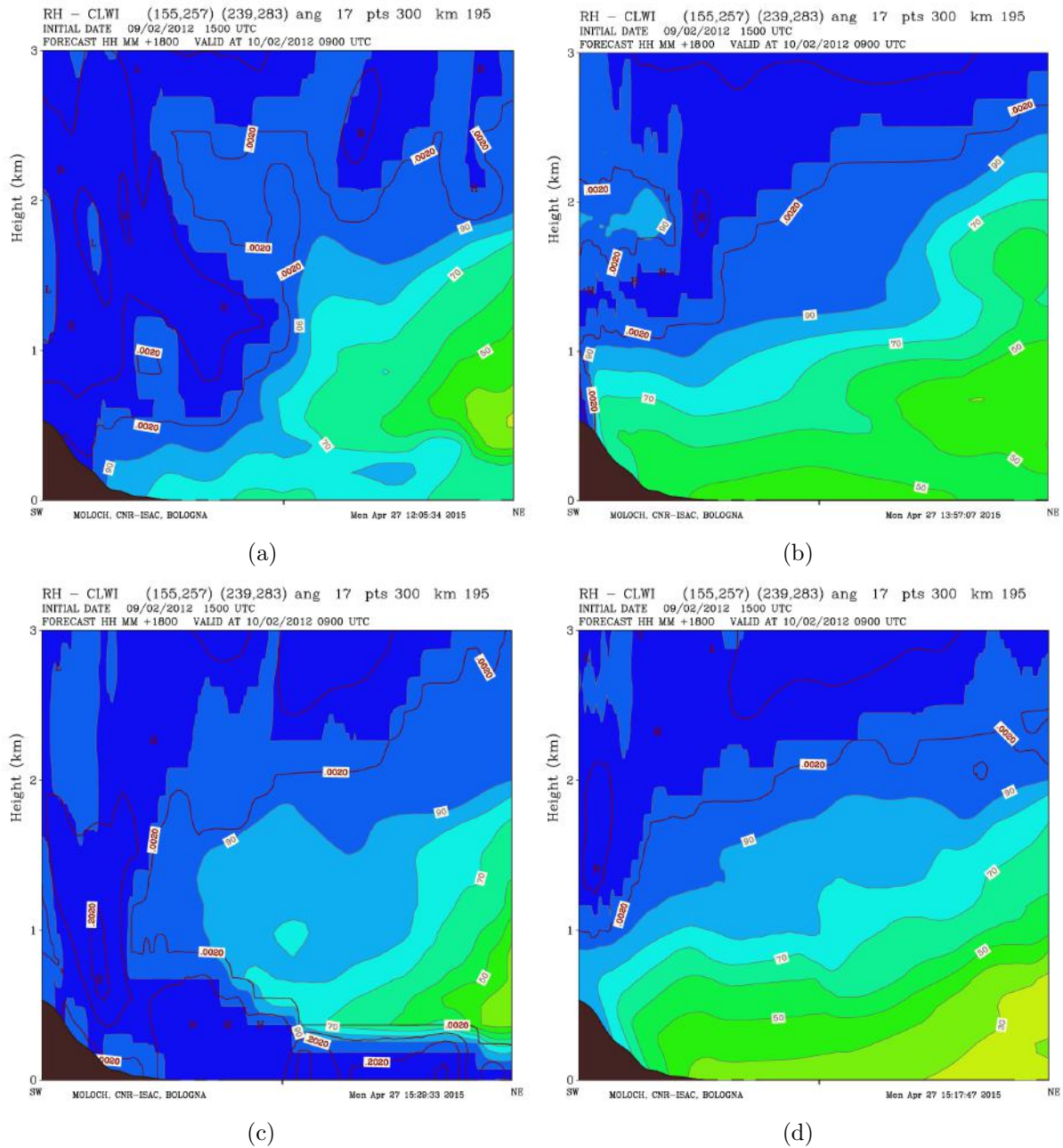
Figure 6.3: Relative humidity and CLWI forecast by MOLOCH on the along-jet cross-section for CNTRL run (a), *nofluxN* run (b), *nosenN* run (c) and *nolatN* run (d), valid at 09 UTC on 10 February 2012.
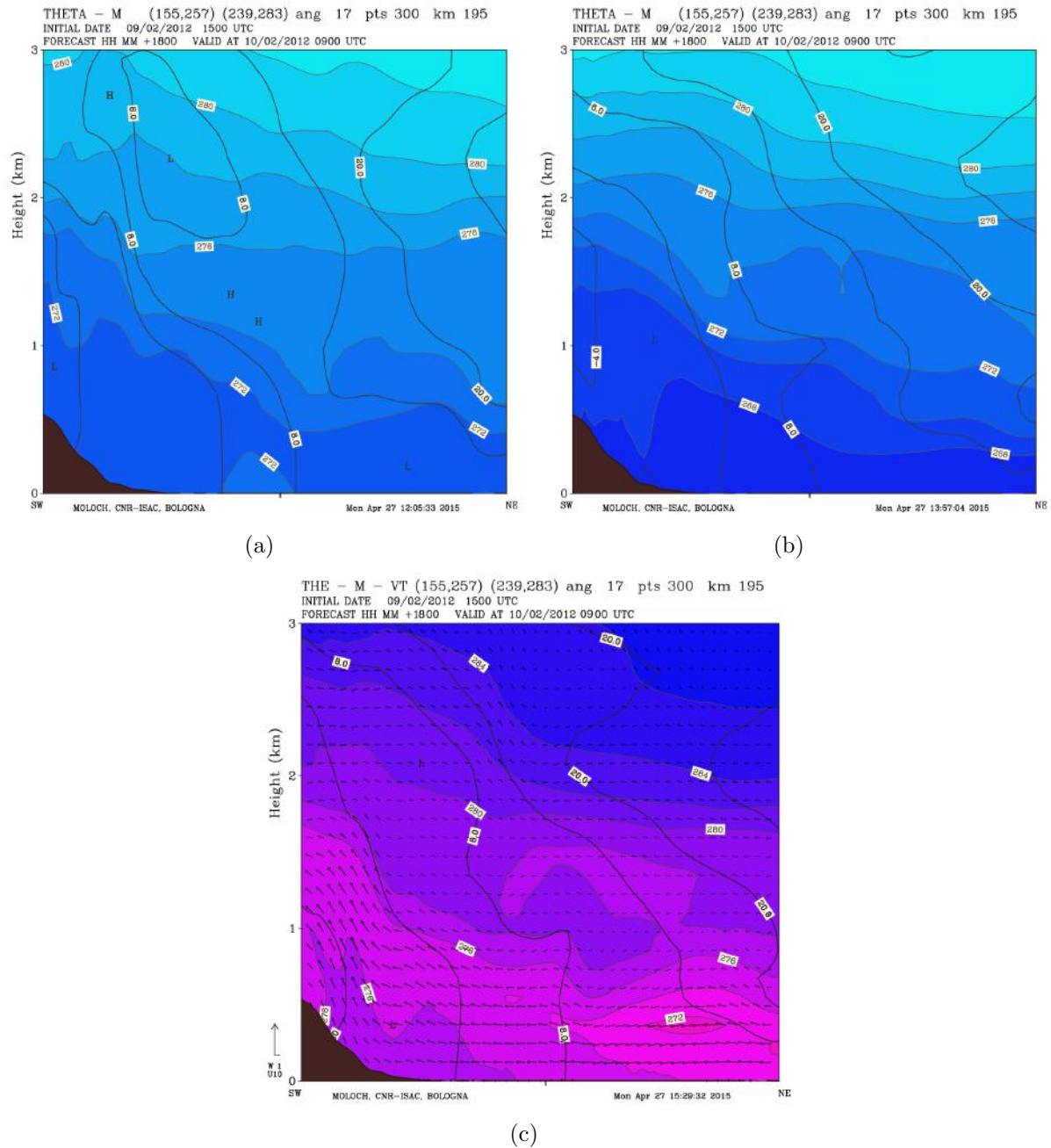
(a)

(b)

(c)

Figure 6.4: Potential temperature and momentum foreacast by MOLOCH on the along-jet cross-section for CNTRL run (a) and *nofluxN* run (b). Equivalent potential temperature, momentum and tangential wind vectors forecast by MOLOCH on the along-jet cross-section for *nosenN* run. Valid at 09 UTC on 10 February 2012.

6.1.2   Case of September 2012

In order to verify if the features observed for the February 2012 case are common to other Bora cases or, on the contrary, it should be considered as an anomaly, also the September case has been taken into account for sensitivity experiments and diagnostics. The analysis for the September case shows good agreement with the February one and allows to extend the previous results at least for the cyclonic Bora cases.

In Fig. 6.5a and Fig. 6.5b the CNTRL-*nofluxN* wind speed differences are shown on the across-sea and on the along-coast cross-section, respectively. In the *nofluxN* run the strongest wind speed areas (four narrow bands od positive differences) tend to be displaced at higher altitude from the surface on both cross-sections . It is worth noting that the along-coast cross-section (Fig. 6.5b) is shifted to the South with respect to the across-sea cross-section, thus it does not show the northernmost jet. Fig. 6.5b clearly shows that the easterly jets blow also at higher altitude above the surface while approaching the coast with respect to the across-sea cross-section (Fig. 6.5a). Negative values in the lowest 1000m indicate weaker easterly winds for the *nofluxN* simulation. The lifting of the flow impinging on the Apennines starts at a larger distance from the orography and consequently higher wind speeds are predicted between 1000m and 2000m with respect to CNTRL run.

The along-jet relative humidity pattern for the CNTRL run (Fig. 6.5c) and for the *nofluxN* run (Fig. 6.5d) confirms a sharper stratification in the simulation without surface fluxes: layer characterised by drier air extends all along the Adriatic Sea and conditions close to saturation are clearly confined above 1000m.
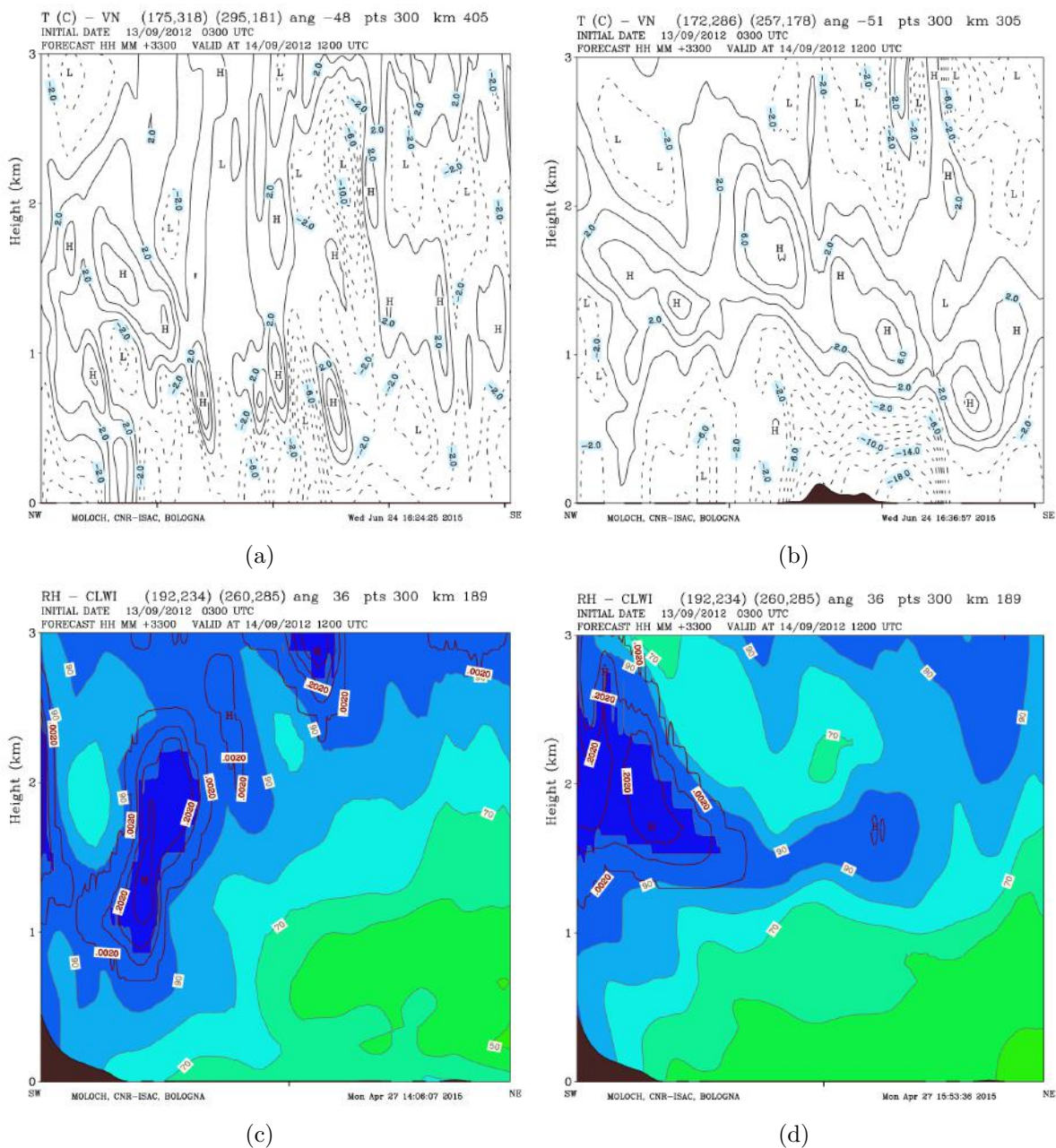
(a)

(b)

(c)

(d)

Figure 6.5: CNTRL-*nofluxN* wind speed difference on the across-sea cross-section (a) and on the along-coast cross-section (b). Continuous (dashed) lines refer to positive (negative) differences. Relative humidity and CLWI for CNTRL run (c) and *nofluxN* run (d) on the along-jet cross-section. Valid at 12 UTC on 14 September 2012.

6.2 Orography sensitivity tests

According to the analysis the precipitation field over Central Italy associated with Bora occurrences is critically influenced by air-sea heat fluxes over the Adriatic Sea.

However heat fluxes may not be the only reason since, as outlined at the end of Ch. 5 and in the introductory chapter to Bora events (Ch. 2), the issue is more complex. The behaviour of a a flow crossing a barrier is faced from the dynamical point of view through the analysis of the stability of the flow upstream and of the different regimes that may establish depending on the barrier physical features. Moreover the results of the atmospheric water balance show that the role of latent heat flux is not as relevant for the cyclonic cases as expected by considering the strong impact on the precipitation field predicted for the *nofluxN* and *nolatN* simulations. It follows that further analysis is needed to take into account other aspects that can lead to similar results in terms of precipitation decrease. Thus a comprehensive work should include the evaluation of the role of the orography that can affect the Bora propagation and, consequently, the precipitation field as well.

To assess indipendently the effect of the Adriatic basin orography (mainly the Apennine range) on the wind field over the Adriatic Sea, two distinct orography tests are performed for the February case only. The orography sensitivity tests consist in running simulations changing the orography height, in particular multiplying its elevation for a factor of 2 (*orogplus*) or 0.5 (*orogless*) over a prescribed area that encompasses the northern and central Apennines (Fig. 6.6).
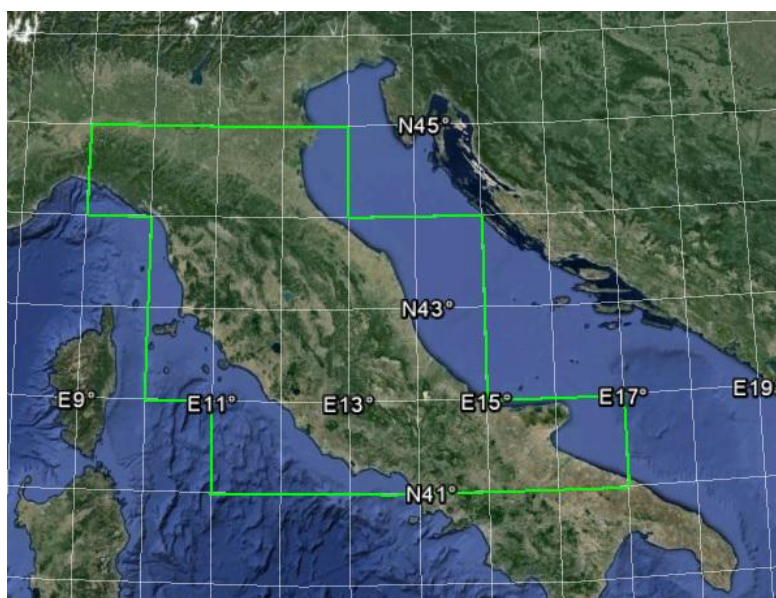

Figure 6.6: Area affected by modified orography.

Precipitation and wind fields are considered in order to analyse the MOLOCH results for the orography sensistivity tests. In the *orogplus* run (Fig. 6.7b) a small decrease of the total precipitation amount with respect to the CNTRL run (Fig. 6.7a) is simulated, in particular in the area next to the northern peak whose intensity decreases from 172 mm to 138mm. The southern peak is predicted more to the East in correspondence to the coastline where the convergence between the Bora flow and the southern cyclonic flow occurs. On the contrary, the precipitation dramatically decreases all over the domain for the *orogless* run (Fig. 6.7c): the two peaks attain 50 mm and 63 mm, respectively.

The wind field (Fig. 6.8) experiences significant changes with respect to CNTRL run as regards the crucial issue of the propagation and the strength of the Bora wind jets. In the simulation with raised orography (Fig. 6.8b) the wind jets are weaker so that the third and the fourth ones from the North hardly affect the Italian coast. A northwesterly wind is simulated between Monte Conero promontory and Gargano promontory that has been already recognised as an area favourable for barrier wind formation.

It is worth noting that the wind pattern is similar in the *orogplus* and *nofluxN* experiments. More precisely weaker wind speeds and narrower wind bands are observed concerning the two northernmost jets while the third and fourth jets rapidly decay and are confined in the eastern part of the Adriatic Sea. They are deflected to the South and merge with the barrier wind developed along the coast. This pattern also inhibits the role of the cyclonic counterclockwise flow which is conveyed towards the barrier wind instead of impinging on the Apennines. This means that the weakening of the wind jets due to higher orography downstream favours the *flow-around* regime (that is upstream blocking and flow deceleration) instead of the *flow-over* regime especially in correspondence to the highest peaks which are raised up to almost 6000m in this simulation.

The *orogless* run (Fig. 6.8c), on the contrary, does not show significant differences with respect to the CNTRL run: a slight decrease in wind speed is just predicted in the southern part of the area affected by the Bora wind.

Fig. 6.9a and Fig. 6.9c show the wind vector on the cross-section along the jet for the *orogplus* and *orogless* simulation, respectively. The steeper orography clearly force the easterly flow to lift at large distance from the Appenines and to reach the saturation before impinging on them. This behaviour can explain the fact that, although weaker jets are predicted at the coast, no significant effects are expected on the precipitation field. On the other hand, in the *orogless* experiment the Bora wind blows at the lower levels above the sea and a slight uplift is observed inland.

Looking at the relative humidity profiles for the orography sensitivity tests it is observed that the dry layer above the sea surface still occurs for the *orogless* test (Fig. 6.9d), while no significant differences with respect to CNTRL run are predicted for *orogplus* (Fig. 6.9b, to be compared with Fig. 6.3a). The more intense uplift observed for the *orogless* experiment prevents the dry layer to form since the Bora flow is forced to rise up to higher altitudes.

(a)

(b)

(c)
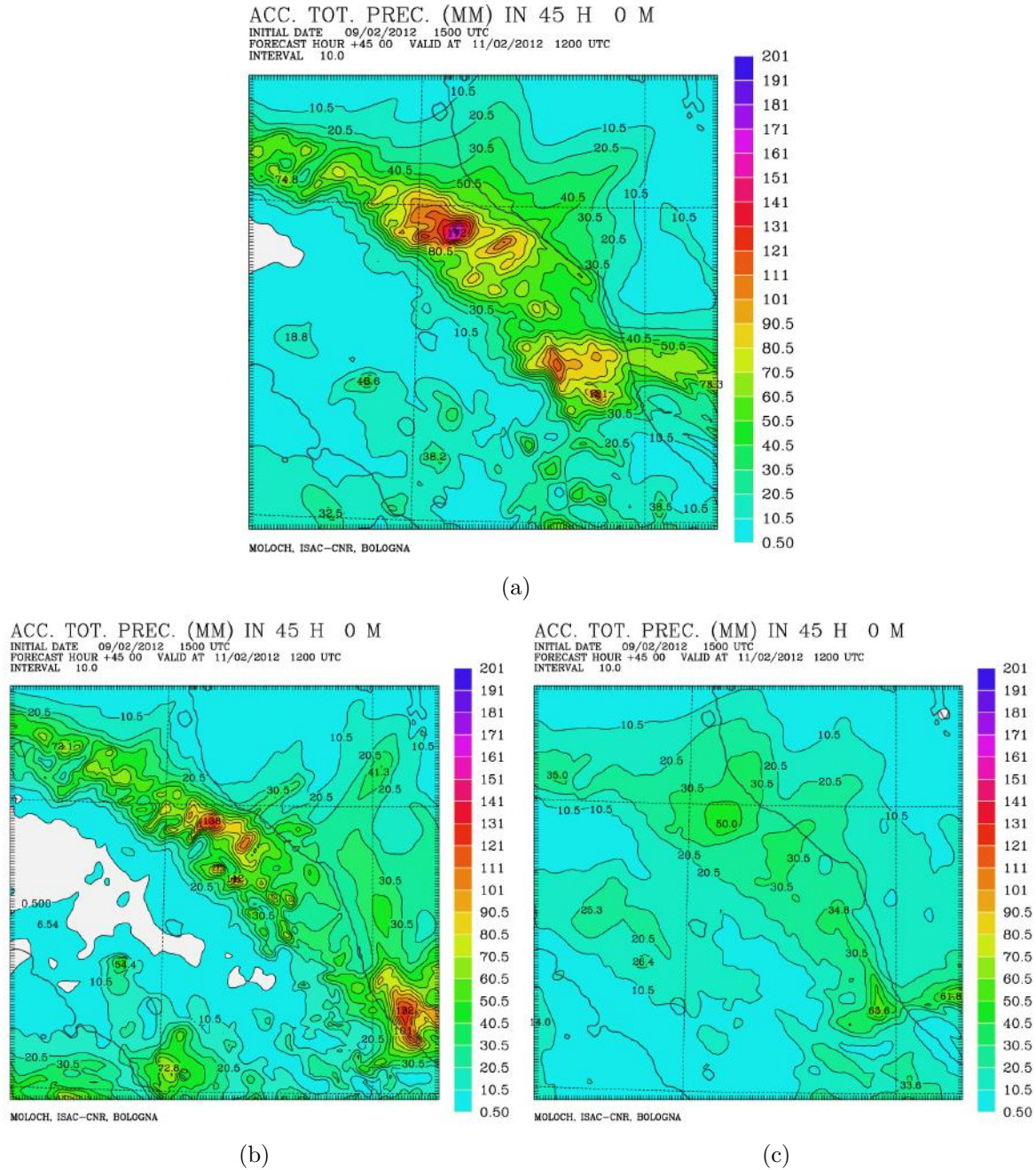
Figure 6.7: Total precipitation amount forecast by MOLOCH in 45h from 15 UTC, 9 February 2012 to 12 UTC, 11 February 2012 for CNTRL run (a), *orogplus* run (b) and *orogless* run (c).

(a)

(b)

(c)
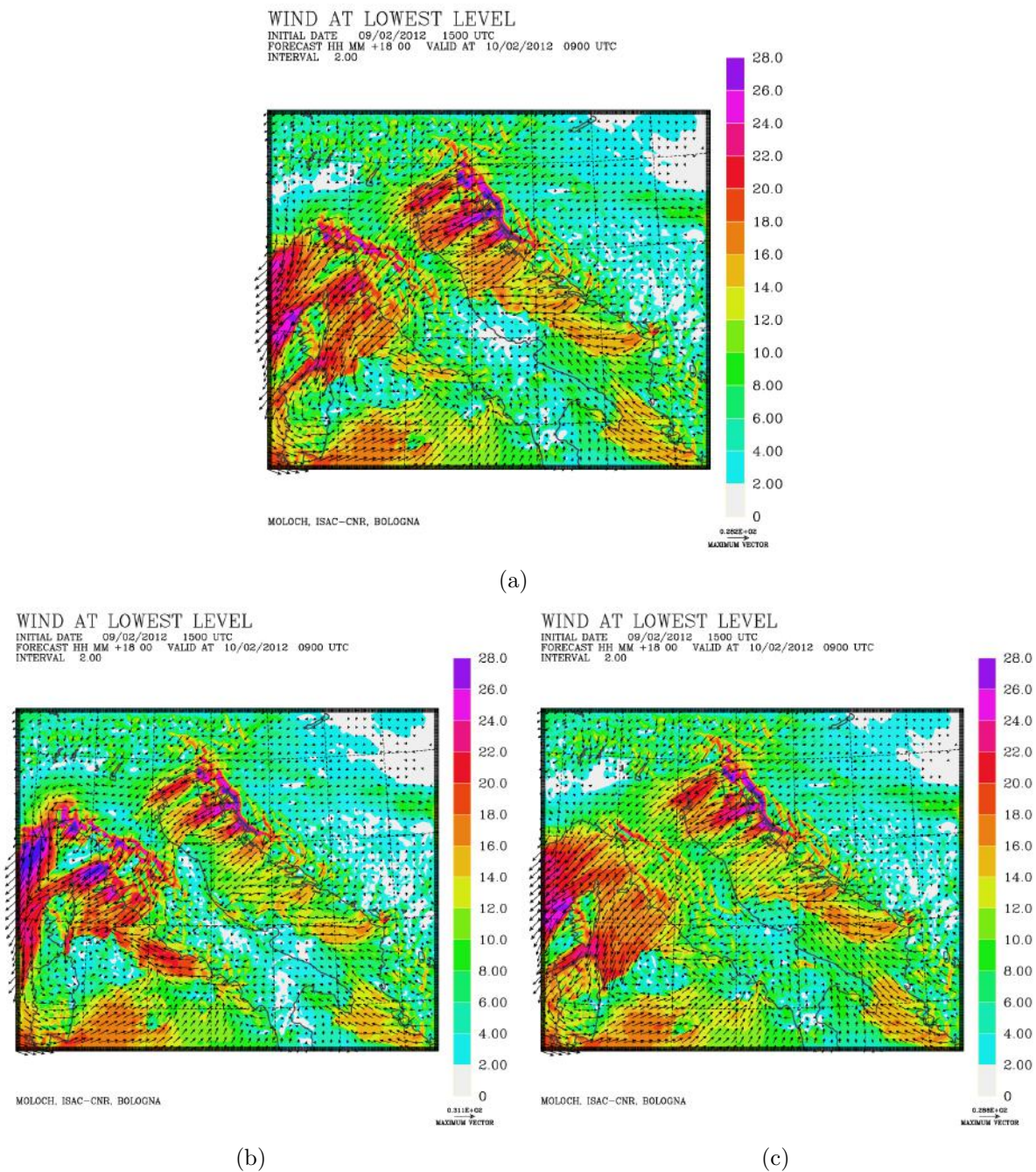
Figure 6.8: Wind field forecast by MOLOCH at lowest level for CNTRL run (a), *orogplus* run (b) and *orogless* run (c), valid at 09 UTC on 10 February 2012.

(a)

(b)

(c)

(d)
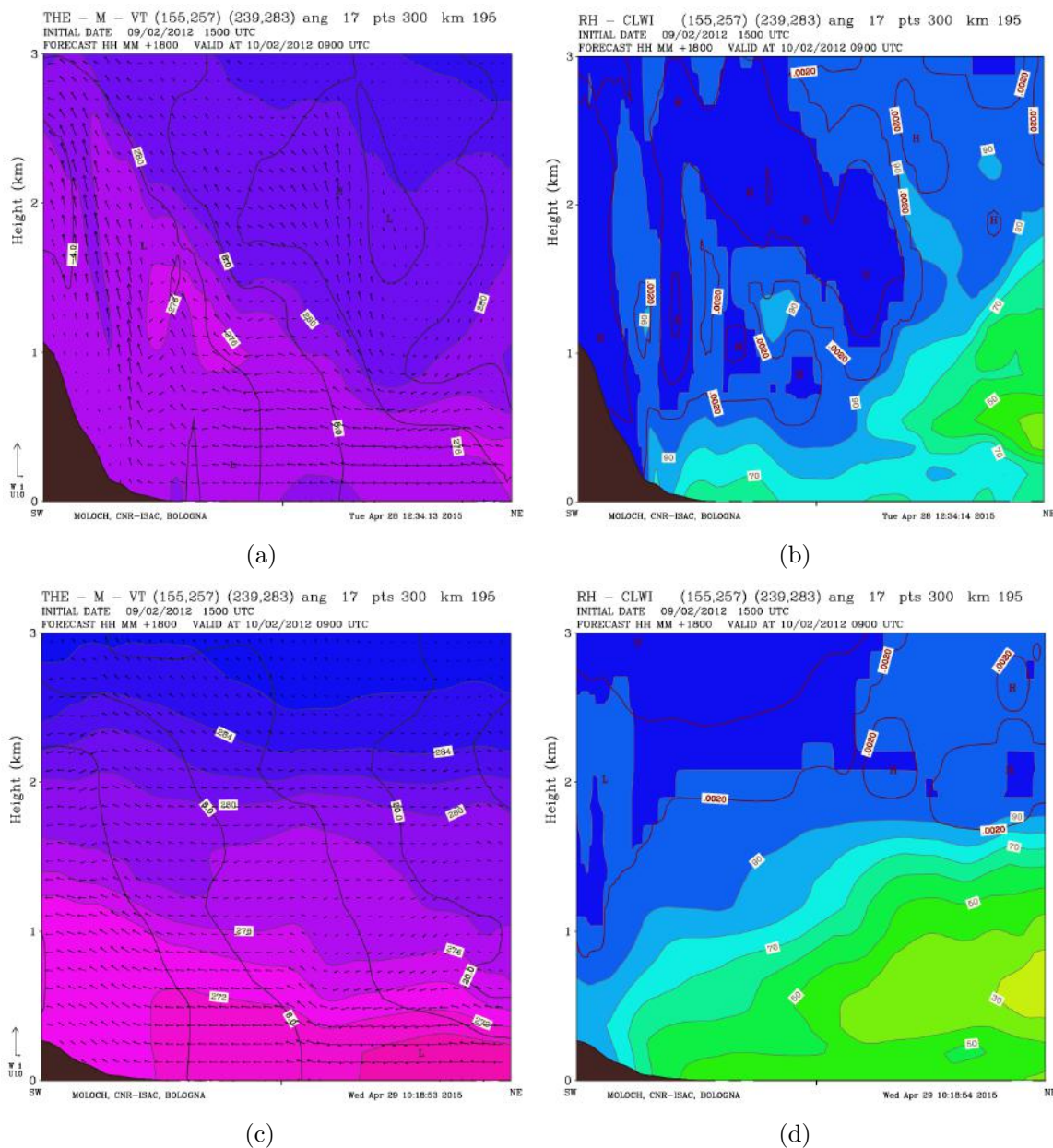
Figure 6.9: θ_e, momentum and tangential wind vector forecast by MOLOCH on the along-jet cross-section for *orogplus* (a) *orogless* (c) tests. Relative humidity and CLWI forecast by MOLOCH on the along-jet cross-section for the *orogplus* (b) and *orogless* (d) cases. Valid at 09 UTC on 10 February 2012.

6.3   Results overview

The analysis of the cross-sections carried out in this chapter allows to examine the
dynamics leading to a weakening of the wind predicted over the Adriatic Sea for all the
noflux sensitivity tests. It shows that the weakening of the wind in the lowest layers, up
to 500m on average, corresponds to a simultaneous increase in the wind strenght above,
typically between 500m and 1000m. This feature indicates that the jet-pattern is still
occurring even if at a different height. The relative humidity patterns on the along-jet
cross-sections show that a layer with different properties establishes above the sea up to
500m or more (as in the September case). For the *nofluxN* and *nolatN* (*nosenN*) the
lack of air-sea heat fluxes prevents the vertical mixing within the lower layer to occur
and allows a drier (wetter) layer (MBL) to form. Thus the Bora wind is displaced at
some distance from the surface so that maximum speed values are no more predicted at
sea level. The θ distribution on the along-jet cross-sections confirms that the MBL is
characterised by different stability properties: it is more stable for for the *nofluxN* and
nolatN experiments and less stable (or even locally unstable) for the *nosenN* one.

   This feature is coherent with the precipitation field forecasts for the sensitivity tests.
The sensitivity tests (Ch. 4) show that the *nofluxN* and *nolatN* runs produce similar results
in terms of the precipitation pattern. On the contrary, the *nosenN* test behave differently:
the decrease of total precipitation amount for this experiment is less pronounced, typically
less than half the values predicted for *nofluxN* and *nolatN* (-20% instead of -60% for the
Romagna and Appennines box and no reduction or even an increase for the sea box).
This features confirms the results of the cross-section analysis: for this case the boundary
layer which develops above the sea surface is characterised by relative humidity close
to saturation (since the latent heat flux is allowed). Moreover the θ_e vertical gradient
shows an inversion in the lowest layers of the western part of the cross-section which
indicates more favourable conditions for moist convection. Meanwhile, *nofluxN* and
nolatN typically behave the same way.

   Finally, the orography sensitivity tests show that the downstream orography (the
Apennines chain) also plays a crucial role. The *orogplus* test demonstrates that an
increase of the Appenines height implies a reduction of the Bora wind strenght and the
disappereance of the jet-pattern in the western part of the Adriatic due to the forced uplift
and the development of a northwesterly barrier wind along the coast. Meanwhile, the dry
layer is not observed and the precipitation field does not show significant differences with
respect to CNTRL run. As supposed, the effect of raising orography is, to some extent,
similar to that obtained by removing the heat fluxes. However, this is true as regards the
dynamics of the Bora wind but differences are observed concerning precipitation.

   Looking at relative humidity on the along-jet cross-section no MBL establishes when
the orography is raised, as in CNTRL run. On the contrary, in the *orogless* experiment
drier air penetrates at sea level too. For this case no wind speed decrease occurs but a
decrease of total precipitation amount with respect to CNTRL run is predicted.

Chapter 7

Conclusions

In the present study some significant Bora events have been addressed: according to the known distinction based on the synoptic pattern preceding the event, three cyclonic Bora episodes and two anticyclonic Bora episodes have been considered. The MOLOCH model, nested in the BOLAM model, which, in turn, is initialized with the ECMWF analysis, is used to perform a number of simulations for each case study. The cyclonic cases turn out to be the most challenging and severe. For this reason, a large number of experiments have been carried out for them.

The evolution of each Bora event has been analysed at the synoptic scale and, more carefully, at the mesoscale. During the analysis, an interesting mesoscale feature has been discovered for the cyclonic cases: a vertical wind shear is present over the Adriatic associated with a southerly warm flow, blowing above the northeasterly Bora, belonging to the mesoscale circulation driven by the cyclone. The prevalent wind direction over the Adriatic basin turns to south-southeasterly above 1500m, while the cyclonic flow merges with the easterly Bora wind below 1500m. Typically this sharp convergence line is associated with an intense precipitation band above the sea extending inland as well. The presence of a vertical wind shear for these cases characterises the common classification into cyclonic/anticyclonic Bora, which is mainly based on synoptic scale features.

A CNTRL run has been performed for each case study and has been compared with observational data in order to validate the model simulations. A good agreement between the simulated and the observational data has been achieved especially concerning the precipitation forecasts, while some discrepancies have been observed for the pressure fields. The model displayed some uncertainties in simulating the location of the Adriatic cyclone and, consequently, the evolution of the meteorological fields was not always properly simulated.

Apart from the above preliminary investigations, the main objective of the thesis is to examine the dynamics of the Bora wind over the Adriatic Sea and to identify the key factors responsible for heavy precipitation events over the eastern Italian coast and

the eastern flanks of the Apennines in conjunction with severe Bora outbreaks. Such an analysis requires at first an evaluation of the role of the air-sea heat fluxes over the Adriatic which are known to provide heat and moisture to the impinging flow. Then an investigation of the dynamical aspects of the Bora wind propagation over the Adriatic Sea has been considered.

Sensitivity tests have been performed by modifying the SST initial values for the Adriatic Sea. The increasing of the SST produced an increase of precipitation over Romagna area and over the sea and a decrease over the central Apennines. Since the air-sea temperature difference strongly affects the vapour fluxes in terms of sensible heat flux (the larger the temperature difference, the larger the flux), this behaviour is expected. The different impact over the Apennines is due to the fact that a warmer sea may favour the development of moist convection and the consequent depletion of the water vapour, thus decreasing the moisture of the air column approaching the coast. An opposite behaviour has been observed by decreasing the SST.

Additional sensitivity tests, performed by removing the air-sea heat fluxes, have been carried out. Latent and sensible fluxes have been removed separately in the southern part of the Adriatic Sea and in the northern part. The removal of heat fluxes in the northern part of the Adriatic Sea produces remarkable effects with respect to the CNTR run: a drop of total precipitation amount over Italy by more than 50% on average, a weakening of the Bora wind-jet and the onset of a barrier wind along the central Italian coast. The results are similar when both the fluxes or latent heat only are removed. The latent heat flux over the Adriatic, in fact, is observed to be larger than the sensible heat flux during Bora events, thus its role turned out to be the most relevant.

To better understand the results of the heat flux sensitivity tests, two diagnostic tools have been developed. The column water vapour flux along the Italian coastline has been computed and yielded to the following considerations. First, it shows that the horizontal water vapour flux is mainly confined below 1500m over the North Adriatic where the Bora wind blows and above 2000m over the South Adriatic where the cyclonic circulation prevails. Then the column water vapour flux shows that the southernmost Bora wind-jet, characterised by a merging with the mesoscale cyclonic flow, is the most intense among the different jets. This feature confirms that the water vapour coming from the South can strongly affect the precipitation pattern over the Apennines. Finally, it has been observed that the water vapour flux computed along the Italian coastline significantly decreases in the sensistivity tests with removed heat fluxes with respect to the CNTRL run. Also in this case, the test with latent heat flux removal behaves similarly to the test when both the fluxes are removed.

The second tool developed is the computation of the atmospheric water balance that has been evaluated in a volume box over the Adriatic Sea and has demonstrated that even if the heat fluxes (especially the latent heat flux) have a dramatic impact on the precipitation field, their contribution to the water balance is relatively small. Moreover,

considering the western section of the box, close to the Apennines, it turned out that the water content outflow is almost totally correlated with the contributions of the other three lateral sections rather than to the bottom face. This behaviour has been observed for the cyclonic cases, while for the anticyclonic ones the contribution of the bottom latent heat fluxes is more relevant since the advection across the lateral sections is quite weak. Furthermore, the water balance evaluation has assessed the importance of the southern cyclonic flow, whose contribution to the balance is not significantly lower with respect to that of the eastern section, which is associated with the Bora wind and it is expected to be the largest one.

In the last chapter of the thesis a more detailed analysis of the dynamics of the Bora wind over the Adriatic Sea has been carried out. In order to better understand, from a dynamical point of view, the decrease of the total precipitation amount simulated for the heat flux sensitivity tests with respect to the CNTRL run, several cross-sections have been considered. A drier and more stable boundary layer have been observed for those experiments characterized by the largest decrease in precipitation. This dry PBL above the Sea constrains the Bora flow at some distance above the sea surface and this pattern prevents the saturation over the Sea, the coast and the foothills of the Appenines leading to the decrease of the total precipitation amount forecast. Moreover the θ distribution on the cross-sections has shown that a weaker stratification and a lower stability characterise the boundary layer above the sea in the CNTRL run which is associated with heavier precipitation.

Since the role of the dowstream orography, as discussed in Ch. 2, can be crucial in affecting the flow propagation towards an obstacle, further sensitivity tests have been performed, for the February case only, to account for this issue. The orography of the MOLOCH model has been changed in order to increase and decrease the Apennines height. In the test with increased orography, the Bora wind is forced to lift from the sea surface up to 1500m at large distance upstream from the Apennines, just at some distance after it descends from the Dinaric Alps slopes. The sharp ascent favours the saturation of the air impinging on the Apennines, thus no significant decreases as regards the precipitation field is observed over Italy with respect to the CNTRL run. On the contrary, diminishing the orography allows the dry Bora wind to flow at lower levels and prevents the condensation to occur over the mountains. In this case a dramatic decrease in the total precipitation amount is predicted with respect to the CNTRL run.

The evaluation of the evolution of the stability of an atmospheric layer characterised by strong wind, intense surface heat fluxes and interacting with orography is a very complex issue. In the present work an empirical approach has been followed in order to identify several mechanisms responsible for influencing the atmospheric layers during Bora wind events. In a theoretical framework a deep understanding of the role of these processes can be achieved only considering individually each mechanism playing a role in

the whole phenomenon. The onset of the Bora wind across the Dinaric Alps depends on the upstream dynamics of the flow and on the barrier features. However the Bora flow affecting Italy, once descended along the Dinaric steep slopes, is in turn influenced by the Apennines. Moreover the air-sea heat fluxes and, consequently, the moisture play a role in affecting the marine boundary layer characteristics and the properties of the boundary layer characterise the flow upstream the Apennines. Therefore, all these processes are involved in an interesting and complex feedback mechanism.

Acronyms

ABL Atmospheric Boundary Layer

AdDW Adriatic Dense Water

AGU American Geophysical Union

ALPEX Alpine Experiment

AMS American Meteorological Society

ARPA Agenzia Regionale Protezione Ambiente

ASE Adriatic Sea Effect

BiOS Bimodal Oscillating System

BOLAM Bologna Limited Area Model

CAPE Convective Potential Available Energy

CFL Courant-Friedrichs-Lewy

CLWI Cloud Liquid Water Ice

CNR Consiglio Nazionale delle Ricerche

COMPARE Comparison of Mesoscale Prediction and Mesoscale Experiment

CRM Convection Resolving Model

DWF Dense Water Formation

ECMWF European Centre for Medium-range Weather Forecast

GFS Global Forecast System

GM Global Model

HyMeX HYdrological MEditerranean Cycle

HP High Pressure

HPE High Precipitation Events

IFS Integrated Forecast System

IOP Intesive Observation Period

ISAC Istituto di Scienze dell'Atmosfera e del Clima

ISMAR Istituto di Scienze MARine

IWV Integrated Water Vapour

LAM Limited Area Model

LCL Lifting Condensation Level

LIW Levantine Intermediate Water

LLJ Low Level Jets

LP Low Pressure

LW Long Wave

LES Lake-Effect Snow

MAP Mesoscale Alpine Project

MBL Marine Boundary Layer

McICA Monte-Carlo Independent Column Approximation

MCS Mesoscale Convective System

MOLOCH MOdello LOCale in coordinate H

NAdDW North Adriatic Dense Water

NCAR National Center for Atmospheric Research

NCEP National Centers for Environmental Prediction

NCL NCAR Command Language

NWP Numerical Weather Prediction

PBL Planetary Boundary Layer

PDE Partial Differential Equation

PV Potential Vorticity

QPF Quantitative Precipitation Forecast

RISKMED Weather Risk Reduction for the Mediterannean

RITMARE Ricerca Italiana per il Mare

RRTM Rapid Radiative Transfer Model

SAP South Adriatic Pit

SAR Synthetic-aperture radar

SODAR SOnic Detection And Ranging

SOP Special Observation Period

SST Sea Surface Temperature

SW Short Wave

SWH Significant Wave Height

TKE Turbulence Kinetic Energy

UKMO United Kingdom Meteorological Office

UTC Universal Time Coordinated

WAC Western Adriatic Current

WAF Weighted Average Flux

WMO World Meteorological Organization

References

[Alpers et al., 2009] Alpers, W., A.Ivanov, and J.Horstmann (2009). Observations of Bora Events over the Adriatic Sea and Black Sea by Spaceborne Synthetic Aperture Radar. *Monthly Weather Review*, 137(3).

[Arakawa and Lamb, 1977] Arakawa, A. and Lamb, V. (1977). *Computational design of the basic dynamical processes of the UCLA general circulation model*, chapter 17, pages 173–265. Academic Press.

[ARPA-SIMC, 2012a] ARPA-SIMC (2012a). Le nevicate di Febbraio 2012: i dati disponibili. Technical report, ARPA Emilia Romagna - Servizio IdroMeteoClima - Area Reti di Monitoraggio.

[ARPA-SIMC, 2012b] ARPA-SIMC (2012b). Rapporto dell'evento meteorologico dal 31 Gennaio al 5 Febbraio 2012 . Technical report, ARPA Emilia Romagna - Servizio Idro-Meteo-Clima.

[ARPA-SIMC, 2012c] ARPA-SIMC (2012c). Rapporto dell'evento meteorologico dal 7 al 12 Febbraio 2012 . Technical report, ARPA Emilia Romagna - Servizio Idro-Meteo-Clima.

[ARPA-SIMC, 2013a] ARPA-SIMC (2013a). Annali Idrologici 2013.

[ARPA-SIMC, 2013b] ARPA-SIMC (2013b). Rapporto dell 'evento idrologico e meteo-marino del 10-12 novembre 2013 . Technical report, ARPA Emilia Romagna - Servizio Idro-Meteo-Clima.

[Artegiani et al., 1997] Artegiani, A., Paschini, E., and Russo, A. (1997). The Adriatic Sea general circulation. Part I: Air-sea interactions and water mass structure.

[Askari et al., 2003] Askari, F., Signell, R., and Chiggiato, J. (2003). RADARSAT mapping of Bora/Sirocco winds in the Adriatic Sea.

[Barker et al., 2008] Barker, H. W., Cole, J. N. S., Morcrette, J.-J., Pincus, R., Räisänen, P., von Salzen, K., and Vaillancourt, P. A. (2008). The Monte Carlo Independent

Column Approximation: an assessment using several global atmospheric models. *Quarterly Journal of the Royal Meteorological Society*, 134(635):1463–1478.

[Bartzokas et al., 2010] Bartzokas, A., Azzopardi, J., Bertotti, L., Buzzi, A., Cavaleri, L., Conte, D., Davolio, S., Dietrich, S., Drago, A., Drofa, O., Gkikas, A., Kotroni, V., Lagouvardos, K., Lolis, C. J., Michaelides, S., Miglietta, M., Mugnai, A., Music, S., Nikolaides, K., Porcù, F., Savvidou, K., and Tsirogianni, M. I. (2010). The RISKMED project: philosophy, methods and products. *Natural Hazards and Earth System Science*, 10(7):1393–1401.

[Belušić et al., 2013] Belušić, D., Hrastinski, M., Vecenaj, Z., and Grisogono, B. (2013). Wind Regimes Associated with a Mountain Gap at the Northeastern Adriatic Coast. *Journal of Applied Meteorology and Climatology*.

[Billet and Toro, 1997] Billet, S. J. and Toro, E. F. (1997). On the Accuracy and Stability of Explicit Schemes for Multidimensional Linear Homogeneous Advection Equations. *Journal of Computational Physics*, 131(1).

[Blackadar, 1962] Blackadar, A. K. (1962). The vertical distribution of wind and turbulent exchange in a neutral atmosphere. *Journal of Geophysical Research*, 67(8):3095–3102.

[Bougeault et al., 2001] Bougeault, P., Binder, P., Buzzi, A., and Dirks, R. (2001). The MAP special observing period.

[Bougeault and Lacarrère, 1989] Bougeault, P. and Lacarrère, P. (1989). Parameterization of orographic induced turbulence in a mesobeta scale model. *Monthly Weather Review*, 117:1872–1890.

[Buzzi et al., 2003] Buzzi, A., D'Isidoro, M., and Davolio, S. (2003). A case-study of an orographic cyclone south of the Alps during the MAP SOP. *Quarterly Journal of the Royal Meteorological Society*, 129(591):1795–1818.

[Buzzi et al., 1994] Buzzi, A., Fantini, M., Malguzzi, P., and Nerozzi, F. (1994). Validation of a limited area model in cases of mediterranean cyclogenesis: Surface fields and precipitation scores. *Meteorology and Atmospheric Physics*, 53(3-4):137–153.

[Buzzi and Foschini, 2000] Buzzi, A. and Foschini, L. (2000). Mesoscale Meteorological Features Associated with Heavy Precipitation in the Southern Alpine Region. *Meteorology and Atmospheric Physics*, 72(2-4):131–146.

[Calwagen, 1926] Calwagen, E. G. (1926). *Zur Diagnose und Prognose lokaler Sommerschauer Aerologische Flugzeugaufstiege in Ostnorwegen*. Oslo Cammermeyers Boghandel.

[Camuffo, 1981] Camuffo, D. (1981). Fluctuation in wind direction at Venice, related to the origin of the air masses.

[Camuffo, 1990] Camuffo, D. (1990). *Acidic Precipitation Research in Italy*, volume 5 of *Advances in Environmental Science*. Springer New York.

[Cavaleri et al., 2010] Cavaleri, L., Bertotti, L., Buizza, R., Buzzi, A., Masato, V., Umgiesser, G., and Zampieri, M. (2010). Predictability of extreme meteo-oceanographic events in the Adriatic Sea. *Quarterly Journal of the Royal Meteorological Society*, 136(647):400–413.

[Cesini et al., 2004] Cesini, D., Morelli, S., and Parmiggianil, F. (2004). Analysis of an intense bora event in the Adriatic area. *Natural Hazards and Earth System Science*, 4(2):323–337.

[C.F.Marche, 2012a] C.F.Marche (2012a). Annali Idrologici 2012 .

[C.F.Marche, 2012b] C.F.Marche (2012b). Rapporto di evento 1-13 Febbraio 2012 . Technical report, Regione Marche - Dipartimento per le politiche integrate di sicurezza e per la protezione civile - Centro funzionale per la meteorologia, l'idrologia e la sismologia.

[C.F.Marche, 2013] C.F.Marche (2013). Rapporto di evento 10-13 Novembre 2013 . Technical report, Regione Marche - Dipartimento per le politiche integrate di sicurezza e per la protezione civile - Centro funzionale per la meteorologia, l'idrologia e la sismologia.

[C.F.Umbria, 2013] C.F.Umbria (2013). Evento alluvionale 11-12 Novembre 2013 - Rapporto d'evento . Technical report, Regione Umbria - Direzione Programmazione, Innovazione e Competitività dell'Umbria - Servizio Protezione Civile - Centro Funzionale.

[Charnock, 1955] Charnock, H. (1955). Wind stress on a water surface. *Quarterly Journal of the Royal Meteorological Society*, 81(350):639–640.

[Davolio et al., 2007] Davolio, S., Buzzi, A., and Malguzzi, P. (2007). High resolution simulations of an intense convective precipitation event. *Meteorology and Atmospheric Physics*, 95(3-4):139–154.

[Davolio et al., 2009a] Davolio, S., Mastrangelo, D., Miglietta, M., Drofa, O., Buzzi, A., and Malguzzi, P. (2009a). High resolution simulations of a flash flood near Venice. *Natural Hazards and Earth System Science*, 9(5):1671–1678.

[Davolio et al., 2009b] Davolio, S., Miglietta, M. M., Moscatello, A., Pacifico, F., Buzzi, A., and Rotunno, R. (2009b). Numerical forecast and analysis of a tropical-like cyclone in the Ionian Sea. *Natural Hazards and Earth System Science*, 9(2):551–562.

[Davolio et al., 2015] Davolio, S., Stocchi, P., Benetazzo, A., Bohm, E., Riminucci, F., Ravaioli, M., Li, X.-M., and Carniel, S. (2015). Exceptional Bora outbreak in winter 2012: validation and analysis of high-resolution atmospheric model simualtions in the northern Adriatic Area.

[Davolio et al., 2013] Davolio, S., Stocchi, P., Miglietta, M., Buzzi, A., Malguzzi, P., Fantini, M., and Drofa, O. (2013). RITMARE - Ricerca ITaliana per il MARE: prima validazione dei modelli atmosferici.

[Dorman et al., 2006] Dorman, C., , and and (2006). February 2003 marine atmospheric conditions and the bora over the northern Adriatic. *Journal of Geophysical Research*, 112(C3).

[Drobinški, 2014] Drobinški, P. e. a. (2014). HyMeX: A 10-Year Multidisciplinary Program on the Mediterranean Water Cycle. *Bulletin of the American Meteorological Society*, 95(7).

[Drofa and Malguzzi, 2004] Drofa, O. and Malguzzi, P. (2004). Parameterization of microphysical processes in a non hydrostatic prediction model. In *Proc. 14th Intern. Conf. on Clouds and Precipitation (ICCP)*.

[Ducrocq et al., 2008] Ducrocq, V., Nuissierl, O., Ricardl, D., Lebeaupinl, C., and Thouvenin, T. (2008). A numerical study of three catastrophic precipitating events over southern France. II: Mesoscale triggering and stationarity factors. *Quarterly Journal of the Royal Meteorological Society*, 134(630):131–145.

[Ducrocq, 2014] Ducrocq, V. e. a. (2014). HyMeX-SOP1: The Field Campaign Dedicated to Heavy Precipitation and Flash Flooding in the Northwestern Mediterranean. *Bulletin of the American Meteorological Society*, 95(7).

[Duffourg and Ducrocq, 2011] Duffourg, F. and Ducrocq, V. (2011). Origin of the moisture feeding the heavy precipitating systems over southeastern France. *Natural Hazards and Earth System Science*, 11(4):1163–1178.

[Durran, 1990] Durran, D. (1990). Mountain Waves and Downslope Winds.

[Enger and Grisogono, 1998] Enger, L. and Grisogono, B. (1998). The response of bora type flow to sea surface temperature.

[Ferrarese et al., 2009] Ferrarese, S., Cassardol, C., Elmi, A., Genovese, R., Longhetto, A., M-Manfrin, and Richiardone, R. (2009). Air-sea interactions in the Adriatic Basin: simulations of Bora and Sirocco wind events. *Geofizika*, 26(2).

[Ferrarin et al., 2013] Ferrarin, C., Roland, A., Bajo, M., Umgiesser, G., Cucco, A., Davolio, S., Buzzi, A., Malguzzi, P., and Drofa, O. (2013). Tide-surge-wave modelling and forecasting in the Mediterranean Sea with focus on the Italian coast . *Ocean Modelling*, 61(0):38 – 48.

[Ferretti, 2014] Ferretti, R. e. a. (2014). Overview of the first HyMeX Special Observation Period over Italy: observations and model results. *Hydrology and Earth System Sciences*, 18(5):1953–1977.

[Gaberšek and Durran, 2004] Gaberšek, S. and Durran, D. (2004). Gap flows through idealized topography. Part I: Forcing by large-scale winds in the nonrotating limit. *Journal of the Atmospheric Sciences*, 61(23):2846–2862. cited By 26.

[Gačić et al., 2010] Gačić, M., Borzelli, G. L. E., Civitarese, G., Cardin, V., and Yari, S. (2010). Can internal processes sustain reversals of the ocean upper circulation? the ionian sea example. *Geophysical Research Letters*, 37(9):n/a–n/a.

[Gohm, Alexander and Mayr, Georg J. and Fix, Andreas and Giez, Andreas, 2008] Gohm, Alexander and Mayr, Georg J. and Fix, Andreas and Giez, Andreas (2008). On the onset of bora and the formation of rotors and jumps near a mountain gap. *Quarterly Journal of the Royal Meteorological Society*, 134(630):21–46.

[Grazzini, 2013] Grazzini, F. (2013). Cold spell prediction beyond a week: extreme snowfall events in February 2012 in Italy. *ECMWF Newsletters*, (136).

[Grisogono and Belušić, 2009] Grisogono, B. and Belušić, D. (2009). A review of recent advances in understanding the meso- and microscale properties of the severe Bora wind. *Tellus A*, 61(1).

[Grubišíc, 2004] Grubišíc, V. (2004). Bora-driven potential vorticity banners over the Adriatic. *Quarterly Journal of the Royal Meteorological Society*, 130(602):2571–2603.

[Grubišic and Orlic, 2007] Grubišic, V. and Orlic, M. (2007). Early Observations of Rotor Clouds by Andrija Mohorovičic.

[Horvath et al., 2009] Horvath, K., Ivatek-Šahdan, S., Ivančan-Picek, B., and Grubišić, V. (2009). Evolution and Structure of Two Severe Cyclonic Bora Events: Contrast between the Northern and Southern Adriatic. *Weather and Forecasting*, 24(4).

[Janecović et al., 2014] Janecović, I., Mihanovic, I., I.Vilibic, and M.Tudor (2014). Extreme cooling and dense water formation estimates in open and coastal regions of the Adriatic Sea during the winter of 2012. *Journal of Geophysical Research: Oceans*, 119(5).

[Jeffries and Lee, 2007] Jeffries, M. and Lee, C. M. (2007). A climatology of the northern Adriatic Sea response to bora and river forcing. *Journal of Geophysical Research: Oceans (1978–2012)*, 112(C3).

[Jiang and Doyle, 2005] Jiang, Q. and Doyle, J. D. (2005). Wave breaking induced surface wakes and jets observed during a bora event. *Geophysical Research Letters*, 32(17).

[Jurčec, 1981] Jurčec, V. (1981). On mesoscale characteristics of bora conditions in yugoslavia. In Liljequist, G., editor, *Weather and Weather Maps*, Contributions to Current Research in Geophysics, pages 640–657. Birkhäuser Basel.

[Kain, 2004] Kain, J. (2004). The Kain-Fritsch convective parameterization: an update.

[Kain and Fritsch, 1990] Kain, J. S. and Fritsch, J. M. (1990). A One-Dimensional Entraining/Detraining Plume Model and Its Application in Convective Parameterization. *Journal of the Atmospheric Science*, 47:2784–2802.

[Koffi et al., 2013] Koffi, E. N., Graham, E., and Mätzler, A. (2013). The water vapour flux above Switzerland and its role in the August 2005 extreme precipitation and flooding. *Meteorologische Zeitschrift*, 22(3):328–341.

[Kraljević and Grisogono, 2006] Kraljević, L. and Grisogono, B. (2006). Sea-surface temperature effects on 3D bora-like flow. *Meteorologische Zeitschrift*, 15(2).

[Kuzmić et al., 2013] Kuzmić, M., Li, X., Grisogono, B., Tomažić, I., and Lehner, S. (2013). TerraSAR-X observations of the northeastern Adriatic bora: early results.

[Lazić and Tošić, 1997] Lazić, L. and Tošić, I. (1997). A real data simulation of the Adriatic bora and the impact of mountain height on bora trajectories. *Meteorology and Atmospheric Physics*, 66(3):143–155.

[Lebeaupin et al., 2006] Lebeaupin, C., Ducrocq, V., and Giordani, H. (2006). Sensitivity of torrential rain events to the sea surface temperature based on high-resolution numerical forecasts. *Journal of Geophysical Research: Atmospheres*, 111(D12):n/a–n/a.

[Lehmann, 1993] Lehmann, R. (1993). On the choice of relaxation coefficients for Davies' lateral boundary scheme for regional weather prediction models. *Meteorology and Atmospheric Physics*, 52(1-2):1–14.

[Lionello et al., 2012] Lionello, P., Cavaleri, L., Nissen, K., Pino, C., Raicich, F., and Ulbrich, U. (2012). Severe marine storms in the Northern Adriatic: Characteristics and trends. *Physics and Chemistry of the Earth, Parts A/B/C*, 40-41.

[Ludwig et al., 2014] Ludwig, P., Pinto, J. G., Reyers, M., and Gray, S. L. (2014). The role of anomalous SST and surface fluxes over the southeastern North Atlantic in the explosive development of windstorm Xynthia. *Quarterly Journal of the Royal Meteorological Society*, 140(682):1729–1741.

[Makjanić, 1978] Makjanić, B. (1978). *Bura, jugo, etezija.* Prilozi poznavanju vremena i klime u SFRJ. Savezni hidrometeorološki zavod.

[Malguzzi and Tartagione, 1999] Malguzzi, P. and Tartagione, N. (1999). An economical second-order advection scheme for numerical weather prediction. *Quarterly Journal of the Royal Meteorological Society*, 125(558):2291–2303.

[Manzato, 2007] Manzato, A. (2007). The 6 h climatology of thunderstorms and rainfalls in the Friuli Venezia Giulia Plain. *Atmospheric Research*, 83(2-4).

[Markowski and Richardson, 2010] Markowski, P. and Richardson, Y. (2010). *Mesoscale Meteorology in Midlatitudes.* Wiley.

[Mihanović, 2013] Mihanović, H. (2013). Exceptional dense water formation on the Adriatic shelf in the winter of 2012. *Ocean Science*, 9(3).

[Milivoj et al., 2006] Milivoj, K., Janekovi, I., Book, J. W., Martin, P. J., and Doyle, J. D. (2006). Modeling the northern Adriatic double gyre response to intense Bora wind: A revisit. *Journal of Geophysical Research: Oceans (19782012)*, 111(C3).

[Mlawer et al., 1997] Mlawer, E. J., Taubman, S. J., Brown, P. D., Iacono, M. J., and Clough, S. A. (1997). Radiative transfer for inhomogeneous atmospheres: RRTM, a validated correlated-k model for the longwave. *Journal of Geophysical Research: Atmospheres*, 102(D14):16663–16682.

[Mohorovičic, 1889] Mohorovičic, A. (1889). Interesting cloud pictures over the Bay of Buccari (with a comment from the editor J. Hann) - Wolkenbildung über der Bucht von Buccari. *Meteorol. Z.*, (24).

[Monin and Obukhov, 1954] Monin, A. S. and Obukhov, A. M. (1954). *On the Accuracy and Stability of Explicit Schemes for Multidimensional Linear Homogeneous Advection Equations*, chapter 151, pages 163–187. Akademija Nauk SSR.

[Morcrette et al., 2008] Morcrette, J., Barker, H. W., Cole, J., M.J.Iacono, and Pincus, R. (2008). Impact of a New Radiation Package, McRad, in the ECMWF Integrated Forecasting System. *Monthly Weather Review*, 136:4773–4798.

[Morcrette, 1991] Morcrette, J.-J. (1991). Radiation and cloud radiative properties in the European Centre for Medium Range Weather Forecasts forecasting system. *Journal of Geophysical Research: Atmospheres*, 96(D5):9121–9132.

[Nuissier et al., 2008] Nuissier, O., Ducrocql, V., Ricard, D., Lebeaupinl, C., and Anquetinl, S. (2008). A numerical study of three catastrophic precipitating events over southern France. I: Numerical framework and synoptic ingredients. *Quarterly Journal of the Royal Meteorological Society*, 134(630):111–130.

[Orlandi et al., 2010] Orlandi, E., Fierli, F., Davolio, S., Buzzi, A., and Drofa, O. (2010). A nudging scheme to assimilate satellite brightness temperature in a meteorological model: Impact on representation of African mesoscale convective systems. *Quarterly Journal of the Royal Meteorological Society*, 136(647):462–474.

[Orlic et al., 1992] Orlic, M., Gacic, M., and Laviolette, P. (1992). The currents and circulation of the Adriatic Sea. *Oceanologica Acta*, 15(2):109–124.

[Pandžić and Likso, 2005] Pandžić, K. and Likso, T. (2005). Eastern Adriatic typical wind field patterns and large-scale atmospheric conditions. *International Journal of Climatology*, 25(1):81–98.

[Pasarić et al., 2009] Pasarić, Z., Belusić, D., and Klaić, Z. B. (2009). Orographic effects on meteorological fields over the Adriatic from different models. *Journal of Marine Systems*, 78.

[Poje, 1992] Poje, D. (1992). Wind persistence in Croatia. *International Journal of Climatology*, 12(6):569–586.

[Pratizzoli, 2012] Pratizzoli, W. (2012). Agrometeorologia: le minime di Febbraio 2012 e confronto con altri eventi di gelo invernale . Technical report, ARPA Emilia Romagna - Servizio Idro-Meteo-Clima.

[Prtenjak and Grisogono, 2007] Prtenjak, M. T. and Grisogono, B. (2007). Sea/land breeze climatological characteristics along the northern croatian adriatic coast. *Theoretical and Applied Climatology*, 90(3-4):201–215.

[Pullen et al., 2007] Pullen, J., Doyle, J. D., Haack, T., Dorman, C., Signell, R. P., and Lee, C. M. (2007). Bora event variability and the role of air-sea feedback. *Journal of Geophysical Research*, 112(C3).

[Pullen et al., 2006] Pullen, J., Doyle, J. D., and Signell, R. P. (2006). Two-Way Air–Sea Coupling: A Study of the Adriatic. *Monthly Weather Review*.

[Rachev and Purini, 2001] Rachev, N. and Purini, R. (2001). The Adriatic response to the bora forcing: A numerical study. *Nuovo Cimento C Geophysics Space Physics C*, 24:303.

[Raicich et al., 2013] Raicich, F., Malacic, V., Celio, M., Giaiotti, D., Cantoni, C., R.R.Colucci, Cermelj, B., and Pucillo, A. (2013). Extreme air-sea interactions in the Gulf of Trieste (North Adriatic) during the strong Bora event in winter 2012. *Journal of Geophysical Research: Oceans*, 118(10).

[Richard et al., 2007] Richard, E., Buzzi, A., and Zängl, G. (2007). Quantitative precipitation forecasting in the Alps: The advances achieved by the Mesoscale Alpine Programme. *Quarterly Journal of the Royal Meteorological Society*, 133(625):831–846.

[Richard et al., 2003] Richard, E., Cosma, S., Benoit, R., Binder, P., Buzzi, A., and Kaufmann, P. (2003). Intercomparison of mesoscale meteorological models for precipitation forecasting. *Hydrology and Earth System Sciences Discussions*, 7(6):799–811.

[Ritter and Geleyn, 1992] Ritter, B. and Geleyn, J.-F. (1992). A Comprehensive Radiation Scheme for Numerical Weather Prediction Models with Potential Applications in Climate Simulations. *Monthly Weather Review*, 120:303–325.

[Rotach et al., 2009] Rotach, M. W., Ambrosetti, P., Appenzeller, C., Arpagaus, M., Fontannaz, L., Fundel, F., Germann, U., Hering, A., Liniger, M. A., Stoll, M., et al. (2009). MAP D-PHASE: Real-time demonstration of weather forecast quality in the Alpine region. *Bulletin of the American Meteorological Society*, 90(9):1321–1336.

[Senatore et al., 2014] Senatore, A., Mendicino, G., Knoche, H., and Kunstmann, H. (2014). Sensitivity of modeled precipitation to sea surface temperature in regions with complex topography and coastlines: A case study for the Mediterranean. *Journal of Hydrometeorology*, 15(6):2370–2396. cited By 0.

[Signell et al., 2010] Signell, R., Chiggiato, J., Horstmann, J., Doyle, J., Pullen, J., and Askari, F. (2010). High-resolution mapping of Bora winds in the northern Adriatic Sea using synthetic aperture radar. *Journal of Geophysical Research*, 115(C4).

[Smith et al., 2010] Smith, B., Yuter, S., Neiman, P., and Kingsmill, D. (2010). Water Vapor Fluxes and Orographic Precipitation over Northern California Associated with a Landfalling Atmospheric River. *Monthly Weather Review*, 138(1).

[Smith, 1985] Smith, R. (1985). On severe downslope winds.

[Smith, 1987] Smith, R. (1987). Aerial observations of the Yugoslavian bora.

[Smith, 1989] Smith, R. B. (1989). Hydrostatic airflow over mountains. *Advances Geophysics*, 31:1–41.

[Stravisi, 1987] Stravisi, F. (1987). Climatic variations at Trieste during the last century.

[Supić et al., 2012] Supić, N., Kraus, R., Kuzmić, M., Paschini, E., Precali, R., Russo, A., and Vilibićl, I. (2012). Predictability of northern Adriatic winter conditions. *Journal of Marine Systems*, 90(1).

[Tettamanti and Zardi, 2002] Tettamanti, R., P. M. and Zardi, D. (2002). Numerical simulation of katabatic winds with a non-hydrostatic meteorological model. *Polar Atmospheres*, 1:1–95.

[Ž.Večenaj et al., 2012] Ž.Večenaj, Belušić, D., Grubišić, V., and Grisogono, B. (2012). Along-Coast Features of Bora-Related Turbulence. *Boundary-Layer Meteorology*, 143(3):527–545.

[Vickers and Mahrt, 2004] Vickers, D. and Mahrt, L. (2004). Atmospheric response to sea-surface temperature variability. In *Preprints, 13th Conf. on Interactions of the Sea and Atmosphere, Portland, ME, Amer. Meteor. Soc., CD-ROM*, volume 2.

[Vilibić et al., 2001] Vilibić, I., Orlic, and Mirko (2001). Least-squares tracer analysis of water masses in the South Adriatic (1967-1990). *Deep Sea Research Part I: Oceanographic Research Papers*, 48(10):2297–2330.

[Yoshino, 1976] Yoshino, M. (1976). *Local Wind Bora*. University of Tokyo Press.

[Zampieri et al., 2005] Zampieri, M., Malguzzi, P., and Buzzi, A. (2005). Sensitivity of quantitative precipitation forecasts to boundary layer parameterization: a flash flood case study in the Western Mediterranean. *Natural Hazards and Earth System Science*, 5(4):603–612.

Acknowledgements